# Simplified FE analysis of reinforced concrete slabs

Master's Thesis in the Master's Programme Structural Engineering and Building Technology

MARTIN EKSTRÖM
KRISTIN SKAAR

# Simplified FE analysis of reinforced concrete slabs

*Master's Thesis in the Master's Programme  Structural Engineering and Building Technology*

MARTIN EKSTRÖM

KRISTIN SKAAR

Department of Civil and Environmental Engineering
*Division of Structural Engineering*
*Concrete structures*
CHALMERS UNIVERSITY OF TECHNOLOGY

Göteborg, Sweden 2016

Simplified FE analysis of reinforced concrete slabs
*Master's Thesis in the Master's Programme Structural Engineering and Building Technology*

MARTIN EKSTRÖM

KRISTIN SKAAR

Department of Civil and Environmental Engineering
Division of Structural Engineering
Concrete structures
Chalmers University of Technology
SE-412 96 Göteborg
Sweden
Telephone: + 46 (0)31-772 1000

Cover:
Upper figure: FE-model of a reinforced concrete slab subjected to torsion, modelled as a beam grillage in the FE software ADINA. Lower left: Multilinear moment-curvature relation. Lower right: Multilinear torsion-twist relation.

Simplified FE analysis of reinforced concrete slabs

*Master's thesis in the Master's Programme  Structural Engineering and Building Technology*

MARTIN EKSTRÖM
KRISTIN SKAAR
Department of Civil and Environmental Engineering
Division of Structural Engineering
Concrete structures
Chalmers University of Technology

ABSTRACT

In finite element analyses (FE-analyses), slabs subjected to bending are normally modelled using shell elements. Such models describe the true linear elastic response of the slab to a great extent. Reinforced concrete slabs though, experience a nonlinear behaviour after cracking which is more complex to capture with shell element models. Thus, concrete, reinforcement and the interaction between them are often modelled as different elements, connected together.

Alternatively, the reinforced concrete slabs can be modelled as a beam grillage. Using beam elements is advantageous due to its simplicity and the possibility for more stable solutions. The material properties may be defined by moment-curvature and torsion-twist relations for each beam element separately, which makes it possible to describe varying structural behaviour in different directions.

Previously, the usage of beam grillage models for reinforced concrete slabs in the commercial FE software ADINA has shown inconsistency. The main reason for the disturbance was believed to be related to the difference in behaviour between a beam and a plate with regard to torsion.

In order to investigate the influence of the implemented torsional stiffness in ADINA, reinforced concrete slabs were simulated and the linear and nonlinear behaviour were studied. Successful linear elastic analyses were performed and it was found that the torsional stiffness should be approximated as two times the moment of inertia of a single beam in order to describe the true response of a slab.

For nonlinear analyses, no such relation was found. The flexural cracking moment of the slab may be used as a rough approximation of how to define the torsional cracking moment, but no relation describing the torsional stiffness for the cracked slab could be established.

II

Förenklad FE-analys av armerade betongplattor

Examensarbete inom masterprogrammet Structural Engineering and Building Technology

MARTIN EKSTRÖM
KRISTIN SKAAR
Institutionen för bygg- och miljöteknik
Avdelningen för Konstruktionsteknik
Betongbyggnad
Chalmers tekniska högskola

SAMMANFATTNING

I finita elementanalyser (FE-analyser) modelleras plattor som utsätts för böjning vanligtvis med skalelement. Sådana modeller beskriver i hög grad det sanna linjär-elastiska beteendet. Armerade betongplattor har dock ett olinjärt beteende efter att sprickor uppkommit som är mer komplicerat att beskriva med skalelementmodeller. Därför modelleras ofta betong, armering och samspelet mellan dem som olika, sammankopplade element.

Alternativt kan armerade betongplattor modelleras som balkroster. Användandet av balkelement i jämförelse med skalelement är fördelaktig på grund av dess enkelhet och möjligheten till mer stabila lösningar. Materialegenskaperna definieras av moment-krökning och vridning-vridvinkel relationer för varje separat balkelement vilket gör det möjligt att beskriva olika strukturella beteenden i olika riktningar.

Tidigare har användningen av balkrostmodeller för armerade betongplattor i det kommersiella FEM programmet ADINA genererat inkonsekventa analysresultat. Den främsta orsaken till störningen har förmodats vara relaterad till skillnaden i beteende mellan en balk och en platta med avseende på vridning.

I syfte att undersöka inverkan av den implementerade vridstyvheten i ADINA studerades armerade betongplattors linjära och olinjära beteende. Lyckade linjär-elastiska analyser genomfördes och det konstaterades att vridstyvheten för ospruckna tvärsnitt bör uppskattas som två gånger tröghetsmomentet för en enskild balk i syfte att beskriva den sanna responsen hos en platta.

För olinjära analyser hittades ingen liknande relation. Böjsprickmomentet i plattan kan användas som en grov uppskattning på hur man definierar vridsprickmomentet, men inget samband som beskriver vridstyvheten för en sprucken platta kunde fastställas.

Nyckelord:  Armerade betongplattor, balkrost, linjär FE-analys, olinjär FE-analys, vridstyvhet, vridning-vridvinkel, moment-krökning

# Contents

# Preface

In this master´s Thesis, the linear and nonlinear behaviour of reinforced concrete slabs subjected to torsion have been studied using FE analyses. The possibility to model slabs as beam grillages have been investigated and the results have been compared with shell element models and experimental data.

The work has been carried out at the office of ÅF Sverige AB in Gothenburg, at the period of January to June 2016. This master´s Thesis is a part of the master´s programme Structural Engineering and Building Technology at Chalmers University of Technology, Sweden. It is carried out at the Department of Structural Engineering, Concrete Structures.

Adjunct Professor Morgan Johansson has been the supervisor and examiner of the project. His commitment and helpful guidance throughout the work has been highly appreciated. We would also like to thank ÅF Sverige AB and our co-workers at the office in Gothenburg for their friendly reception.

Gothenburg, June 2016

Martin Ekström and Kristin Skaar

# Notations

**Roman upper case letters**

| | |
|---|---|
| $A$ | Area of cross-section |
| $D$ | Plate stiffness |
| $E$ | Young's modulus |
| $E_c$ | Young's modulus for concrete |
| $G$ | Shear modulus |
| $I$ | Moment of inertia |
| $I_I$ | Moment of inertia for State I cross-sections |
| $I_{II}$ | Moment of inertia for State II cross-sections |
| $I_p$ | Polar moment of inertia |
| $K_v$ | Torsional stiffness |
| $L$ | Diagonal length between supports |
| $L$ | Length of beam segment |
| $M$ | Moment |
| $M_{cr}$ | Flexural cracking moment |
| $M_{Ed}$ | Design value of bending moment |
| $P$ | Applied load |
| $S$ | First moment of area |
| $S_A$ | Shear area |
| $T$ | Torsional moment |
| $T_{cr}$ | Torsional cracking moment |
| $T_{sv}$ | St. Venant's torsional moment |
| $T_w$ | Vlasov's torsional moment |
| $V$ | Shear force |
| $V_{Ed}$ | Design value of shear force |
| $X$ | Global coordinate in ADINA |
| $Y$ | Global coordinate in ADINA |
| $Z$ | Global coordinate in ADINA |

**Roman lower case letters**

| | |
|---|---|
| $a$ | Shorter side of cross-section |
| $a$ | Concrete cover thickness |
| $b$ | Longer side of cross-section |
| $c$ | Diagonal length from support to edge corner |
| $d$ | Effective depth of cross-section |
| $f_{cc}$ | Concrete compressive strength |
| $f_{cm}$ | Mean compressive strength |
| $f_{ct}$ | Concrete tensile strength |
| $f_{ctm}$ | Mean concrete tensile strength |
| $f_{ctm,fl}$ | Flexural mean concrete tensile strength |
| $f_y$ | Yield stress |
| $f_{y,mod}$ | Modified yield stress with seven integration points |
| $h$ | Height of cross-section |
| $k$ | Correction factor due to size effect |
| $k_\lambda$ | Correction factor for shear slenderness |
| $l_{BG}$ | Length of beam grillage model in ADINA |

| | |
|---|---|
| $l_{el}$ | Element length in beam grillage mesh |
| $l_{gross}$ | Length of gross slab geometry |
| $l_{pl}$ | Length of plastic region |
| $m$ | Moment per unit width |
| $m_{cr}$ | Cracking moment per unit width |
| $m_r$ | Design reinforcement moment |
| $m_{xy}$ | Torsional moment per unit width |
| $q$ | Distributed load |
| $q_x$ | Distributed load in x-direction |
| $q_y$ | Distributed load in y-direction |
| $r$ | Radius of curvature |
| $r$ | Local coordinate in ADINA |
| $s$ | Local coordinate in ADINA |
| $s$ | Reinforcement bar spacing |
| $t$ | Local coordinate in ADINA |
| $t$ | Thickness |
| $u$ | Vertical displacement |
| $w$ | Width of cross-section |
| $w_{beam}$ | Width of chosen beams in ADINA |
| $x$ | Coordinate |
| $x$ | Height of compression zone |
| $x_0$ | Distance between maximum moment section and adjacent zero moment section |
| $x_u$ | Height of ultimate compression zone |
| $y$ | Coordinate |

**Greek lower case letters**

| | |
|---|---|
| $\alpha$ | Correction factor |
| $\alpha$ | Torsional rigidity factor |
| $\alpha_{new}$ | Torsional rigidity factor with implemented correction factor |
| $\beta$ | Correction factor |
| $\beta$ | Shear area factor |
| $\varepsilon$ | Strain |
| $\varepsilon_c$ | Concrete strain |
| $\varepsilon_{cc}$ | Concrete compressive strain |
| $\varepsilon_{cu}$ | Ultimate concrete compressive strain |
| $\varepsilon_s$ | Steel strain |
| $\varepsilon_{su}$ | Ultimate steel strain |
| $\Delta\alpha$ | Correction factor for torsional rigidity |
| $\theta$ | Angle of twist |
| $\theta$ | Angle |
| $\theta_{pl}$ | Plastic rotation |
| $\theta_{pl,d}$ | Design value of plastic rotation |
| $\theta_{rd}$ | Plastic rotation capacity |
| $\lambda$ | Shear slenderness |
| $\mu$ | Modification factor |
| $\nu$ | Poisson's ratio |
| $\tau$ | Shear stress |

| | |
|---|---|
| $\phi$ | Reinforcement bar diameter |
| $\chi$ | Curvature |
| $\chi_{pl}$ | Plastic curvature |
| $\chi_u$ | Ultimate curvature |
| $\chi_y$ | Yield curvature |

# 1 Introduction

## 1.1 Background

Finite element (FE) softwares have become an important part in structural design today. FE analyses enable the designer to describe the behaviour of the studied structure in detail which makes it possible to capture a reasonable approximation of the structural response. Modelling of slabs in bending are normally performed using FE models based on shell elements. This way of modelling gives a response that represents the true response to a great extent for linear elastic analyses. However, for reinforced concrete slabs that experience a nonlinear response after cracking, problems may arise when modelling with shell elements. Using shell elements in describing the nonlinear behaviour of reinforced concrete slabs can be complex and time consuming. The method is also restricted in terms of input variables and may convey numerical issues.

Alternative modelling approaches of the nonlinear response in slabs exist though. Using simplified plastic material models combined with equivalent material data to approximate the correct response of reinforced cracked concrete in one way to do so. This can be done using shell elements with a plastic material model. However, the possibility to combine different responses in different directions in such a model is limited. Therefore, another method is to simulate the slab using a beam grillage, i.e. a grid of orthogonally placed beams. Material properties of the beam elements, describing the nonlinear response, are defined to correspond to the response of the concrete slab. Every beam element can be given specific properties, thus it is possible to describe different behaviour in different parts of the structure. In other words, for reinforced concrete slabs which often require varying amount of reinforcement in different sections, usage of a beam grillage model could be beneficial.

This type of modelling has successfully been used for nonlinear analyses of reinforced concrete beams, e.g. in Lim (2013) but a clean transition of this knowledge into slabs has been problematic.

In three Master Theses carried out by Lim (2013), Lindelöf and Walhelm (2014) and Andersson and Antonsson (2015) the usage of beam grillage models for reinforced concrete slabs in the commercial FE software ADINA has shown inconsistency. The main reason for this disturbance is believed to be related to the difference in behaviour between a beam and a plate with regard to torsion. However, successful linear elastic analyses with beam grillage models have been performed but the accuracy of the results is highly dependent on the mesh size.

## 1.2 Aim and objectives

The aim of this Thesis was to investigate the possibility to use simplified methods to simulate the linear elastic and nonlinear response in reinforced concrete slabs. The intention was to analyse how beam grillages modelled in the FE software ADINA behave in comparison with shell element models and experimental tests. The main focus in the comparison was to examine how the torsional stiffness of single beam elements should be defined in order to correctly describe the behaviour of a slab.

## 1.3    Method

First, a general literature study was performed to get an overview of the subject. Earlier research of the same topic was studied to understand the encountered problems with the usage of a beam grillage model.

The main task was then to make a comparison between experiments and FE modelling using shell and beam grillage models. The commercial FE software used for the analyses was the student version of ADINA, version 9.1. As a first step, linear elastic FE analyses were made. The main investigation was how the torsional stiffness in an uncracked slab should be defined for beam grillages and why the mesh dependency problem in previous Theses has occurred. Shell element models were compiled to act as a reference for the true solution. In addition, two different modelling techniques of beam grillages were tested and compared.

When an accurate linear elastic beam grillage model had been established the next step was to use moment-curvature and torsion-twist relations to make the model viable for non-linear analyses. Results from experimentally tested slabs represented the true nonlinear response. In addition, models using shell elements were also compiled in order to compare the two different modelling methods.

## 1.4    Limitations

Due to the short timeframe the analyses were limited to certain boundary conditions and load applications. The static response was investigated and dynamic effects were disregarded. Since the student version of ADINA was limited to 900 nodes all FE models were adapted accordingly.

# 2 Characteristics of reinforced concrete

## 2.1 Response of reinforced concrete

The material response of concrete and reinforcing steel is often described with stress-strain curves as in Figure 2.1.
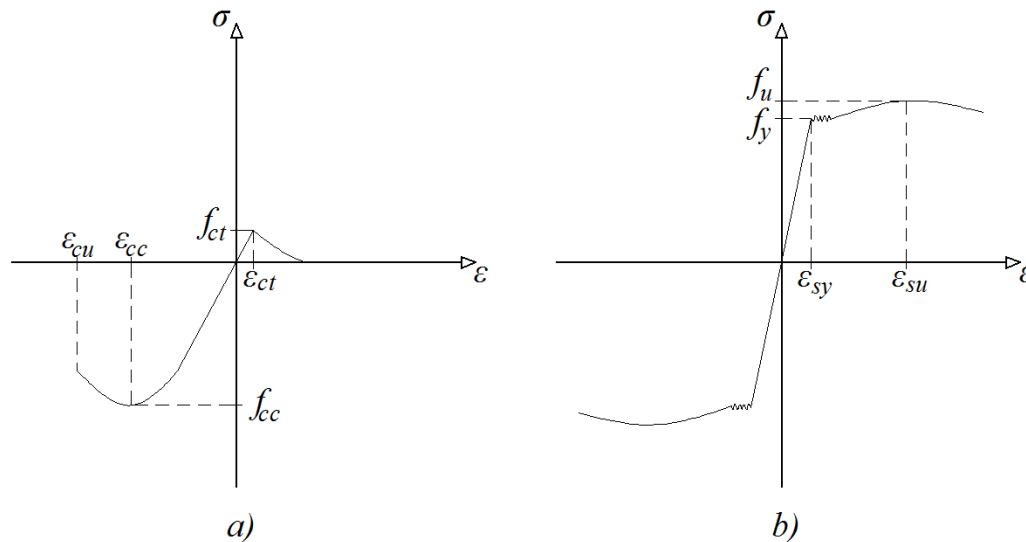


*Figure 2.1   Typical stress-strain relationships for a) plain concrete, b) hot-rolled steel.*

A normal relation for hardened concrete is that the compressive strength $f_{cc}$ of the material is far greater than the tensile strength $f_{ct}$. As a rule of thumb the tensile strength is approximately 10% of the compressive strength. With this relation in mind tensile stresses can induce cracking in concrete structures at low load levels. To determine strength parameters standardised experimental tests are performed. From the tests, strength classes of concrete can be determined and their corresponding stress-strain relations. For further information about strength classes and material characteristics of concrete the reader is referred to Eurocode 2, CEN (2004).

To avoid having the low tensile strength of concrete as a limitation for the load bearing capacity of a structure, reinforcement is normally added. The reinforcement is activated after cracking and is therefore focused to tensile zones of the structure. Steel is commonly used as reinforcing material and able to transfer tensile forces after cracking. The composite section of concrete and steel normally obtain a significantly higher load bearing capacity than a plain concrete section. Furthermore, a significantly more predictable and redundant response of the structure is ensured since the load bearing capacity of the structure is kept intact by the reinforcing steel after cracking.

Reinforcing steel is normally defined by having a stress limit known as the yield stress, $f_y$. The stress-strain relation of steel is linear until the yield stress is reached. After yielding the material starts to behave in a plastic manner. The manufacturing process of the steel is an important factor for the behavior after yielding. Hot-rolled

steel denoted as class B and class C has a pronounced yield plateau which cold worked steel denoted as class A has not. All reinforcement classes have a strain hardening effect after yielding. The effect of strain hardening further increases the load bearing capacity and normally gives a larger contribution to class B and class C steel. For further information about steel classes and their strength parameters the reader is referred to Eurocode 2, CEN (2004).

As can be seen in Figure 2.1 concrete exhibits a non-linear stress-strain relation from the start while steel has a more defined elastic-plastic behavior.

## 2.2    Response of beams in bending

Local- and global response are two terms that are often used in the discussion of the structural response of reinforced concrete beams. The local response is the response of the beam cross-section in a single point or, when in the cracked stage, a small region. It is described by the relationship between the bending moment and the average curvature in that specific point or region. When adding all regional responses together the global response of the beam is obtained.

The curvature, $\chi$, of a cross-section corresponds to the inclination of the local deformation, i.e. strain $\varepsilon$, as can be seen in Figure 2.2 and equation (2-1).
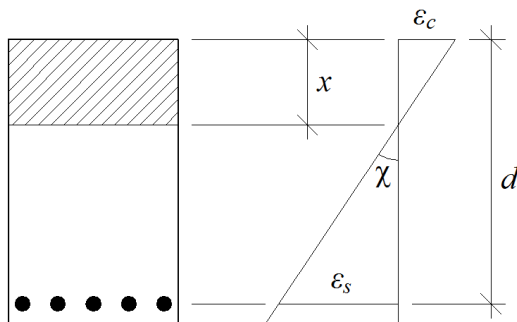


*Figure 2.2     Curvature-deformation relationship.*

$$\chi = \frac{1}{r} = \frac{\varepsilon_s - \varepsilon_c}{d} \tag{2-1}$$

Where:          $\chi =$      Curvature
                 $r =$      Radius of curvature
                 $\varepsilon_s =$      Steel strain
                 $\varepsilon_c =$      Concrete strain
                 $d =$      Effective depth of cross-section

The structural response of a beam cross-section can be divided into three distinct stages; the uncracked stage (State I), the cracked stage (State II) and the ultimate stage (State III). The three stages are illustrated in a moment-curvature graph in Figure 2.3.

*Figure 2.3    Moment-curvature relationship of a reinforced concrete member loaded until failure.*

The response for sections in State II and State III is clearly non-linear but can be simplified to linear relationships. These can be combined in a multiple linear relationship as shown in Figure 2.4. The simplified model can be used as input data in finite element analyses in order to describe the non-linear behaviour of reinforced concrete.
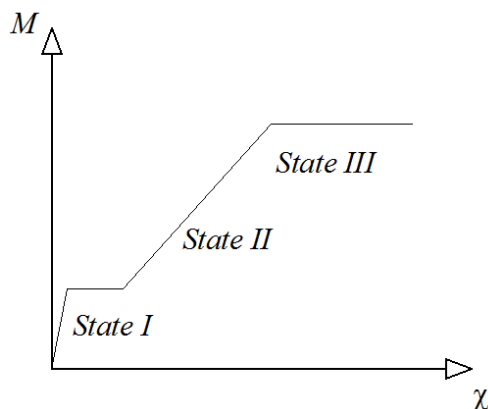


*Figure 2.4    Simplified moment-curvature relationship of a reinforced concrete member loaded until failure.*

## 2.2.1    Uncracked stage (State I)

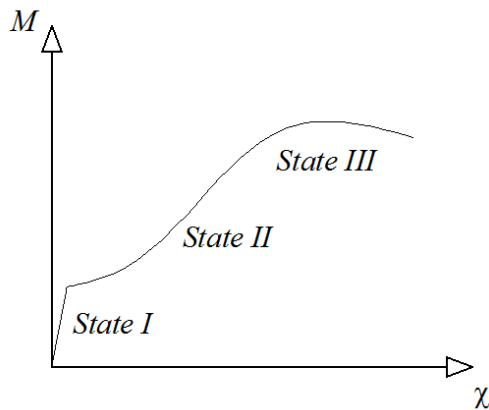In State I the whole beam is still uncracked and the cross-section has a linear response, i.e. the curvature increases linearly with the applied bending moment. The linear response is also reflected in the global response. The influence of the reinforcement with respect to stiffness of the uncracked section is often considered to be small and is neglected. However, according to Engström (2015) the stiffness can, depending on the amount of reinforcement, be increased with more than 20% if the reinforcement is included.

The moment-curvature relationship for a cross-section in State I is expressed in equation (2-2) and is illustrated in Figure 2.5.

$$\chi_I = \frac{M}{E_c I_I} \tag{2-2}$$

Where:  $M =$  Moment
$E_c =$  Young's modulus for concrete
$I_I =$  Moment of inertia for a State I cross-section



*Figure 2.5    Moment-curvature relationship for State I.*

## 2.2.2    Cracked stage (State II)

As long as the concrete stress is lower than the tensile strength of the concrete, $f_{ct}$, the section is assumed to be uncracked. However, if the stress in the outermost fiber of the cross-section reaches $f_{ct}$ the section starts to crack, and State II is initiated.

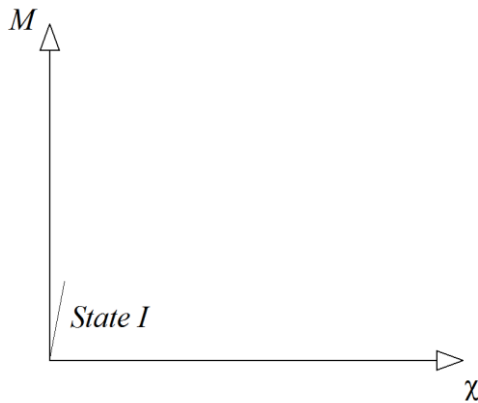When a crack appears the stiffness of that section decreases significantly and there will be a distinct change in the regional response, which can be seen in Figure 2.3. The State II model assumes the beam to be fully cracked immediately after $f_{ct}$ is reached, but that is not true in reality. The cracks emerge with a certain distance and the stiffness of the uncracked parts in between the cracks is contributing to the overall stiffness of the beam. This effect is called tension stiffening and it causes an underestimation of the stiffness in State II. The effect is largest just after the cracking load is reached and decreases with increasing load.

It can also be noted that the calculation model used for State II has limitations and can according to Engström (2015) only be used for steel stresses up to $f_y$ and compressive concrete stresses lower than half of $f_{cc}$. This is due to the assumption in the model that both concrete and steel have a linear elastic material response. For higher stresses, a State III model which allows for non-linear material response is preferable.

The moment-curvature relationship for a cross-section in State II is described with equation (2-3) and is illustrated in Figure 2.6.

$$\chi_{II} = \frac{M}{E_c I_{II}} \tag{2-3}$$

Where:  $I_{II} =$  Moment of inertia for a State II cross-section
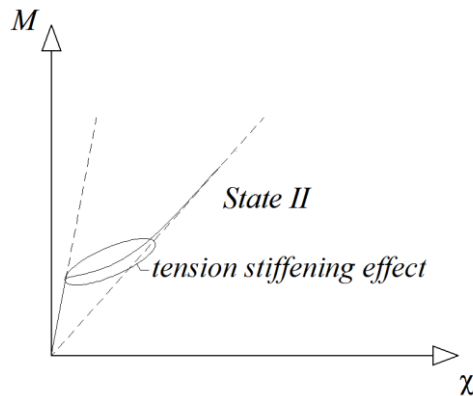
*Figure 2.6      Moment-curvature relationship for State II.*

### 2.2.3    Ultimate stage (State III)

The ultimate stage (State III) is initiated when either of the material obtains a nonlinear behaviour, i.e. the steel stress reaches the yield strength or the concrete stress exceeds half of the compressive strength. However, the ultimate capacity of the beam is not reached yet and the load can still be increased slightly. The increase of load is possible due to effects such as plastic redistribution in the concrete and strain hardening of the tensile reinforcement. When the ultimate moment capacity is reached, the moment-curvature relationship can be described with a straight line where the curvature increases without an increase in load.

The moment-curvature relationship for a cross-section in State III is illustrated in Figure 2.7.



*Figure 2.7      Moment-curvature relationship for State III.*

### 2.2.4    Plastic rotation capacity

The collapse of a reinforced concrete beam can either be due to global or local failure. Global failure is only possible if the structure has sufficient plastic rotation capacity. If this capacity is insufficient, local failure such as crushing of concrete and reinforcement rip off is prone to dominate the collapse of the structure.

According to Engström (2015) the plastic rotation capacity is evaluated based on the assumption that plastic hinges are form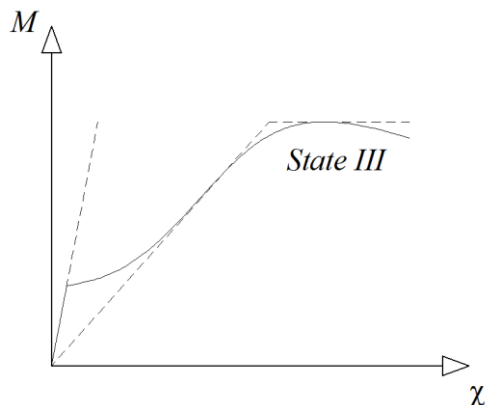ed at certain sections and do not transmit along the member. The rotation of the concentrated hinges when the load is increased from the start of yielding until collapse is denoted as plastic rotation capacity. For all sections between the plastic hinges formed, the reinforcement is assumed to behave linear elastically. Plastic hinges can be single or double depending on the support and boundary conditions of the structure. A fixed end support tends to form a single hinge whilst the span and continuous supports form double hinges. Figure 2.8 exemplifies the formation of single and double hinges.
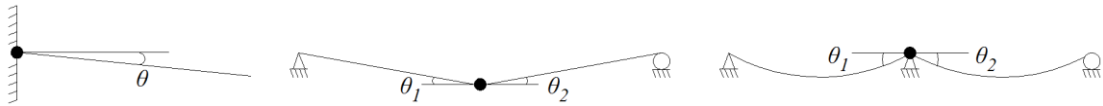


*Figure 2.8    Formation of single and double plastic hinges in different regions.*

The assumption that a plastic hinge is locked to a certain section is not true in reality. Plastic hinges in real structures have a tendency to transmit a certain distance along the member. The propagation length of plastic hinges is denoted as $l_{pl}$ where the tensile steel strain exceeds the yield strain, see Figure 2.9.

Double plastic hinges are influenced from the curvature distribution at each side of the hinge. The sum of the lengths $l_{pl1}$ and $l_{pl2}$ corresponds to the total length of the plastic region $l_{pl}$. The total rotation $\theta_{pl}$ is in analogy the sum of the two rotations $\theta_{pl1}$ and $\theta_{pl2}$, see Figure 2.9.
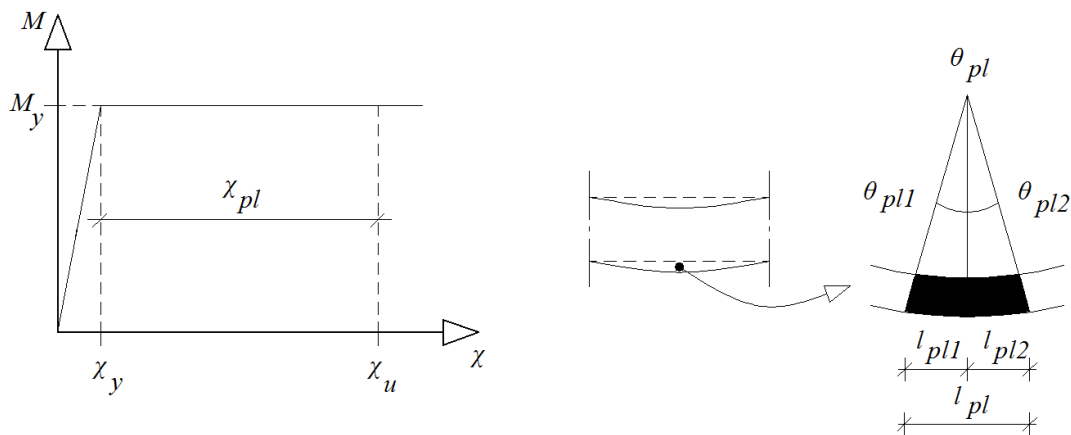


*Figure 2.9    Plastic curvature, plastic rotation and corresponding length of plastic region of a double plastic hinge.*

Integration of the plastic curvature over the propagation length yields the plastic rotation as in equation (2-4).

$$\theta_{pl} = \int_{lpl} (\chi - \chi_y)dx \qquad (2\text{-}4)$$

Where:         $\theta_{pl} =$   Plastic rotation

$$\chi = \quad \text{Total curvature}$$
$$\chi_y = \quad \text{Yield curvature}$$
$$l_{pl} = \quad \text{Length of plastic region}$$

Eurocode 2, CEN (2004), offers a simplified way to estimate the plastic rotation capacity. The diagram shown in Figure 2.10 is available in Eurocode and applicable for reinforced concrete members with shear slenderness, $\lambda$, equal to 3. The curves in the diagram are based on different concrete strength classes, ductility class of the reinforcing steel and the $x_u/d$ ratio of the section. As can be seen in Figure 2.10, the design value of the plastic rotation $\theta_{pl,d}$ increases with increasing $x_u/d$ ratio until a certain peak value is reached. After $\theta_{pl,d}$ has reached its maximum value it decreases if the $x_u/d$ ratio is increased further. The reason for the change of behavior is dependent on which material strain that is limiting the rotational capacity. At low $x_u/d$ ratio the ultimate strain of the reinforcement $\varepsilon_{su}$ is governing. At higher $x_u/d$ ratio the ultimate strain of the concrete $\varepsilon_{cu}$ limits the rotation capacity.
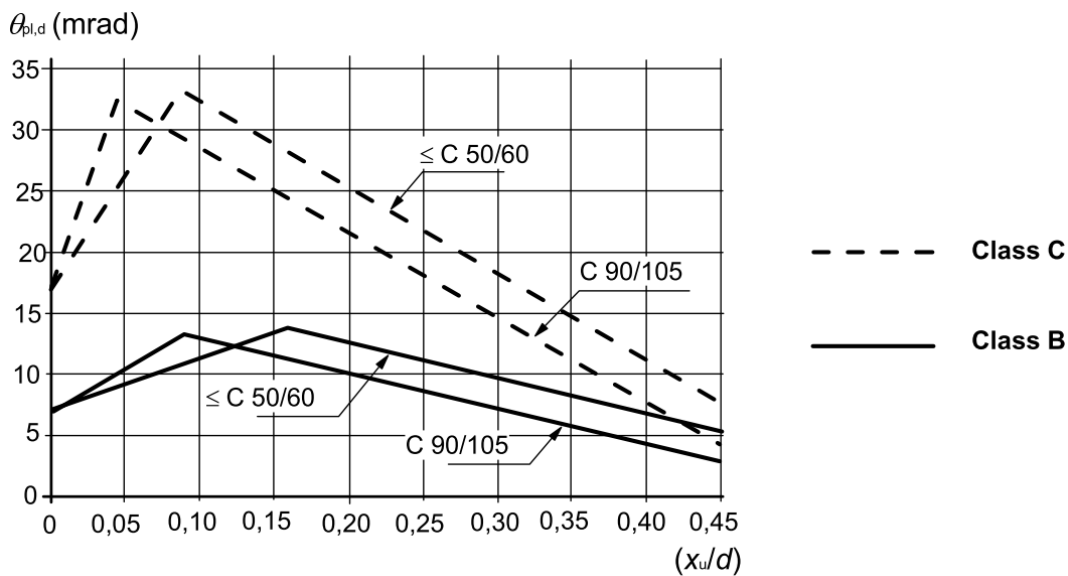


*Figure 2.10    Plastic rotation capacity according to Eurocode 2 (2005) for members with shear slenderness $\lambda = 3$.*

If the shear slenderness of the member $\lambda \neq 3$ Eurocode proposes the use of a correction factor to multiply with the values obtained from Figure 2.10. According to Eurocode 2, CEN (2004) the plastic rotational capacity can be calculated as in equation (2-5).

$$\theta_{rd} = k_\lambda \theta_{pl,d} \tag{2-5}$$

Where:     $k_\lambda = \quad$ Correction factor for $\lambda \neq 3$
           $\theta_{pl,d} =$ Design value of plastic rotation according to Figure 2.10

The correction factor $k_\lambda$ can be calculated from equation (2-6).

$$k_\lambda = \sqrt{\frac{\lambda}{3}} \qquad\qquad (2\text{-}6)$$

Where:  $\lambda =$  Shear slenderness

The shear slenderness can be calculated from equation (2-7) or estimated by a simplification as in equation (2-8).

$$\lambda = \frac{x_0}{d} \qquad\qquad (2\text{-}7)$$

Where:  $x_0 =$  Distance between the maximum moment section and the adjacent zero moment section after plastic redistribution

$d =$  Effective depth of cross-section

$$\lambda = \frac{M_{Ed}}{V_{Ed}d} \qquad\qquad (2\text{-}8)$$

Where:  $M_{Ed} =$ Design value of bending moment

$V_{Ed} =$  Design value of shear force

## 2.3 Response of slabs in bending

### 2.3.1 Definition of slabs

Concrete slabs and their response is the scope of this Thesis and therefore some definitions are needed. Eurocode 2, CEN (2004), defines slabs as structural members where the minimum of the width or length dimension is not less than 5 times the thickness of the member. According to Engström (2014) slabs can be categorized into two main groups; flat slabs and slabs. A slab is denoted as a flat slab if at least one of the supports is a column. Slabs with other support conditions such as line-supports or edge supports, are just referred to as slabs. Figure 2.11 shows examples of a flat slab and a slab.



*a)*           *b)*
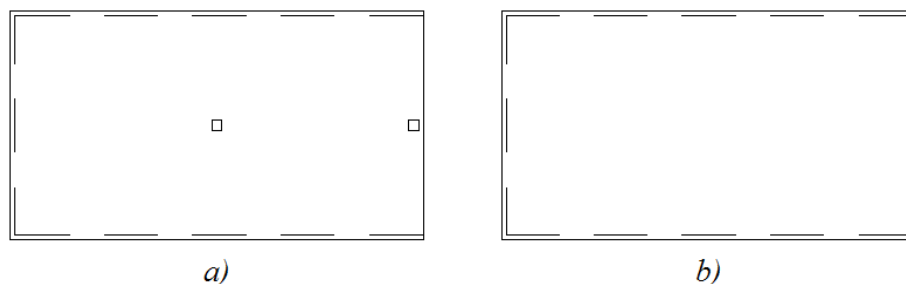
*Figure 2.11    Illustration of a) flat slab, b) slab.*

A slab can carry load in alternative ways depending on support and loading conditions. If only two opposite supports are present, the load is carried in one direction and it is therefore referred to as a one-way slab. If instead a rectangular slab is supported along its four edges it carries load in two main directions perpendicular

to each other and is then denoted as a two-way slab. Figure 2.12 illustrates the difference between a one way slab and two-way slab.
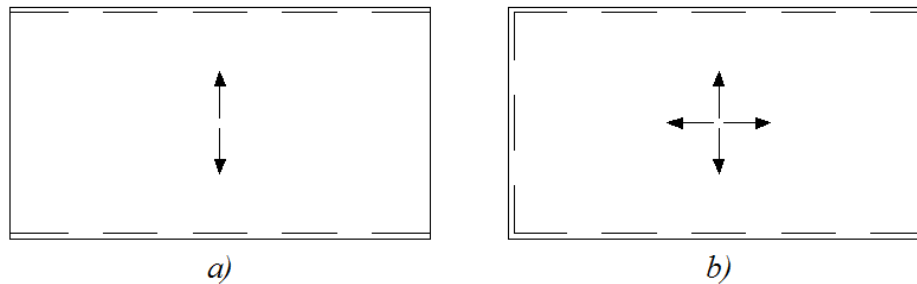


*Figure 2.12    Load carrying in a) one-way slab, b) two-way slab.*

## 2.3.2    Definition of sectional forces

In Engström (2014) the sectional forces in a slab is defined as the sectional force per unit width of 1.0 meter and as concentrated forces. In this Thesis the same approach was used, lower case letters represent sectional forces per unit width, while upper case letters are used to define concentrated sectional forces. To clarify these notations an example is explained in terms of bending moment. The capital letter $M$ was used for concentrated moments with the unit [Nm]. The lower case letter $m$ was used for bending moments per unit width [Nm/m].

Since slabs normally experience bending moments in multiple directions it is convenient to have a coordinate system that relates a certain moment with a specific direction. The coordinate system used in this Thesis was defined by the two main directions of the slab as an x-y system. The coordinate system and the notations for bending moments are shown in Figure 2.13.



*Figure 2.13    Bending moments and coordinate axes.*

Calculation of sectional forces per unit width is in general a statically indeterminate problem for slabs. The task is to find a combination of bending moments $m_x$ and $m_y$ with torsional moments $m_{xy}$ and $m_{yx}$ that fullfills equilibrium conditions with the applied load. According to Engström (2014) reinforced concrete have a plastic

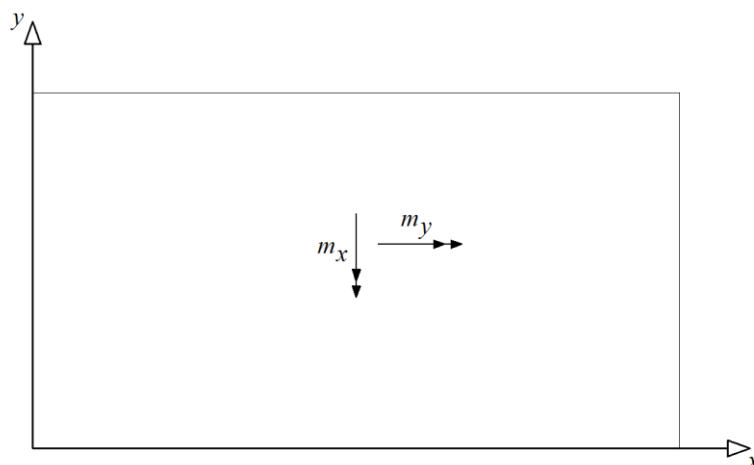response in the ultimate state. Due to the plastic response in the ultimate state, where the moment capacity is determined by reinforcement amount, theory of plasticity can be applied. According to theory of plasticity any moment distribution that fulfills equilibrium can be used in design and will be reached in the ultimate limit state. This means that the designer can choose the moment distribution and control the behavior of the slab by means of reinforcement arrangement.

According to Eurocode 2, CEN (2004), four different ways of determining sectional forces to be used in design exist. The distribution can be distinguished according to:

- Linear elastic analysis
- Linear elastic analysis with limited redistribution
- Plastic analysis
- Non-linear analysis

In this Thesis analytical design approaches will be made based on plastic analysis and used to verify finite element models. For description of the analytical tools that are used the reader is referred to Section 2.3.4 and 2.3.5.

### 2.3.3 Bending of reinforced concrete slabs

The structural behaviour of reinforced concrete slabs is to a high degree based on the sectional response in bending. The sectional response can be defined in terms of the relationship between bending moment, $m$, and curvature, $\chi$. As can be seen in Figure 2.14a, a linear relationship can be distinguished at load levels below the cracking moment, $m_{cr}$. When cracking starts the linear relation no longer holds true and a pronounced non-linear behaviour takes place until the provided reinforcement reach yielding. At yielding a more or less plastic behaviour takes place where the curvature increases without significant increase of the applied moment. Figure 2.14b and c) illustrates the assumed moment-curvature relations used for linear- and plastic analysis, respectively. As can be seen in Figure 2.14, linear analysis agrees well with the true response prior to cracking whilst plastic analysis describes yielding of reinforcement to a certain degree.
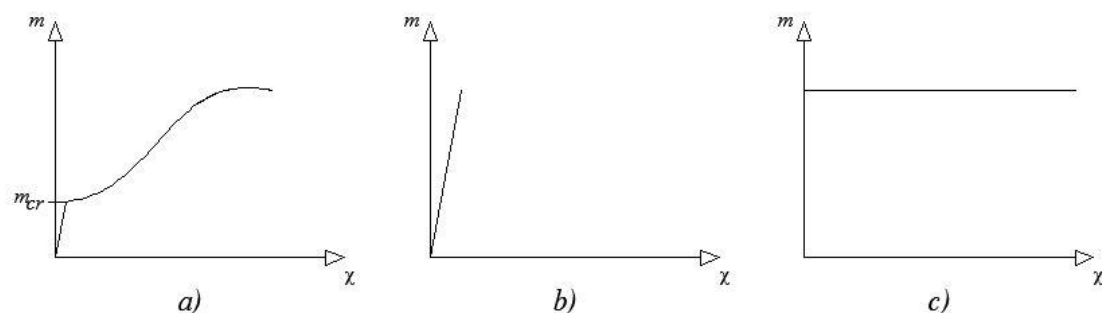


*Figure 2.14   Moment-curvature relations for a) true response, b) linear elastic response, c) plastic response.*

Since the moment-curvature relation has a nonlinear variation it is of interest to study the behaviour of a slab loaded until failure. According to Engström (2014) four main

stages can be distinguished and are referred to as uncracked state (State I), cracked state (State II), ultimate state (State III) and ultimate limit state (collapse).

State I, State II and State III is based on the same theory as is defined in Section 2.2.1 - 2.2.3, i.e. the same behaviour as is described for beams can be directly applied to slabs. The difference for a slab is that reinforcement is usually placed in two main directions whereas there is only one main direction in a beam. Thus, a slightly different response in the ultimate limit state is acquired in a slab.

The ultimate state starts when yielding of a reinforcement bar somewhere in the slab takes place. At yielding a section is utilised to its maximum capacity hence the moment in yielding sections cannot increase further. However, yielding of a section does not lead to collapse of the slab since other sections still provide capacity. If the load is increased further the moment in yielding sections remain constant whilst it increases in other sections through plastic redistribution. The plastic redistribution continues in a complex and nonlinear manner until enough sections yield to form a collapse mechanism.

The ultimate limit state is reached at the end of the ultimate state when the load can be increased no further and yielding sections form a collapse mechanism. When the collapse mechanism is formed the slab deforms under a constant load and portions of the slab rotate as rigid bodies. Since reinforcement arrangements determine the capacity of sections in the ultimate limit state, theory of plasticity is commonly used in design.

### 2.3.4    The strip method

The strip method is a design method based on theory of plasticity. It is a lower bound solution meaning that conservative results are obtained. According to Engström (2014) the general rules for the strip method can be stated as:

- In all elements on the slab the torsional moments are chosen
  $m_{xy} = -m_{yx} = 0$.
- The slab is divided in strips in the main directions x and y.
- The load on an element is distributed between the two strips in x- and y-directions.
- Each strip is designed for one-way action.

The designer is free to choose any moment distribution that fulfils equilibrium and that moment distribution will be obtained in the ultimate limit state. The load on each small element can be divided in any way between two strips in x- and y-direction. However, equilibrium conditions apply meaning that the sum of the load carried by each strip should be equal to the total load.

The equilibrium equation is stated in equation (2-9).

$$q = q_x + q_y \qquad\qquad\qquad (2\text{-}9)$$

Where:        $q =$    Total load on a slab element

$$q_x = \text{Load carried by strip in x-direction}$$
$$q_y = \text{Load carried by strip in y-direction}$$

An important consideration is that the load distribution highly influences the reinforcement arrangement in the ultimate limit state. For recommendations how a reasonable load distribution is estimated the reader is referred to Engström (2014).

### 2.3.5 Yield line method

The yield line method is a kinematic method for plastic analysis of reinforced concrete slabs. The principle is that the designer assumes a pattern of yield lines which forms a possible failure mechanism. Since the true failure mechanism will be as efficient as possible in terms of energy required, the designer has to test several failure mechanisms to find the one that generates the lowest collapse load. Since the true failure mechanism can be complex and there are no guarantees that the real failure mode has been found, the yield line method is an upper bound solution. The acquired results are not on the safe side and the method is therefore not recommended in design.

## 2.4 Shear

### 2.4.1 Shear stress in beams

Shear stresses in beams are defined as the vertical stresses along the length of a beam caused by the acting shear force. Shear stresses can cause shear cracks, shear failure and shear deformations in the structures.

The shear stress distribution for a beam cross-section can be expressed by Zhuravskii's shear stress formula, equation (2-10).

$$\tau(z) = \frac{S(z) \cdot V}{I \cdot w(z)} \tag{2-10}$$

Where:
$$\tau(z) = \text{Shear stress}$$
$$S(z) = \text{First moment of area}$$
$$V = \text{Shear force}$$
$$w(z) = \text{Width of the beam cross-section}$$

Figure 2.15 illustrates the real shear stress distribution for rectangular cross-sections. The parabolic shape is however, according to Al-Emrani *et al.* (2011), normally simplified to a rectangular shape with an equally distributed stress over the cross-section defined as two thirds of the maximum stress.
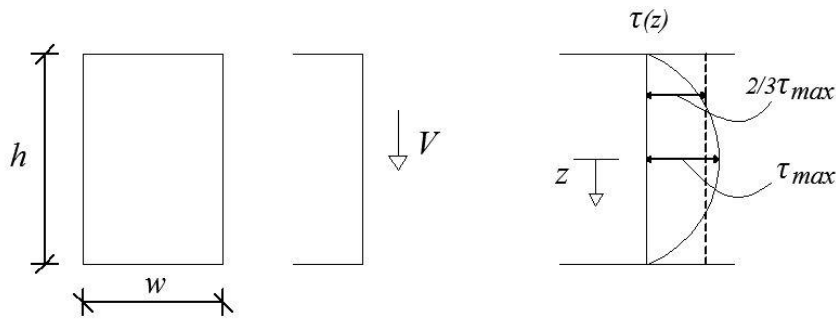
*Figure 2.15    Shear stress distribution based on equation (2-10) for a rectangular cross-section.*

For a rectangular cross-section as in Figure 2.15 the maximum shear stress can be calculated using equation (2-10). Equation (2-11) presents the derivation of the expression.

$$\tau_{max} = \tau(z = 0) = \frac{S(z) \cdot V}{I \cdot w(z)} = \frac{\frac{wh}{2}\frac{h}{4}V}{\frac{wh^3}{12}w} = \frac{3}{2}\frac{V}{wh}$$

(2-11)

Where:     $h =$     Height of the beam cross-section
           $w =$     Width of the beam cross-section

## 2.4.2    Shear deformations

Shear stresses give rise to shear deformations due to a sliding action occurring on a plane normal to the axis of the beam, see Figure 2.16. Shear deformations are normally disregarded in analytical calculations due to it being a rather small portion of the total deflection for beams subjected to bending action. However, if the beams are short and thick, shear deformations may contribute as a large percentage of the total deformation due to the small bending deformations in such beams.
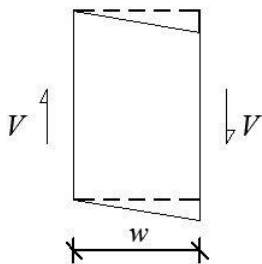


*Figure 2.16    Sliding action due to shear deformation.*

The shear deformation of a beam segment with rectangular cross-section subjected to a constant internal shear force can according to Blake (1985) be calculated as in equation (2-12).

$$\delta_s = \frac{VL}{\frac{5}{6}AG}$$

(2-12)

Where:
- $V =$ Shear force
- $L =$ Length of beam segment
- $A =$ Area of cross-section
- $G =$ Shear modulus

The coefficient 5/6 is used to calculate the equivalent shear area based on the shape of the cross-section and is applicable to rectangular cross-sections.

## 2.5 Torsion

### 2.5.1 Torsion of beams

Torsion of a beam can be expressed as a relation between the applied torsional moment and the corresponding angle of twist. The applied torsional moment leads to twisting of the cross-section and possibly also warping. The torsional moment can be divided in two parts; St. Venant's torsion, $T_{sv}$, and Vlasov's torsion, $T_w$. In the theory of St. Venant's torsion, also called pure torsion, the applied torque is resisted entirely by torsional shear stresses. However, if the torque is resisted by warping moment the theory of Vlasov's torsion, i.e. warping torsion, is applied.

Circular cross-sections are solely subjected to St. Venant's torsion, see Figure 2.17. For solid and closed thin-walled cross-sections both St. Venant's and Vlasov's torsion are present, but the St. Venant's torsion is dominating. The influence of Vlasov's torsion can therefore be neglected for such cases. On the contrary Vlasov's torsion is dominating for open cross-sections. St. Venant's torsional moment can be expressed with equation (2-13).

$$T_{sv} = K_v G \frac{d\theta}{dx}$$

(2-13)

Where:
- $T_{sv} =$ St. Venant's torsional moment
- $K_v =$ Torsional stiffness
- $G =$ Shear modulus
- $\theta =$ Angle of twist
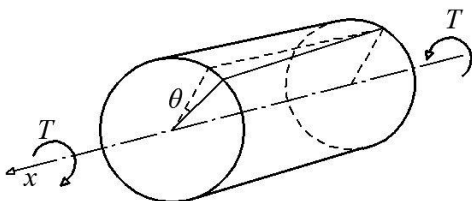- $x =$ Direction along axis of the member



*Figure 2.17   Circular cross-section subjected to St. Venant's torsion.*

The torsional stiffness for a circular cross-section is equal to the polar moment of inertia, equation (2-14).

$$K_v = I_p \qquad (2\text{-}14)$$

Where: $I_p =$ Polar moment of inertia

A common simplification when deriving the torsional moment for non-circular cross-sections is to make the assumption that plane cross-sections remain plane. However, this generalisation leads to a slightly overestimated torsional stiffness of non-circular cross-sections. This can be considered by multiplying the stiffness of the cross-section with a correction factor, $\beta$. The torsional stiffness of a rectangular cross-section can be calculated according to equation (2-15).

$$K_v = \beta b a^3 \qquad (2\text{-}15)$$

Where:
$K_v =$ Torsional stiffness of a rectangular cross-section
$\beta =$ Correction factor depending of height to width ratio
$a =$ Shorter side of cross-section
$b =$ Longer side of cross-section

Values of the correction factor, $\beta$, for cross-sections with different height to width ratios can be found in Table 2.1.

*Table 2.1 Values for correction factor $\beta$ for different $b/a$ ratios for rectangular cross-sections according to Dahlblom and Olsson (2010).*

| $b/a$ | 1.0 | 1.2 | 1.5 | 2.0 | 2.5 | 3.0 | 4.0 | 5.0 | 10.0 | $\infty$ |
|-------|-----|-----|-----|-----|-----|-----|-----|-----|------|----------|
| $\beta$ | 0.141 | 0.166 | 0.196 | 0.229 | 0.249 | 0.263 | 0.281 | 0.291 | 0.312 | 0.333 |

## 2.5.2 Torsion of slabs

In structural engineering, the expression slab is frequently used. However, a more general way to describe this type of element is to use the term plate. Hence, in this section the term plate is used for derivations.

The torsional response of a plate deviates from beams due to the large width to height ratio of the cross-section. Thus, also a beam grillage model compared to a shell element model will have different response. Figure 2.18 describes a plate element loaded by torsional moments $T$.
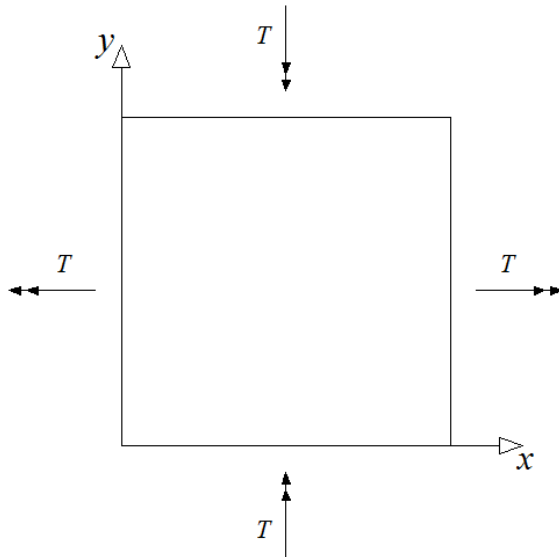
*Figure 2.18    Plate element subjected to torsional moment T.*

For linear elastic response the torsional moment $T$ can be calculated according to equation (2-16).

$$T = D(1 - v)\frac{\partial^2 w}{\partial x \partial y}$$

(2-16)

Where:          $T =$     Torsional moment acting on plate element
                $D =$     Plate stiffness
                $v =$     Poisson´s ratio
                $\frac{\partial^2 w}{\partial x \partial y} =$ Curvature

The plate stiffness $D$ can be calculated as in equation (2-17).

$$D = \frac{EI}{1 - v^2}$$

(2-17)

Where:          $E =$     Young´s modulus
                $I =$     Moment of inertia

For derivation of equation (2-16) the reader is referred to Hallbjörn (2015).

### 2.5.3    Torsion in cracked concrete

From equation (2-15) it can be seen that the geometry of the cross-section is the governing factor for the torsional stiffness of a beam. This expression holds true in linear elastic analyses but as soon as cracks appear the torsional stiffness changes. Calculation of the torsional stiffness for reinforced concrete in State II is a complex problem and propositions in the literature exist on how the stiffness should be estimated.

According to BBK 04, Boverket (2004), the torsional stiffness in State II can be estimated depending on the mode of cracking that is present. If cracking occurs due to bending, 30% of the State I stiffness can be accounted for whilst only 10% can be used in case of shear or torsional cracks. These recommendations are given as guidelines for beams; no recommendations are presented for slabs.

The design guidelines stated in Eurocode does not describe how the loss of torsional stiffness due to cracking should be estimated for any structural members.

# 3 FE modelling

## 3.1 Orientation

The FE analyses in this Thesis were made using the student version of the finite element software ADINA, ADINA (2014). The student version has the same functions as the original version but is limited to a number of 900 nodes. A reinforced concrete slab can be modelled in many different ways and it is possible to choose between several element types which describe the structural behaviour of the slab in different ways. In this Thesis both shell and beam elements were used.

## 3.2 Shell element model

Shell elements belong to the group of structural elements, which mean that they have both transversal and rotational degrees of freedom (DOF), and it is possible to study both sectional forces and moments. A shell element has three transversal and two rotational DOFs, see Figure 3.1.
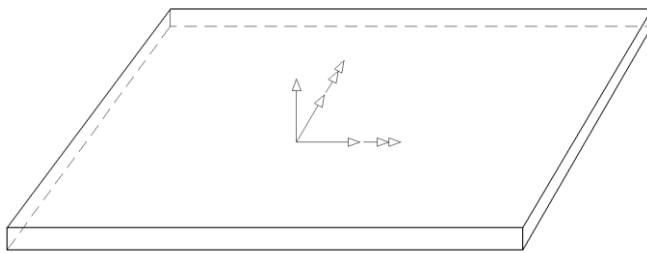


*Figure 3.1    Degrees of freedom in a shell element.*

In ADINA a shell element can be made with 4-32 nodes and with varying thickness. Depending on what is studied, the number of nodes and how they are placed (i.e. midsurface or top/bottom) must be chosen accordingly. Example of shell elements can be seen in Figure 3.2.



*Figure 3.2    Example of shell elements a) midsurface nodes b) top and bottom nodes.*

The program ADINA is treating a shell element as a 3D continuum element but with two assumptions from the Timoshenko beam theory and the Reissner/Mindlin plate theory:

- Material particles that originally lie on a straight line normal to the midsurface of the structure remain on that straight line during the deformations.
- The stress in the direction normal to the midsurface of the structure is zero.

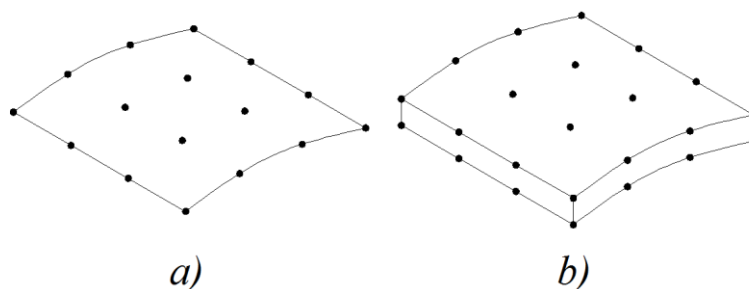By defining the shell elements using Timoshenko beam theory and the Reissner/Mindlin plate theory, the influence of shear deformations is regarded.

Using shell elements is a common way to model reinforced concrete slabs but special attention needs to be paid at concentrated forces and supports. A slab supported on columns and/or subjected to concentrated forces modelled in single nodes give rise to singularities. Sectional forces and moments in these points are tending to infinity. According to Pacoste *et al.* (2012) the reasons why these problems occur are due to simplifications in the geometrical modelling and the modelling of the mechanical properties of the material. However, the problem can be handled either by refining the modelling of the supports or by simply using the results from sections contiguous to the singularity points.

In a 3D analysis of a slab both bending and torsional moments will be computed, see Figure 3.3, and the slab must be designed to resist both these moments. The reinforcement is generally arranged in two perpendicular directions and thus the torsional moments cannot effectively be resisted. To account for the torsional moment in the design of reinforcement it is transformed to bending moment according to equation (3-1) and equation (3-2).



a)    b)
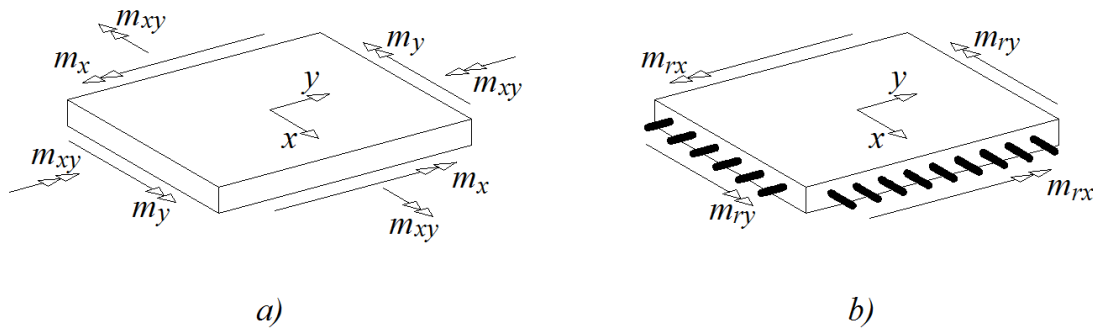
Figure 3.3    *Shell element with a) bending and torsional moments b) transformed reinforcement moment.*

$$m_{rx,pos(neg)} = m_x \pm \mu |m_{xy}| \qquad (3\text{-}1)$$

$$m_{ry,pos(neg)} = m_y \pm \frac{1}{\mu} |m_{xy}| \qquad (3\text{-}2)$$

Where:    $m_{rx}$ = Design reinforcement moment in x-direction
$m_{ry}$ = Design reinforcement moment in y-direction
$m_x$ =  Bending moment in x-direction
$m_y$ =  Bending moment in y-direction

$m_{xy}$ = Torsional moment

$\mu$ = Modification factor depending on practical considerations, usually close to 1.0

With moment directions as defined in Figure 3.3a, the indices *pos* and *neg* refer to the top and bottom reinforcement, respectively.

When using shell elements in ADINA some issues that need extra consideration occurs. First it must be noticed that using plastic material models in ADINA will lead to an increase in the moment capacity of the slab. The effect is based on that ADINA uses Von Mises plastic theory and thereby defines Poisson's ratio as $v = 0.5$ once yielding of the material is initiated, irrespective of what value is given as input, Augustsson and Härenstam (2010).

Secondly, the stress distribution in ADINA when using seven integration points over the cross-section height is described by a polynomial of order six as illustrated in Figure 3.4, Augustsson and Härenstam (2010). Such a stress-distribution is not used in analytical calculations and generates a slightly lower bending moment resistance than analytical calculations do. To compensate for the stress-distribution used in ADINA a correction factor was defined in Augustsson and Härenstam (2010) in order to achieve a correct bending moment resistance. To transform the stress calculated in ADINA to the expected one, a modified yield stress $f_{y,mod}$, calculated as in equation (3-3), can be used as input.
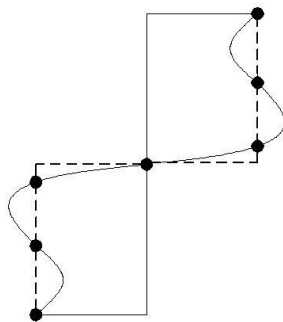


*Figure 3.4    Stress distribution when using seven integration points according to ADINA.*

$$f_{y,mod} = \frac{1}{\alpha} f_y \qquad\qquad (3\text{-}3)$$

Where:        $f_{y,mod}$ =        Modified yield stress to be inserted in ADINA
              $\alpha$ =        Correction factor
              $f_y$ =        Yield stress

In Augustsson and Härenstam (2010) there is a full derivation of the equation and the correction factor, $\alpha$. The equation holds true for homogenous rectangular cross-sections and the correction factor is calculated as $\alpha = 0.231$.

Thirdly, the application of a distributed load to a slab modelled with shell elements is easily accomplished by placing a pressure load on the whole surface. However, applying a point load to a single node may generate local deviations in the shell element model. To avoid these kinds of deviations, the point load could be applied as a pressure load over a certain amount of elements.

## 3.3    Beam grillage model

A beam grillage model is based on beam elements and is illustrated in Figure 3.5. The beam elements are placed orthogonally to each other and the model represents a simplified way of studying the structural response of a slab.
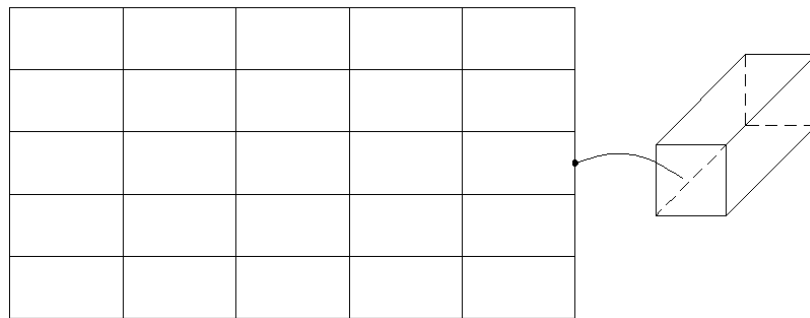
*Figure 3.5     Beam grillage model of a slab.*

Since ADINA is the finite element software that will be used, the beam elements in the models will be 2-node Hermitian beams with constant cross-section. Figure 3.6 shows a beam element with both global (X,Y,Z) and local (r,s,t) coordinate systems as defined in ADINA.
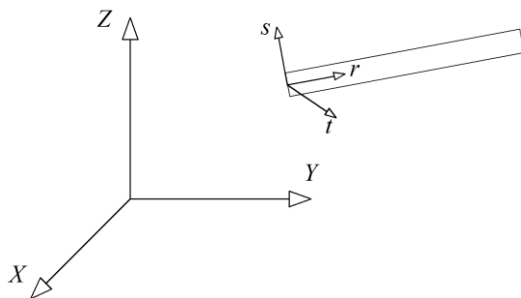
*Figure 3.6     Beam element and coordinate systems in ADINA.*

From the coordinate system presented in ADINA it can be seen that torsion will occur around the $r$-axis whilst bending will be around the $s$- and $t$-axes.

For linear elastic analyses the flexural stiffness properties of each element can be described by the cross-sectional input together with a material model. However, the torsional stiffness needs to be modelled in such a way that a realistic structural behaviour is achieved. The torsional stiffness is in general not an important factor in single beam elements, but when beam elements are combined to a grillage the torsional stiffness may have a major influence.

For nonlinear analyses ADINA offers the possibility to define simplified moment-curvature relations for each beam element. By defining the moment-curvature relations for the elements, varying stiffness properties in different directions can be modelled based on the state each element is in. Figure 3.7 clarifies beams in different states in a grillage model.



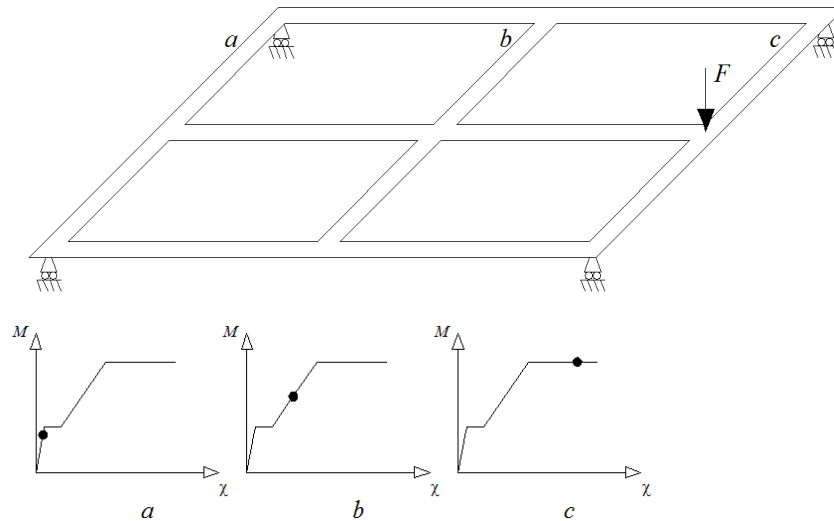*Figure 3.7    Beam grillage model where different sections have reached different levels in their moment-curvature relation.*

To model the torsional stiffness in nonlinear analyses, an approach similar to the flexural response can be used. ADINA offers the possibility to define torsional moment versus angle of twist relations for each beam element. Thus, it is possible to capture varying stiffness properties due to torsional effects in an equivalent manner as is shown for bending action in Figure 3.7.

The application of loads in a beam grillage model differs slightly from how it is done for shell element models. Since pressure loads cannot be applied to beam grillage models alternative solutions were used. For a slab subjected to an evenly distributed load, line loads with a magnitude half as large as the total load are applied to the beams in both directions. Furthermore, the application of a point load to a single node should not cause any local deviations in a beam grillage model. However, concentrated forces were divided into smaller portions acting on adjacent nodes for a smoother load application and to generate a response that is comparable with the pressure loads used in the shell element models. Figure 3.8 shows how a concentrated force can be applied in smaller portions to adjacent nodes in ADINA.
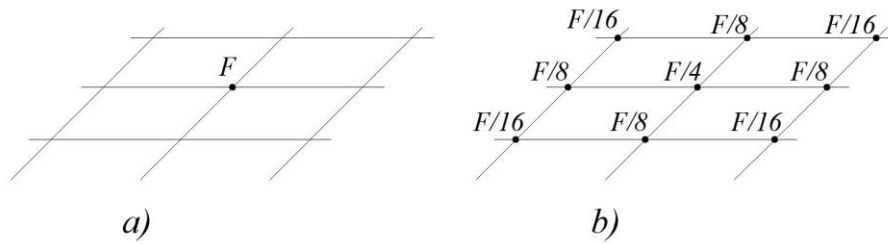
*Figure 3.8      a) point load acting in one node and b) the equivalent loading in beam grillage models in ADINA.*

## 3.4      Previous modelling choices

In Lim (2013) shell element models were compared with beam grillage models of a reinforced cantilever concrete slab. For linear elastic analyses, shell element models were used as reference for the beam grillage models. From the analyses it was concluded that the results from the beam grillage models were highly dependent on the mesh size. The term mesh size in a beam grillage model can be defined as the actual length of the beam elements which also corresponds to the centre distance between the elements, denoted $l_{el}$ in Figure 3.9. The difference between the results obtained from the shell element models and the beam grillage model were only acceptable if the mesh size was set to 0.2 meters, equal to the height of the slab, i.e. quadratic cross-sections of the beam elements yielding $l_{el}/h_{el} = 1.0$. In Section 4.5.3, Lim's cantilever slab is studied more thoroughly and compared with the models in this Thesis.
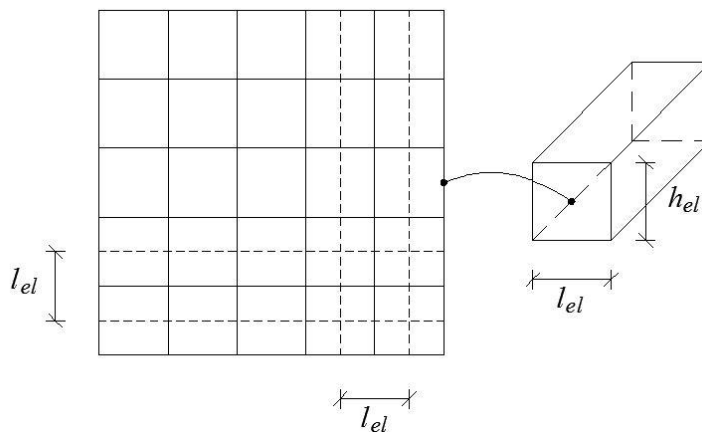


*Figure 3.9      Illustration of mesh size for a beam grillage model.*

Furthermore, in Lindelöf and Walhelm (2014) it was discovered that the torsional stiffness used in the analyses using a beam grillage model, influences the results to a great extent. The torsional stiffness of a beam element is one of the input parameters that need to be chosen when performing nonlinear analyses in ADINA. In Lim (2013), the value was set equal to the elastic torsional stiffness in all analyses, also when the beams were in the cracked state. Lindelöf and Walhelm (2014) made a parametric study to analyse the effect of different torsional stiffness. They studied how the moment distribution and cumulative plastic rotations changed with different

torsional stiffness input in the model. For the case where the torsional stiffness was set constant to its elastic value they got similar results to Lim (2013). When the torsional stiffness was set to zero, the maximum moment was approximately 50% greater than what was obtained when using the elastic stiffness. The moment distribution for the tested torsional stiffness in Lindelöf and Walhelm (2014) is depicted in Figure 3.10.
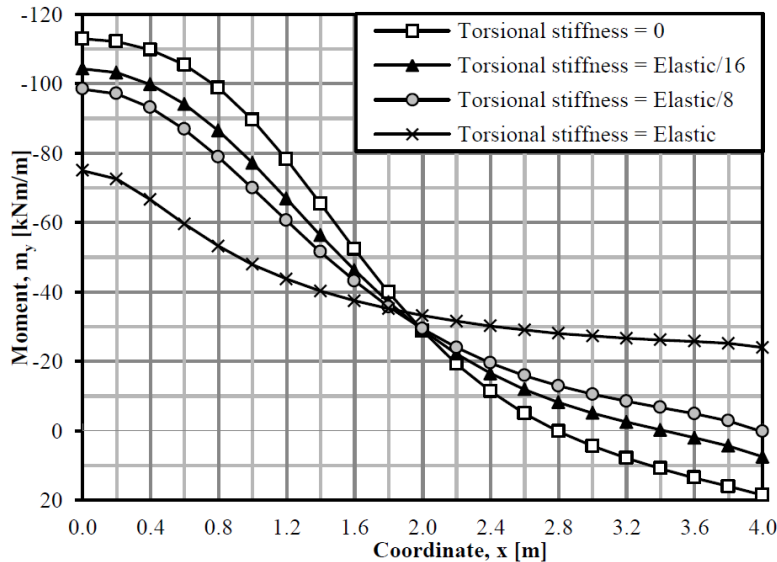


*Figure 3.10*    *Moment distribution in cantilever slab with varying torsional stiffness input for beam grillage models, Lindelöf and Walhelm (2014).*

In Lopes *et al.* (2014) a series of experiments were performed to study the torsional stiffness of reinforced concrete slabs subjected to torsion. Nine quadratic slabs were loaded until failure and the relation between load-displacement and moment-twist were analysed. Three corners of the slab were prevented to move in the vertical direction and at the fourth corner the load was applied in order to create predominantly torsional moments, see Figure 3.11. The experiments showed that the torsional stiffness of the cracked reinforced concrete slabs used in the experiments was 1/17-1/15 of the elastic stiffness, a value much lower than what is assumed for elements predominantly subjected to bending moments. With these tests in mind, Lindelöf and Walhelm (2014) choose their torsional stiffness to be 1/16 of the elastic stiffness in all states.

*Figure 3.11    Illustration of the experimental setup used in Lopes et al. (2014).*

Accordingly, in the Master Thesis of Andersson and Antonsson (2015) a beam grillage model with a mesh size equal to the height of the slab and a reduced torsional stiffness 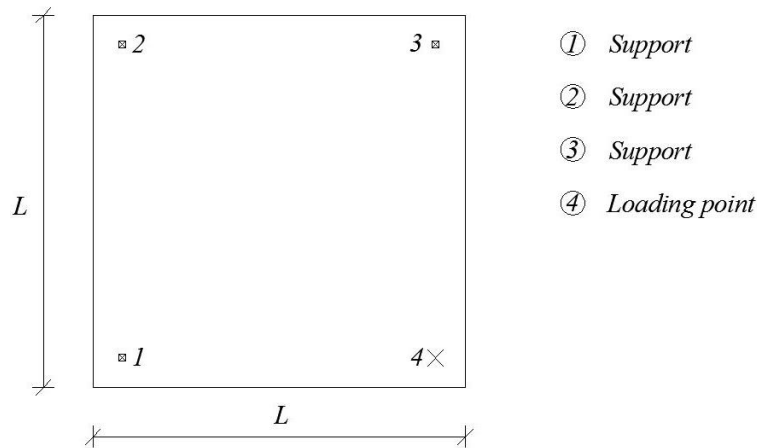of 1/16 of the elastic torsional stiffness was used. This model worked well for all analyses except for when an elastic-fully plastic material model was used. The elasto-plastic model showed a considerably lower internal resistance than a comparable shell element model as well as hand calculations using the strip method, even though the strip method is considered to be well on the safe side. Furthermore, the load distribution of the elasto-plastic beam grillage model did not correspond to the one assumed with the strip method; the load was not distributed to the corner regions, yielding an unreasonable failure mode in the model, see Figure 3.12.



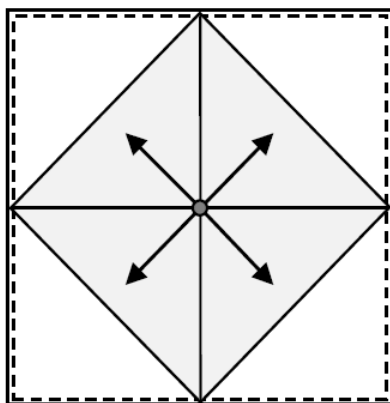*Figure 3.12    Load distribution at failure of elasto-plastic beam grillage model discovered in Andersson and Antonsson (2015).*

Andersson and Antonsson (2015) performed attempts to solve the problem by modelling diagonal beams but the model was still not able to describe the true behaviour of the slab. They considered the elasto-plastic beam grillage model to be non-viable and used shell elements for further studies.

# 4 Linear elastic analyses

## 4.1 Orientation

Successful linear elastic analyses of slabs subjected to torsional moments, modelled with a beam grillage in the FE-software ADINA, have been performed in earlier Master Theses. However, the results received were highly dependent on the mesh size. As described in Section 3.4, satisfactory results were obtained only if the mesh width was set equal to the height of the slab. This was believed to be related to how the torsional stiffness was implemented in the model. To be able to find a well-functioning nonlinear beam grillage model, a more general linear elastic model first had to be established.

## 4.2 Torsional stiffness in ADINA

In the FE software ADINA there is two different ways of implementing the torsional rigidity of a beam. Either, the modulus of elasticity and the geometry of the cross-section of the beam element are defined and the torsional rigidity is calculated by ADINA. Or the torsional moment versus angle of twist and flexural moment versus curvature relationships that describes the stiffness of the beam can be inserted in the program.

For the first case, where material parameters and the geometry of the cross-section are defined, ADINA calculates the torsional rigidity of a beam with rectangular cross-section using equation (4-1).

$$K_v = \frac{1}{3}\left(1 - 0.63\frac{a}{b}\left(1 - \frac{a^4}{12b^4}\right)\right)a^3b, \qquad a \leq b \tag{4-1}$$

Where:    $K_v =$    Torsional stiffness of a beam with rectangular cross-section
          $a =$    Shorter side of cross-section
          $b =$    Longer side of cross-section

Equation (4-1) can be compared with equation (2-15); both equations describe the torsional stiffness of rectangular beams. In order to verify that the values obtained in ADINA correspond to the ones in Table 2.1 different $b/a$ ratios were inserted in the equation. From the study it was concluded that both equations yielded the same results.

However, when modelling a beam grillage the torsional rigidity of the model should reflect the stiffness of an elastic isotropic slab, not a beam. According to Hallbjörn (2015) this can be achieved by multiplying the moment of inertia for a single beam with a factor two, equation (4-2). For a full derivation of this expression the reader is referred to Appendix A.

$$K_v = 2I_I \tag{4-2}$$

Where:    $K_v =$    Torsional stiffness of a beam in a beam grillage

In ADINA there is a factor called *torsional rigidity factor* which can be used to modify the torsional stiffness calculated with equation (4-1). This factor can be utilised when a beam grillage is modelled and the stiffness of a slab is required. The torsional rigidity factor is set to 1.0 as default. However, by using the relationship in equation (4-3) the factor can be used to represent the stiffness of an elastic isotropic slab.

$$\alpha K_v = 2I_I \ \rightarrow \ \alpha = \ 2I_I/K_v \tag{4-3}$$

Where:    $\alpha =$    Torsional rigidity factor in ADINA
          $K_v =$    Torsional stiffness of a beam calculated with equation (4-1)

## 4.3    Torsional rigidity factor

To analyse how the torsional rigidity factor changes with changing cross-section dimensions, a parametric study was performed. Cross-sections with a constant height of 1 meter were tested. The width was successively increased from 0.2 meters to 2 meters with a step size of 0.2 meters. The results are expressed as the width to height ratio of the cross-section versus the corresponding torsional rigidity factor, see Figure 4.1. Equation (4-3) was used as reference for all tested width to height ratios. The default value in ADINA, $\alpha = 1.0$ is presented to enable comparison. The torsional rigidity factor for cross-sections having a width to height ratio of 0.2 is much higher than for the other ratios and thus left out in the figure. However, all torsional rigidity factors determined are specified in Table 4.1.



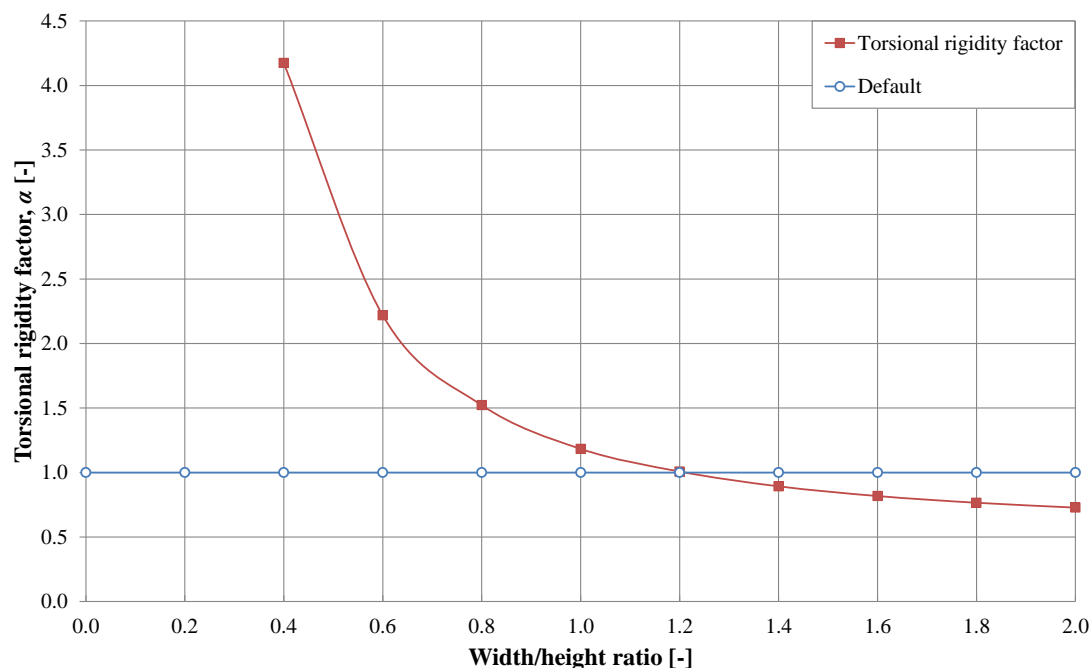*Figure 4.1    Width to height ratio versus torsional rigidity factor.*

From Figure 4.1 it can be concluded that beams with larger height than width generates a torsional rigidity factor that deviates further away from the default value of 1.0 compared to cross-sections with larger width than height. Thus, adjusting the torsional rigidity factor can be of considerable importance for accurate analyses.

A torsional rigidity factor of 1.0 is achieved if the width to height ratio is equal to 1.211. If the width to height ratio is increased towards infinity the torsional rigidity factor tends to a value of 0.5. The reason why width to height ratios below 1.0 seems to deviate more for each step is based on the fact that the moment of inertia is proportional to $h^3$.

*Table 4.1       Torsional rigidity factors for different width to height ratios.*

| w/h | Torsional rigidity factor, $\alpha$ |
|:---:|:---:|
| 0.2 | 14.3 |
| 0.4 | 4.17 |
| 0.6 | 2.22 |
| 0.8 | 1.52 |
| 1.0 | 1.18 |
| 1.2 | 1.01 |
| 1.4 | 0.89 |
| 1.6 | 0.82 |
| 1.8 | 0.77 |
| 2.0 | 0.73 |
| ∞ | 0.50 |

To see analytical calculations of the torsional rigidity factor the reader is referred to Appendix B.

In both Lim (2013), and Lindelöf and Walhelm (2014) it has been concluded that a beam grillage model with the width of the beam equal to the height yields the most satisfying results in an isotropic linear elastic analysis. This outcome can be explained by means of the torsional rigidity factor. From equation (4-1), it can be found that a quadratic cross-section generates a torsional rigidity factor of 1.18, which is rather close to the default value of 1.0. Both Lim (2013), and Lindelöf and Walhelm (2014) compared the quadratic cross-section with cross-sections having a width to height ratio of 0.5 and 2. The corresponding torsional rigidity factors are in those cases 2.91 and 0.73, respectively, i.e. further from the default value and thus further from the true results of the analyses.

## 4.4     Verification of torsional stiffness

### 4.4.1   Orientation

In order to investigate the correctness of equation (4-2), proposed by Hallbjörn, a series of tests were performed in ADINA. They were carried out to ensure that the statement holds true for varying slab geometries as well as varying beam cross-sections. To verify that the correct torsional stiffness was implemented, a pair of models was generated for each test. A beam grillage model and an equivalent shell element model were designed as suggested in Hallbjörn (2015). The shell element models were built up using four-node isoparametric shell elements. If nothing else is

stated, the modulus of elasticity and Poisson's ratio were defined as in Hallbjörn (2015), where $E = 20$ GPa and $\nu = 0$, respectively.

### 4.4.2 Modelling technique practiced by Hallbjörn

For the comparison, the modelling technique practiced by Hallbjörn was used. It means that the geometry of the ADINA model was based on chosen beam widths and not the gross geometry of the slab. The slab in Figure 4.2 can be used as an example to explain how the modelling was performed.
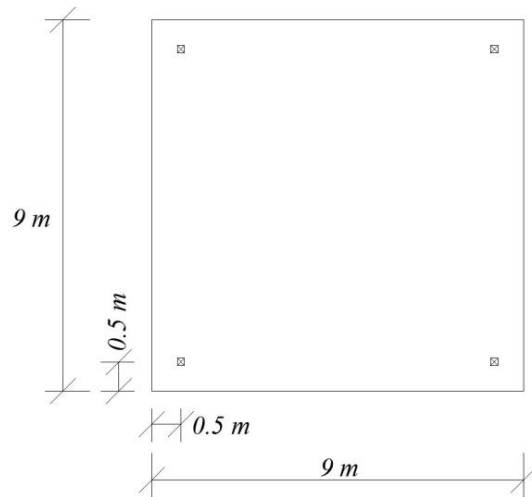


*Figure 4.2    Geometry of the slab used to illustrate the modelling technique practiced in Hallbjörn (2015).*

Figure 4.2 shows the gross geometry of a 9 x 9 meters slab, simply supported on four point supports indented 0.5 meters. However, when using the modelling technique suggested by Hallbjörn, the geometry of the beam grillage model depends on the beam cross-section and not the gross slab geometry. The slab in Figure 4.2 is therefore decreased in both main directions of the slab. Since the geometry established in ADINA is based on the centrelines of the beams the modification can be described by equation (4-4).

$$l_{BG} = l_{gross} - w_{beam} \qquad\qquad (4\text{-}4)$$

Where:     $l_{BG} =$        Length of beam grillage model
           $l_{gross} =$      Length of gross slab geometry
           $w_{beam} =$       Width of chosen beams in ADINA

Due to the support locations, using beams with a width of 1.0 meter is an appropriate choice. Thus, if the width of the beams is chosen to 1.0 meter and the expression above is utilised, the geometry of the ADINA model will be as is shown in Figure 4.3.
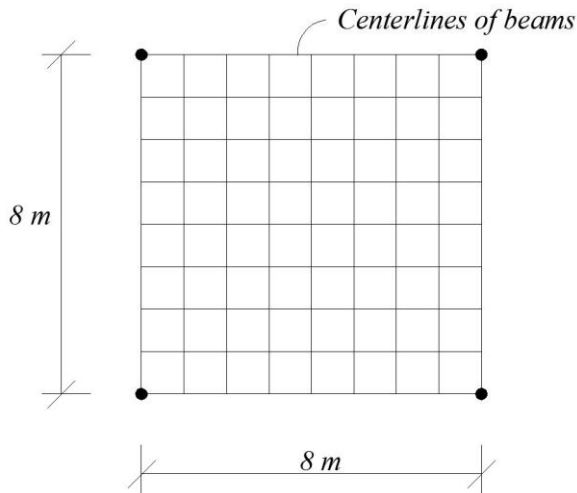
*Figure 4.3    Beam grillage model in ADINA based on the modelling technique suggested in Hallbjörn (2015).*

To further explain the modelling technique, the cross-section of the slab can be studied, see Figure 4.4. The cross markings represent the centreline of each beam. It can be seen that beams with a width of 1 meter, gives a model with a length of 8 meter in ADINA. However, the fictitious cross-section is equivalent with the gross geometry of the slab, i.e. 9 meters.
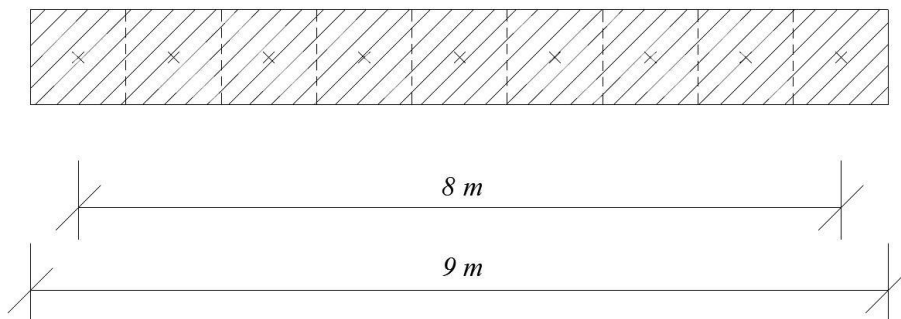


*Figure 4.4    Cross-section of the slab modelled as a beam grillage.*

### 4.4.3   Quadratic slab with varying cross-sections

The first test in the analysis of equation (4-3) was designed to study how well the equation serves for different beam cross-sections. Several slabs with different cross-sections of the beams were modelled using the torsional rigidity factor calculated with equation (4-3) and compared with corresponding shell element models. For slabs with beam cross-sections with a width to height ratio larger than 1.0 a slab with dimensions, supports and loading according to Figure 4.5 was modelled in ADINA. The width of the beams was constantly 1.0 meter but the height varied between 0.1 and 1.0 meter with a step size of 0.1 meters.

*Figure 4.5      Geometry of the a) shell element model and b) beam grillage model for width to height ratios larger than 1.0.*

On the contrary, slabs with beam cross-sections having a width to height ratio smaller than 1.0 the slab shown in Figure 4.6 was studied. 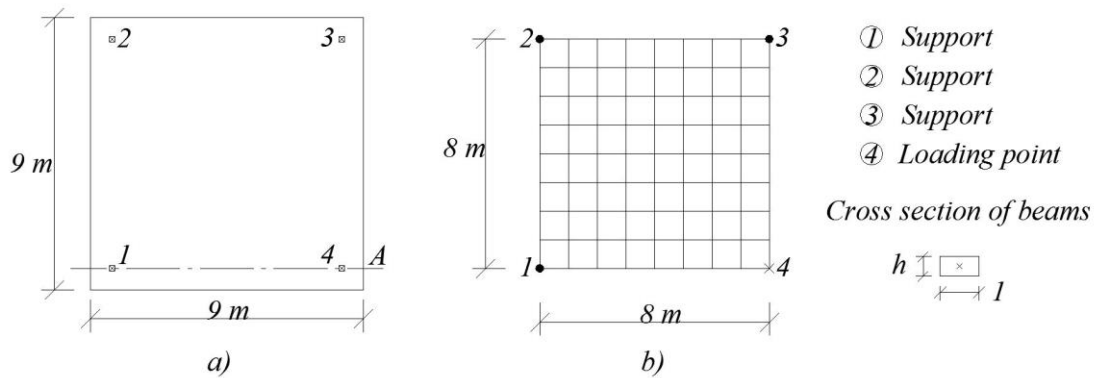The width of the beams was constant 0.2 meters but the height varied between 0.2 and 1.0 meter. The reason for looking at different slabs depending on the width to height ratio was to study slabs with conventional geometries. If a slab with beams having a width of 1.0 meter were used for all ratios the height would become unreasonably high for small ratios.
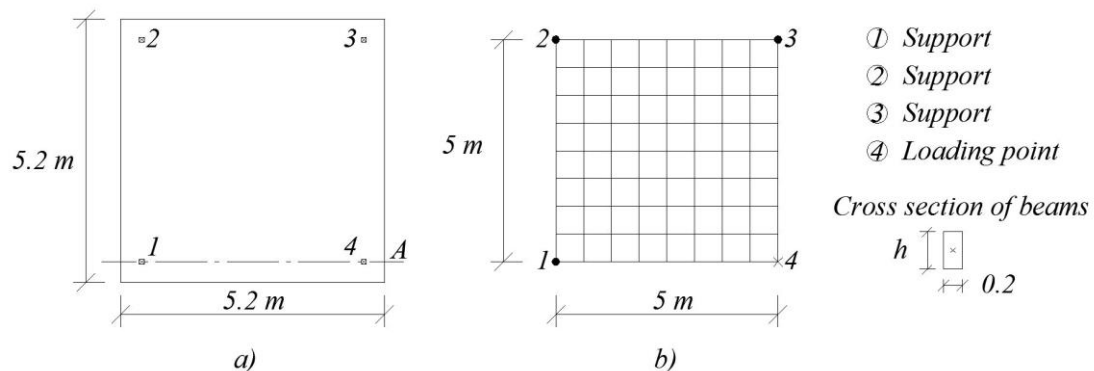


*Figure 4.6      Geometry of the a) shell element model and b) beam grillage model for width to height ratios smaller than 1.*

All analyses were performed with the material input data described in Section 4.4.1. Thus the only parameter varying was the height of the slab. The point supports were simply supported and the point load had a magnitude of 100 kN.

The vertical displacement along Line A shown in Figure 4.5 and Figure 4.6 was measured and plotted with the x-coordinates. Results for the slabs with ratios 0.2, 0.4, 1.0, 1.67 and 5, are shown in Figure 4.7. For results of all slabs the reader is referred to Appendix C.
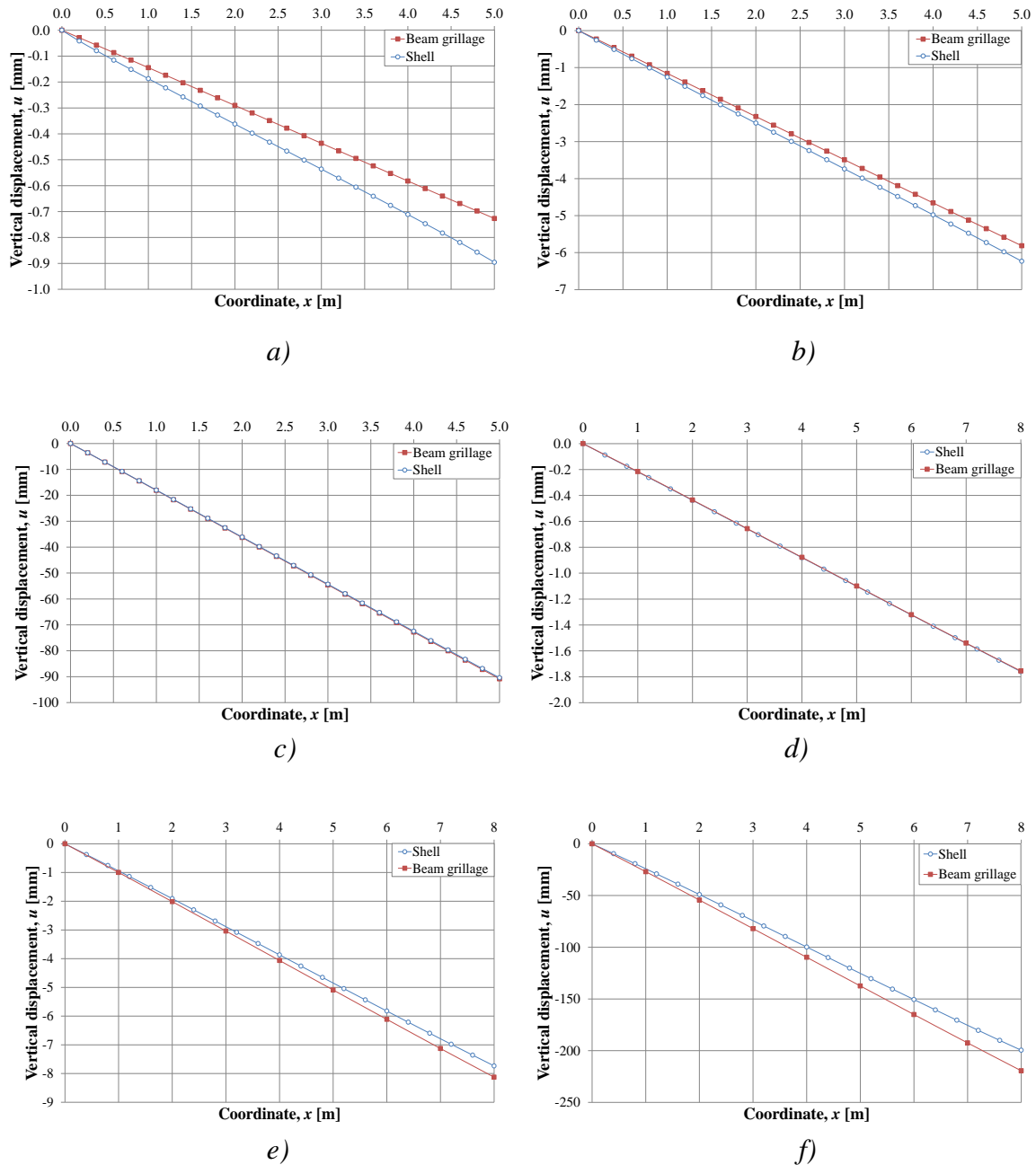
*Figure 4.7    Vertical displacement, u along Line A for beam grillages with varying cross-sections. Width to height ratio: a) 0.20, b) 0.40, c) 1.00 d) 1.00, e) 1.67 and f) 5.00.*

It was observed that the relationship proposed by Hallbjörn (2015) holds true for certain choices of beams in the beam grillage model. A beam grillage with beams having quadratic cross-sections obtains deformations almost identical to the shell element model. However, for a width to height ratio that increases or decreases from the value 1.0 the results deviate further from the true solution. Beam grillages with ratios smaller than 1.0 yield displacements smaller than the shell element models. By contrast, beam grillages with larger ratios than 1.0 generate displacements larger than the shell element models. The maximum vertical displacements for the slabs presented in the figures above are presented in Table 4.2.

*Table 4.2*     *Maximum vertical displacement, u for shell element models and beam grillages with different width to height ratios.*

| Width/height ratio | 0.20 | 0.40 | 1.00 | 1.00 | 1.67 | 5.0 |
|---|---|---|---|---|---|---|
| Shell element model, maximum vertical displacement, $u$ [mm] | 0.90 | 6.23 | 90.4 | 1.76 | 7.73 | 200 |
| Beam grillage model, maximum vertical displacement, $u$ [mm] | 0.73 | 5.81 | 90.8 | 1.76 | 8.13 | 219 |

Even if the relationship seems to be valid for beams with quadratic cross-sections a more general correlation was sought. It was investigated if there was a way to modify equation (4-3) to achieve accurate deformations for any arbitrary cross-section. Therefore, the slabs illustrated in Figure 4.5 and Figure 4.6 were studied again. Through an iterative process where the torsional rigidity factor was altered, a new factor which gave the same vertical displacement as the corresponding shell element model was found. The torsional rigidity factor calculated with equation (4-3) denoted as $\alpha_{old}$ and the new iterated value $\alpha_{new}$ was used as in equation (4-5) to determine the difference between them, i.e. the "correction factor" $\Delta\alpha$.

$$\Delta\alpha = \alpha_{new} - \alpha_{old} \tag{4-5}$$

Where:     $\Delta\alpha =$     Correction factor
           $\alpha_{new} =$     Iterated value
           $\alpha_{old} =$     Torsional rigidity factor as in equation (4-3)

Numerical values for different cross-sections are presented in Table 4.3 and Table 4.4.

*Table 4.3*     *Calculated torsional rigidity factors, α and the correction factor, Δα for the slab in Figure 4.6 with different width to height ratios.*

| Ratio | 0.20 | 0.22 | 0.25 | 0.29 | 0.33 | 0.40 | 0.50 | 0.67 | 1.0 |
|---|---|---|---|---|---|---|---|---|---|
| $\alpha_{old}$ | 14.30 | 11.77 | 9.495 | 7.469 | 5.695 | 4.175 | 2.913 | 1.917 | 1.183 |
| $\alpha_{new}$ | 11.60 | 9.800 | 8.200 | 6.620 | 5.200 | 3.910 | 2.800 | 1.900 | 1.183 |
| Δα | -2.702 | -1.973 | -1.295 | -0.849 | -0.495 | -0.265 | -0.113 | -0.017 | 0 |

*Table 4.4*     *Calculated torsional rigidity factors, α and the correction factor, Δα for the slab in Figure 4.5 with different width to height ratios.*

| Ratio | 1.0 | 1.11 | 1.25 | 1.43 | 1.67 | 2.00 | 2.50 | 3.33 | 5.00 | 10.0 |
|---|---|---|---|---|---|---|---|---|---|---|
| $\alpha_{old}$ | 1.183 | 1.078 | 0.974 | 0.881 | 0.799 | 0.728 | 0.668 | 0.617 | 0.572 | 0.534 |
| $\alpha_{new}$ | 1.183 | 1.090 | 0.999 | 0.915 | 0.841 | 0.777 | 0.722 | 0.675 | 0.632 | 0.594 |
| Δα | 0 | 0.013 | 0.026 | 0.034 | 0.042 | 0.049 | 0.054 | 0.058 | 0.060 | 0.060 |

The relation between the width to height ratio and the correction factor $\Delta\alpha$ for ratios smaller than 1.0 can be seen in Figure 4.8. For ratios larger than 1.0, see Figure 4.9.

*Figure 4.8*    *Relation between width to height ratios smaller than 1.0 and the calculated correction factor Δα. Notice that the horizontal axis starts at 0.2.*



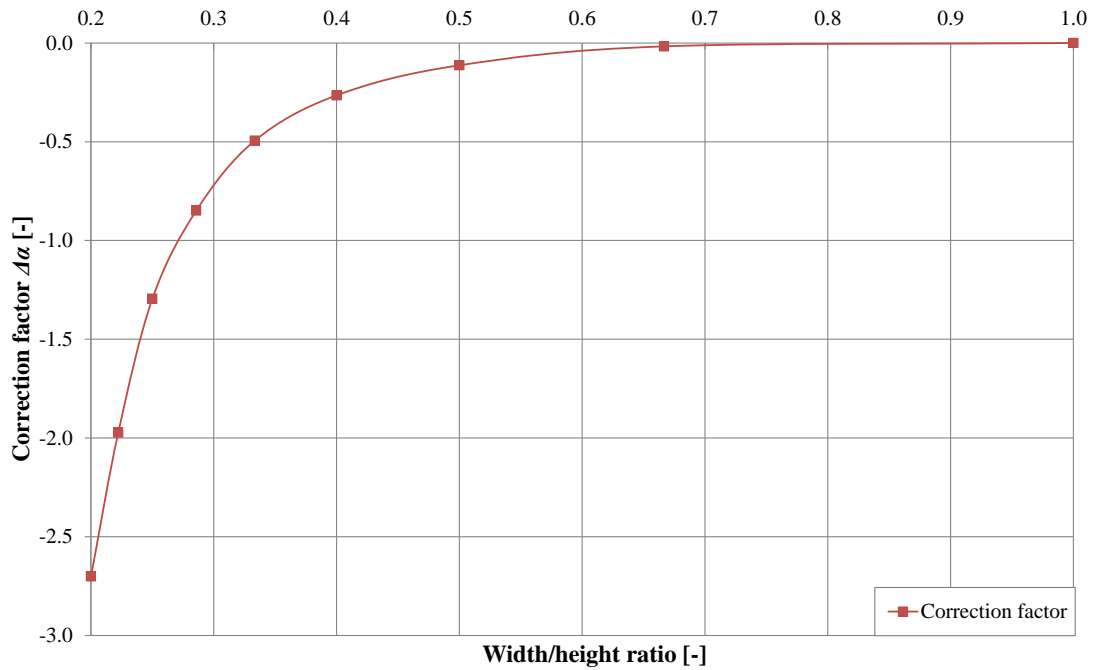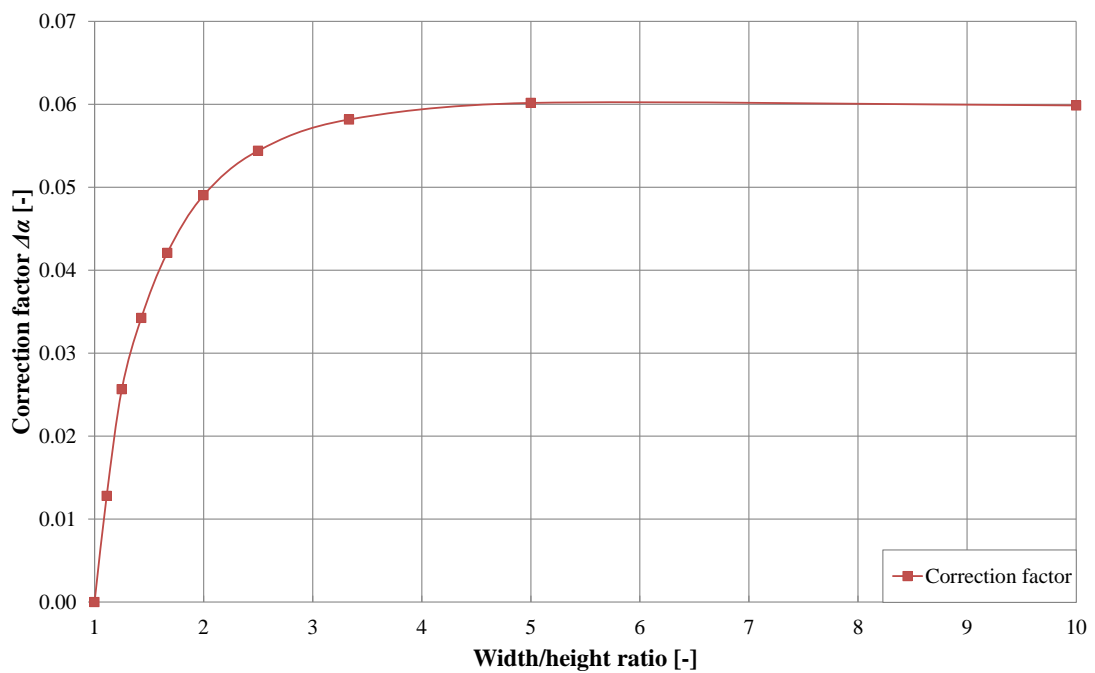*Figure 4.9*    *Relation between width to height ratios larger than 1.0 and the calculated correction factor Δα. Notice that the horizontal axis starts at 1.0.*

As can be seen from the results in Figure 4.8, for width to height ratios smaller than 1.0, the correction factor is negative. For ratios larger than 1.0 however, it is a positive

value, see Figure 4.9. The difference in magnitude of the correction factor is due to how the moment of inertia is calculated for a rectangular cross-section.

When implementing the correction factor $\Delta\alpha$ in equation (4-3), the relationship can be described with equation (4-6).

$$(\alpha + \Delta\alpha)K_v = 2I_{beam} \tag{4-6}$$

Where:        $\Delta\alpha =$    Correction factor for the torsional rigidity factor in ADINA

Equation (4-6) is more general than equation (4-3) since it describes the relationship not only for quadratic cross-sections but also for rectangular cross-sections. Values for the correction factor $\Delta\alpha$ can be found in Table 4.3 and Table 4.4 and for intermediate ratios, linear interpolation can be used.

### 4.4.4    Rectangular slab

The correction factors for the torsional rigidity factor that are presented in Table 4.3 and Table 4.4 were intended to be general for all slab geometries. They were generated from quadratic slabs subjected to torsion effects. Thus, it was of interest to test if they also hold true for a different geometry, such as a rectangular slab. All tested slabs had simply supported point supports and a load magnitude of 100 kN.

As a first test it was determined to use beams with quadratic cross-sections. By using quadratic cross-sections the correction factor from Table 4.3 or Table 4.4 was set to zero, i.e. the slab geometry was the only investigated parameter. The beam cross-section was chosen to have a side length of 0.3 meters. Figure 4.10 shows the tested slab with its gross geometry and the corresponding beam grillage model.
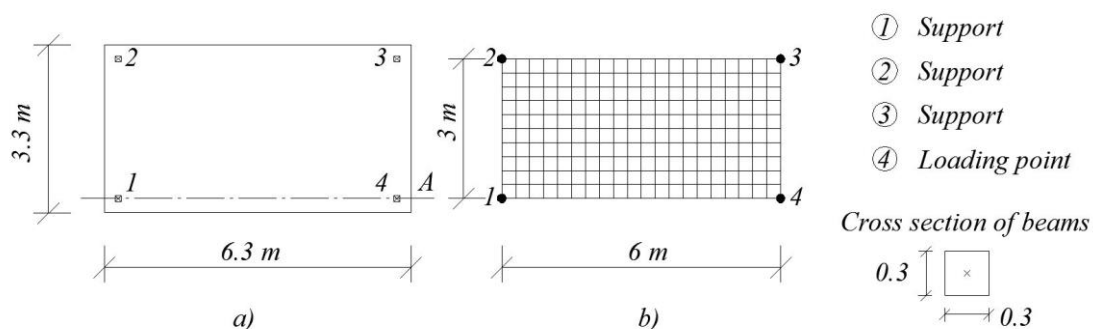


*Figure 4.10    Geometry of the a) shell element model and b) beam grillage model of the rectangular slab with quadratic beam cross-sections.*

For verification of the beam grillage model, Figure 4.11 shows the displacement of the slab along Line A.
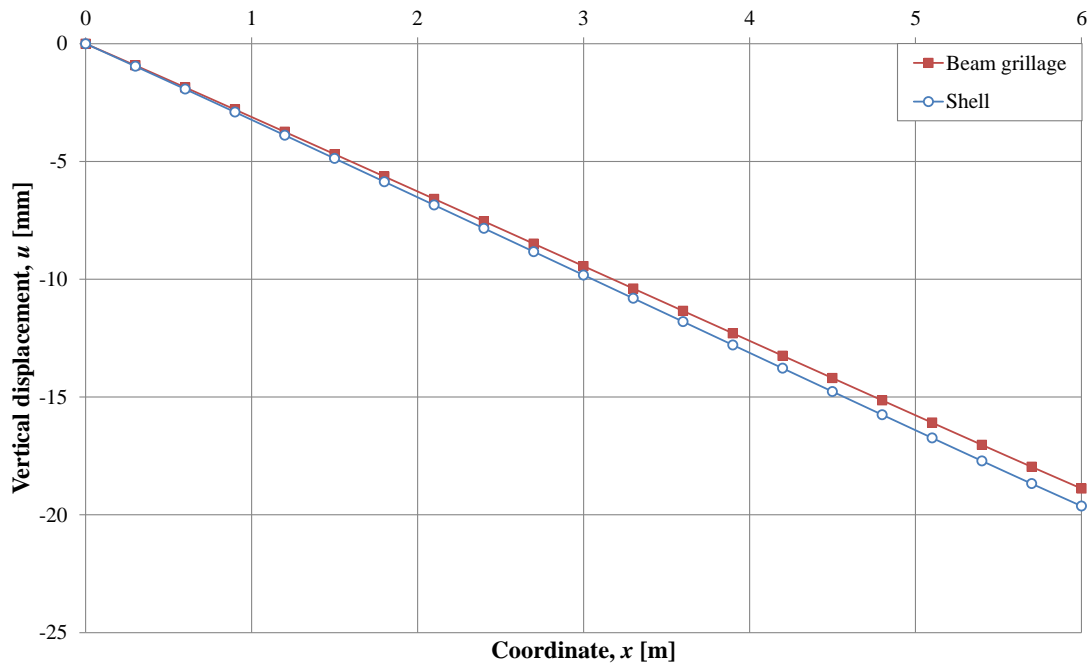
*Figure 4.11    Vertical displacement, u along Line A for the rectangular slab with quadratic cross-sections in Figure 4.10.*

From Figure 4.11 it can be seen that there is a small deviation in terms of deformation of the two models. If the maximum displacement is studied, the differences between the models are approximately 3.6 %. If the same difference is studied for a quadratic slab with quadratic beam cross-sections, the error is smaller (0.6 %). Hence, it was concluded that the slab geometry influences the results. Hallbjörn's suggestion of how the torsional stiffness should be modelled seems to hold true only for quadratic slabs.

The same test as was performed with quadratic beam cross-sections was also performed with rectangular cross-sections. Thus, the correction factor from Table 4.3 is no longer zero.

The beam cross-sections were chosen to a width, $w = 0.2$ meters and a height, $h = 0.6$ meters yielding a ratio $w/h = 0.33$. This cross-section was chosen since it was also used to extract the corrected torsional rigidity factor $\alpha_{new} = 5.2$ from Table 4.3. By using the same cross-section, the risk of cross-section geometry influencing the results was eliminated and the change of slab geometry could once again be investigated. Figure 4.12 shows the geometry of the slab and its corresponding beam grillage.
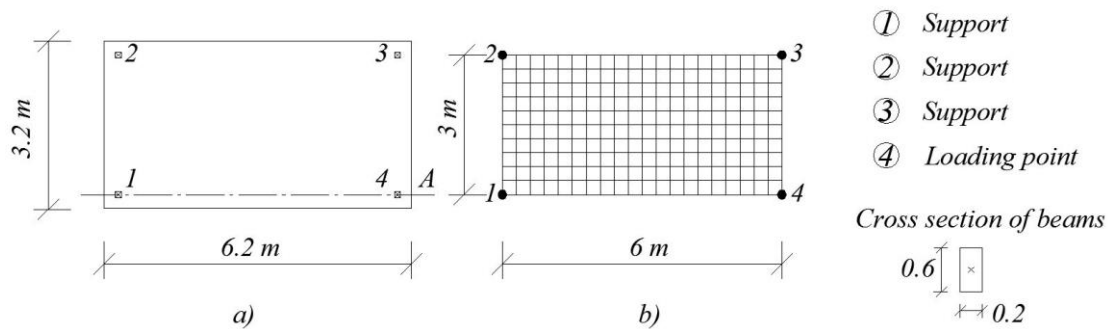
*Figure 4.12    Geometry of the a) shell element model and b) beam grillage model of the rectangular slab with rectangular beam cross-sections.*

Once again the displacement along Line A was studied and is presented in Figure 4.13.
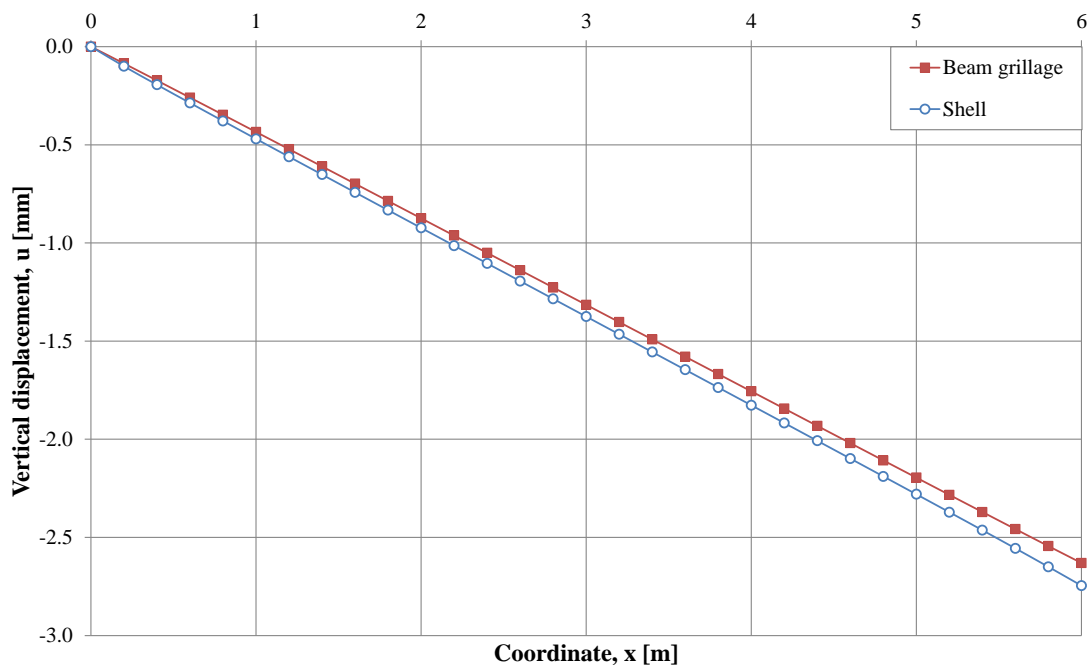


*Figure 4.13    Vertical displacement, u along Line A for the rectangular slab with rectangular cross-sections in Figure 4.12.*

From Figure 4.13 it can be seen that the displacement in the beam grillage was less than in the shell element model. If the maximum displacement is studied, the difference between the beam grillage and the shell element model equals 4.2 %. This error is slightly larger compared to the case of quadratic beam cross-sections with an error of 3.6 %. Since the difference between quadratic and rectangular cross-sections with correction factors was small, it was concluded that the cross-sectional geometry has negligible influence on the results.

As a summation, modelling the torsional stiffness as two times the moment of inertia in rectangular slabs as suggested by Hallbjörn (2015) generates a slight error even for models with quadratic beam cross-sections. The influence of using rectangular cross-

sections with correction factors according to Table 4.3 and Table 4.4 works satisfactory for a rectangular slab. In Section 4.6, the influence of shear deformations as a possible reason for the deviations is discussed.

### 4.4.5 Influence of cross-section geometry

A study of how the correction factors in Table 4.3 and Table 4.4 were influenced by the cross-section geometry was required to be able to consider them as general. The correction factors were tested for different cross-sections by means of the quadratic slab presented in Figure 4.14. A quadratic slab was chosen to avoid generating the slight error described in Section 4.4.4.
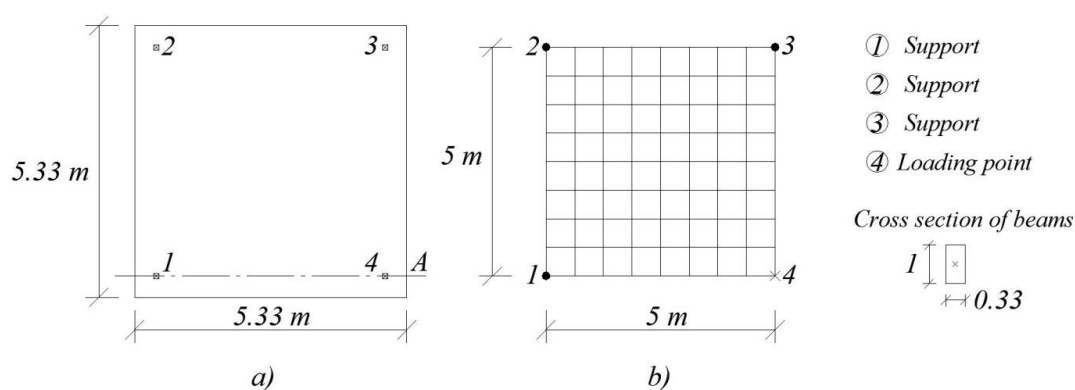


*Figure 4.14    Geometry of the a) shell element model and b) beam grillage model.*

The slab was modelled with rectangular beam cross-sections with a width to height ratio of 0.33. According to Table 4.3, the torsional rigidity factor for such cross-sections should be chosen as $\alpha_{new} = 5.2$. A width to height ratio that equals 0.33 can be achieved with several possible widths and heights. Thus, the slab in the figure above was modelled with beam cross-sections as $w/h = 0.33/1 = 0.33$. The displacement along Line A is presented in Figure 4.15 for the beam grillage model and its corresponding shell element model.
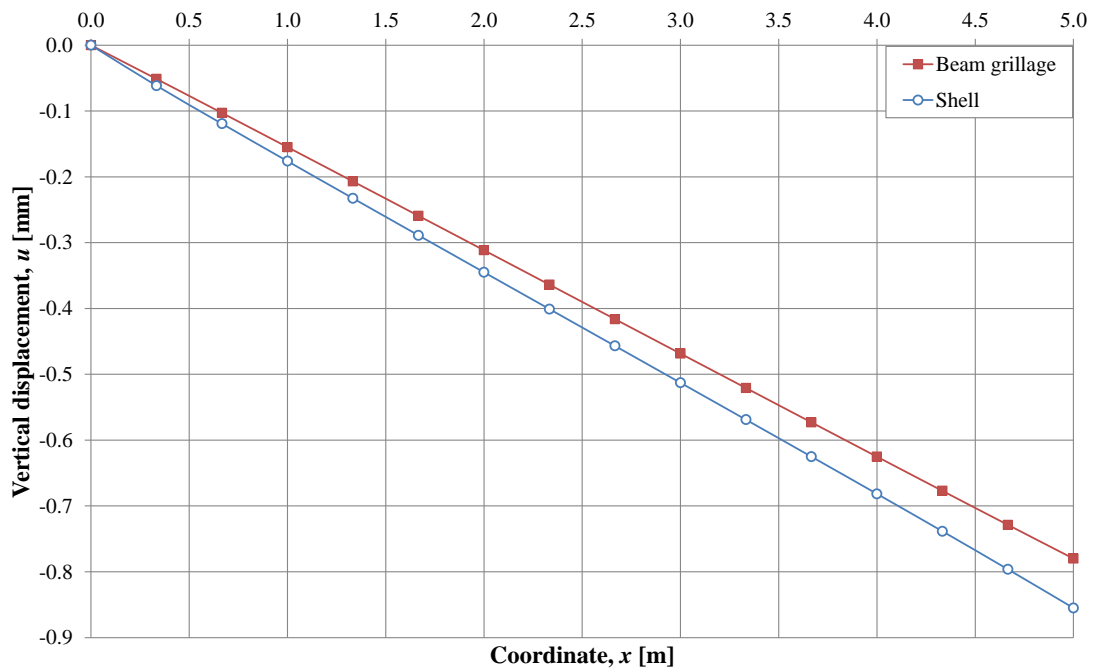
*Figure 4.15    Vertical displacement,* u *along Line A for the quadratic slab with rectangular cross-sections in Figure 4.14.*

By looking at Figure 4.15 it is clearly seen that deviations occur. At the maximum displacement there is a 9.8 % difference between the models. The torsional rigidity factor $\alpha_{new} = 5.2$ was interpolated from cross-sections where $w/h = 0.2/0.6$. This means that the correction factors presented in Table 4.3 does not hold true for all cross-sections based on the width to height ratio but rather depends on the actual cross-sectional geometry. In other words the correction factors presented holds true only for cross-sections with the width, $w = 0.2$ meters. Accordingly, the correction factors presented in Table 4.4 holds true only for cross-sections with the width $w = 1.0$ meter.

### 4.4.6   Moment distribution

As deviations occurred in the deformation measurements presented. It was of interest to study the moment distributions in beam grillage models compared to shell element models. Thus the slab presented in Figure 4.5 was modelled as a beam grillage using quadratic beams with a side length equal to 1.0 meter. The moment distribution for the beam grillage model and an equivalent shell element model along Line A is presented in Figure 4.16.

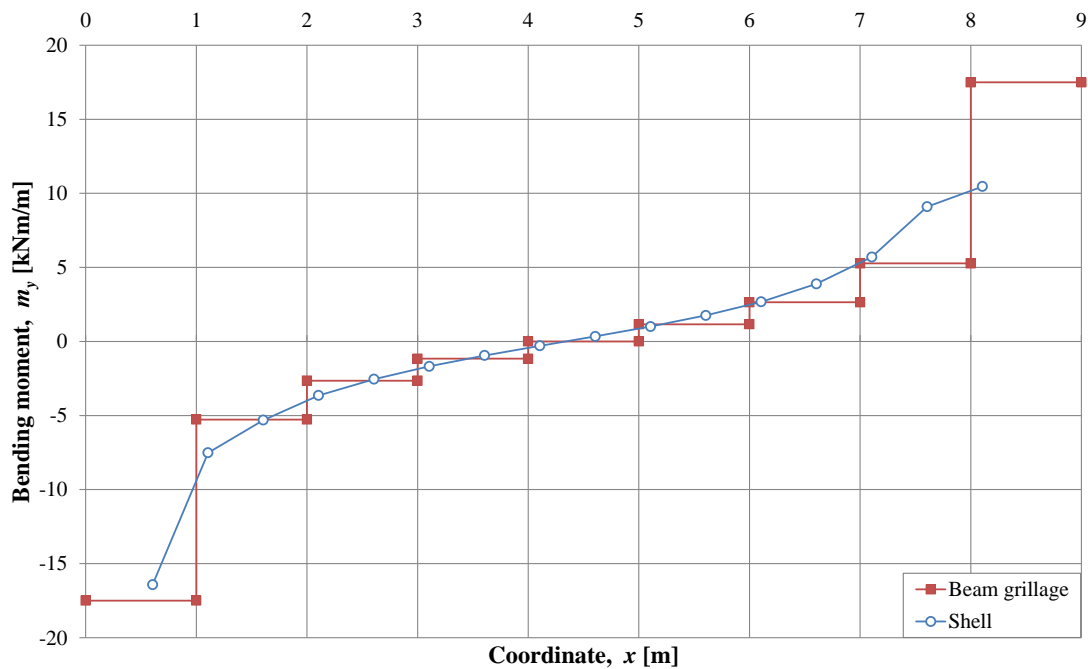*Figure 4.16    Moment distribution, $m_y$ along Line A for the beam grillage model and shell element model.*

Figure 4.16 clarifies that the models distribute the moment in a similar manner. The results of the beam grillage model are presented as a constant average moment in each beam element. The moment distribution corresponds exactly to what is presented in Hallbjörn (2015), leading to believe that the deviations in displacement is not related to the moment distribution. Hence the modelling technique was considered valid with regard to moment distribution. In addition, since the moment distribution was valid, the ides that shear deformations may cause the deviation in displacements is strengthen.

### 4.4.7    Slab subjected to bending

Another interesting study to perform was to move the loading point from the corner to the middle of the slab and adding a fourth support. The slab was then predominantly subjected to bending moments. In theory the torsional rigidity factor should not influence the result of a slab that is not subjected to torsional moments hence the aim of the study was to see if the theory is correct. By looking at a similar slab as described in Section 4.4.3, the influence of the torsional rigidity factor was studied. The geometry of the slab can be seen in Figure 4.17. The outer dimensions were 9 x 9 meters and the cross-section of the beams was set to 0.33 x 0.33 meters. Further, four simply supported point supports were placed in the corners and the point load was modelled in the same way as described in Section 3.3 with a total magnitude of 100 kN.

*Figure 4.17    Geometry of a) the shell element model and b) the equivalent beam grillage model for the quadratic slab.*

For the beam grillage models, three different torsional rigidity factors were used. The first one was based on the theory of Hallbjörn to $\alpha = 1.18$. The other two values were chosen arbitrarily to $\alpha = 0.7$ and $\alpha = 7.0$. The vertical displacement along line A, see Figure 4.17, was studied and the results for the shell element model and the three beam grillage models are presented in Figure 4.18. The maximum displacements are also stated in Table 4.5.
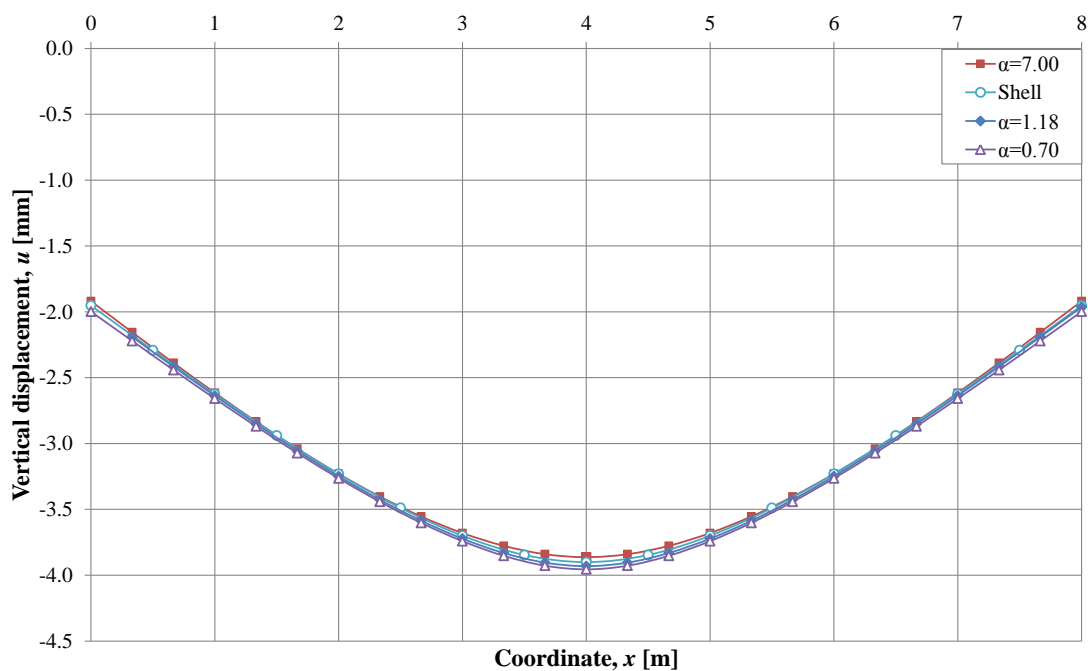


*Figure 4.18    Vertical displacement, u along line A for the quadratic slab with centric loading for different torsional rigidity factors.*

*Table 4.5*     *Maximum vertical displacement, u for the quadratic slab in Figure 4.17.*

| Model | Shell | Beam grillage α =0.70 | Beam grillage α =1.18 | Beam grillage α =7.00 |
|---|---|---|---|---|
| Maximum vertical displacement, $u$ [mm] | -3.90 | -3.96 | -3.90 | -3.86 |

The results of the beam grillage models only differ slightly from the shell element model. From these results it can be concluded that the torsional rigidity factor has very little influence in analyses of slabs subjected to mainly bending moments. For the beam grillages themselves, the results are as expected. The difference between the models can be omitted but, as was presumed, the model with the highest $\alpha$-value i.e. the highest torsional stiffness generates the smallest displacement. However, to verify that the torsional rigidity factor has negligible influence for slabs mainly subjected to bending not only with quadratic geometry, the same test was performed for a slab with rectangular geometry.

Thus, a rectangular slab with beam cross-sections of 0.3 x 0.3 meters and geometry as in Figure 4.19 was tested. Simply supported point supports were, just as in the previous test, placed in the corners and a point load of 100 kN was applied in the middle of the slab in the same way as for the quadratic slab.
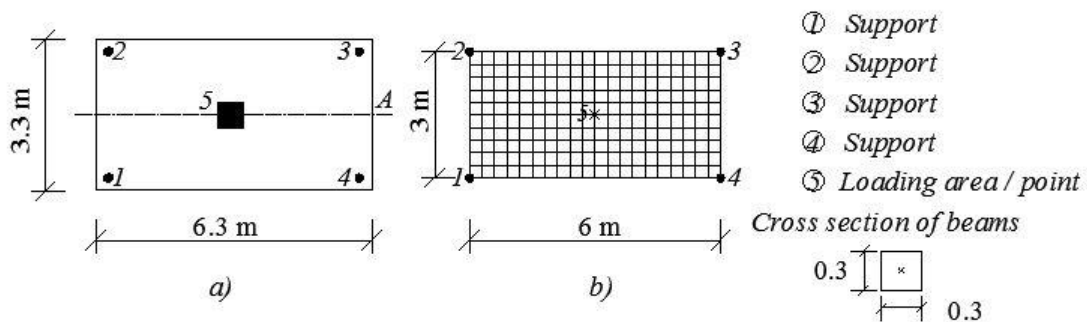


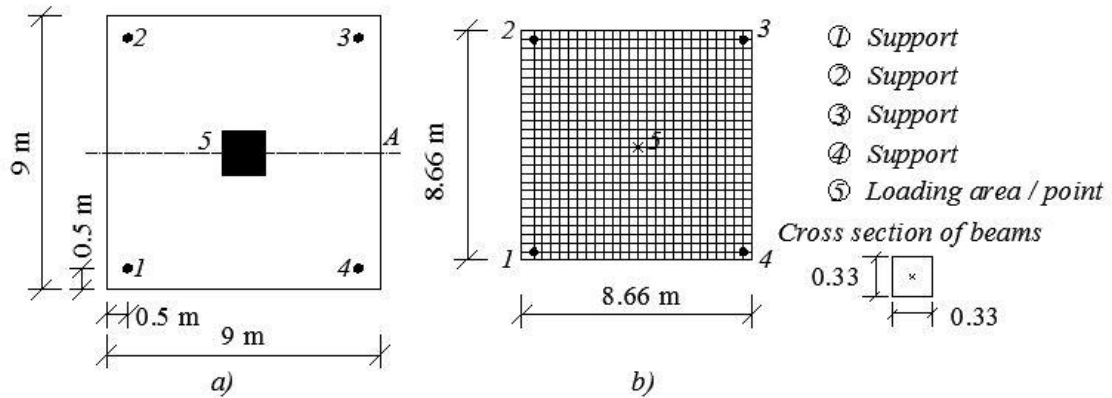*Figure 4.19*     *Geometry of a) the shell element model and b) the equivalent beam grillage model for the rectangular slab.*

For the first model, the torsional rigidity factor was set to $\alpha =1.18$ based on the theory of Hallbjörn. Model two and three were given the factors $\alpha =0.7$ and $\alpha =7.0$, respectively. Vertical displacement along Line A in Figure 4.19 were compiled and plotted in the graph in Figure 4.20. The corresponding maximum values are specified in Table 4.6.
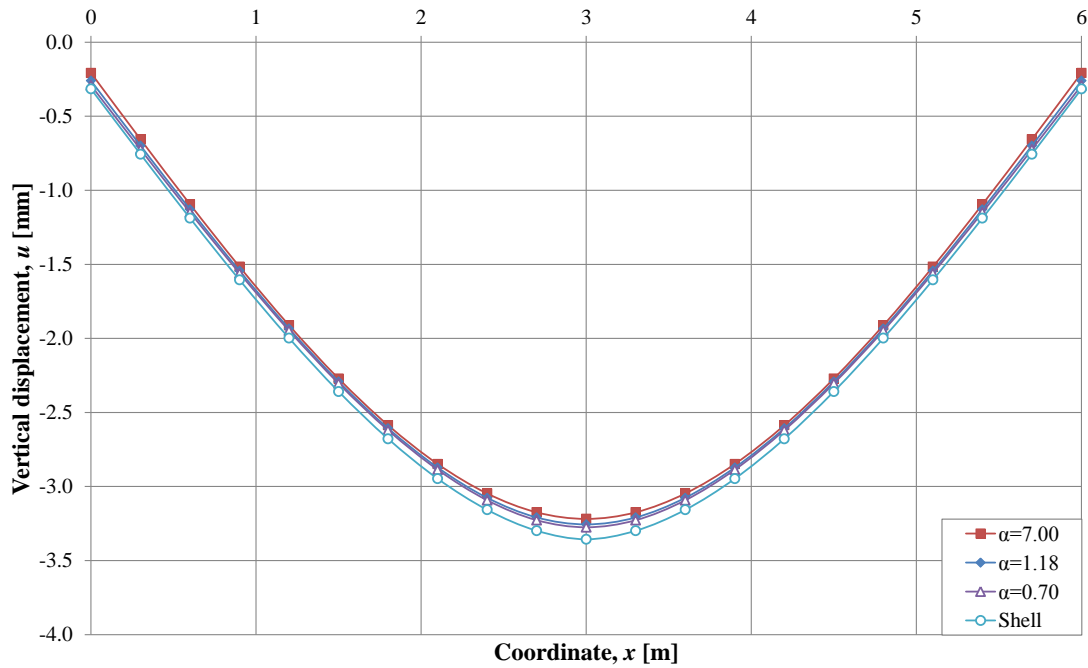
*Figure 4.20    Vertical displacement, u along line A for the rectangular slab with different torsional rigidity factors.*

*Table 4.6      Maximum vertical displacement, u for the rectangular slab in Figure 4.19.*

| Model | Shell | Beam grillage $\alpha$ =0.70 | Beam grillage $\alpha$ =1.18 | Beam grillage $\alpha$ =7.00 |
|---|---|---|---|---|
| Max. vertical displacement, $u$ [mm] | -3.36 | -3.28 | -3.26 | -3.22 |

Just as for the quadratic slab, there is no significant difference between the vertical displacement for the different beam grillage models. However, all beam grillage models are stiffer than the shell element model. This was believed to be due to the rectangular shape of the slab as described in Section 4.4.4 and not related to torsional rigidity factor. In conclusion, the torsional rigidity factor has no notable influence on the results for slabs subjected to mainly bending moments. This ascertainment holds true for both quadratic and rectangular slabs.

## 4.5    Cantilever slab

### 4.5.1    Orientation

The linear elastic response of concrete slabs, using beam grillage models was tested in Lim (2013). Lim performed a parametric study where three mesh densities were compared to a shell element model. However, Lim did not modify the torsional rigidity of the beam elements, i.e. the default value of the torsional rigidity factor of $\alpha = 1.0$ was used for all mesh densities. Section 4.4 concludes that the torsional stiffness of the beams has a major influence on the results of the analyses if torsional effects are present. Therefore, it was decided to reproduce Lim's cantilever slab whilst

implementing the torsional stiffness of two times the moment of inertia as suggested by Hallbjörn (2015).

## 4.5.2 Modelling technique

In Lim (2013), just as in the two other previous Theses by Lindelöf and Walhelm (2014) and Andersson and Antonsson (2015), another modelling technique than the one described in Section 4.4.2 was used. Instead of changing the geometry of the beam grillage model with respect to the beam cross-sections, the gross geometry of the slab was modelled. To illustrate how the modelling technique works the slab in Figure 4.21 is used as an example.



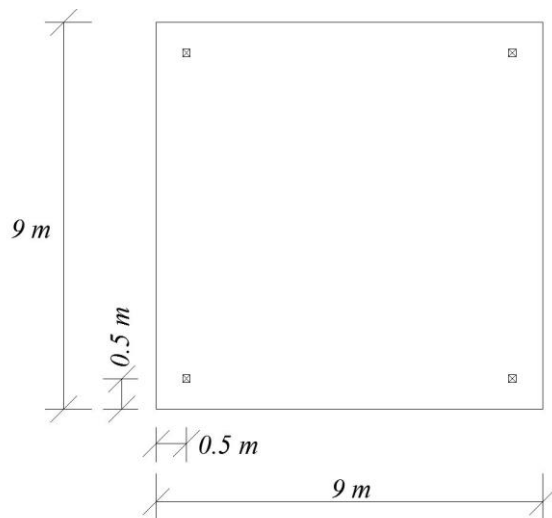*Figure 4.21    Geometry of the slab.*

For the corresponding beam grillage model the gross geometry is used, i.e. a grid of beams of 9 x 9 meters. Due to the support locations an appropriate beam width is 0.5 meters. To model the rim, edge beams are implemented and given a width half as wide as the inner beams in the model to keep the area of the slab constant. The beam grillage model is shown in Figure 4.22.
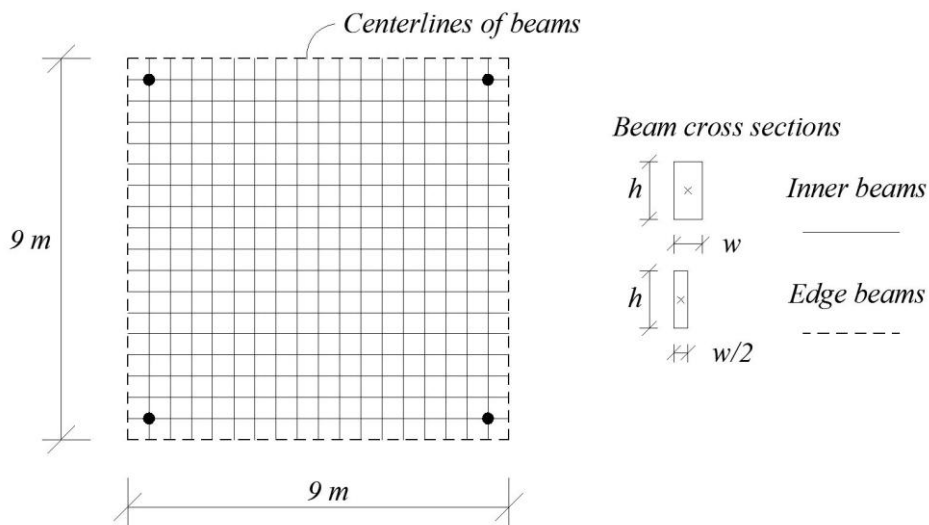
*Figure 4.22 Beam grillage model based on gross geometry with modified edge beams.*

Since the beams in a beam grillage are modelled as the centerline, a gap between the edge beams and the adjacent beams will occur from a geometrical viewpoint. Figure 4.23 is meant to illustrate this gap created at the edges of the slab. The outer dimensions of the fictitious slab will be 9.25 x 9.25 meters, but the true geometry of the slab is still 9 x 9 meters. The reasoning behind this modelling approach is that the outer part of the edge beams will cover the loss of stiffness that is created by the gaps.
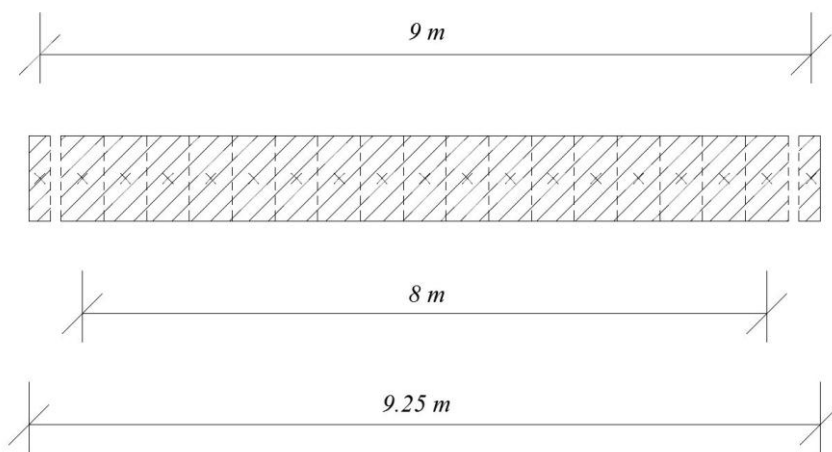


*Figure 4.23 Cross-section of a slab modelled with modified edge beams.*

### 4.5.3 Response when subjected to point load

The geometry of Lim's cantilever slab is presented in Figure 4.24. The height of the slab was 0.2 meters. Young's modulus was defined as $E = 30$ GPa and Poisson's ratio as $\nu = 0$. Lim performed a convergence study of shell element models with different mesh densities and concluded that a density of 0.2 meters was adequate. Based on Lim's study, the same mesh density was used in the following analyses. Due to the dense meshing, a symmetry line was implemented to not excess the maximum

number of 900 nodes. The applied point load was 100 kN, positioned at the end of the symmetry line.
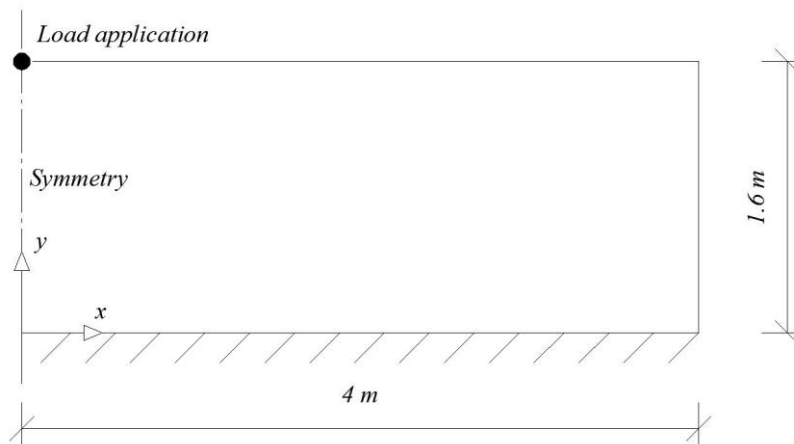


*Figure 4.24    Geometry of cantilever slab.*

Lim modelled the corresponding beam grillage in three different ways, see Figure 4.25. The varying parameter was the cross-section geometry; beam widths of 0.1, 0.2 and 0.4 meters were tested. Lim found that a beam width of 0.2 meters, i.e. a quadratic cross-section, gave the most satisfying results.
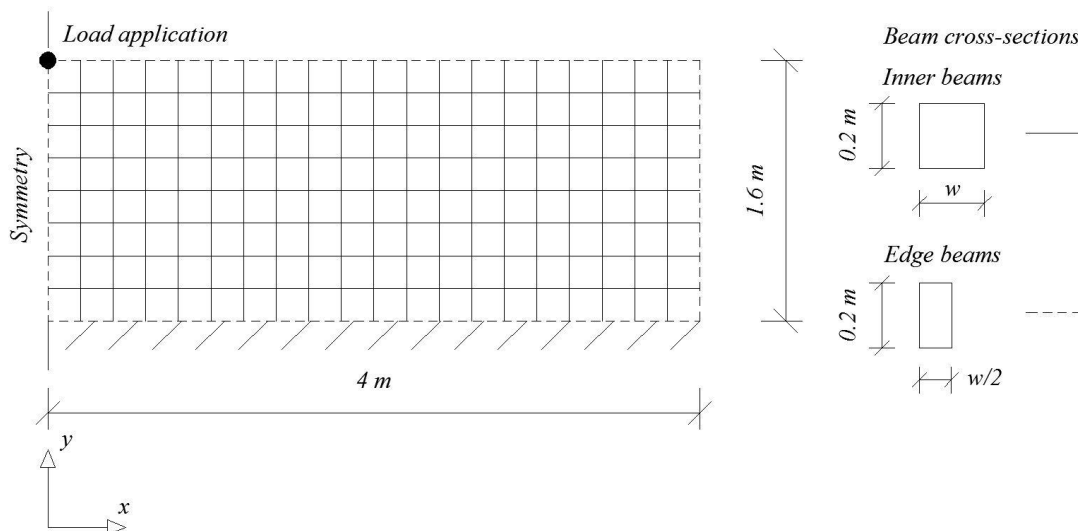


*Figure 4.25    Beam grillage model of cantilever slab.*

In order to compare the results from Lim (2013), where the difference in torsional stiffness between a single beam and a beam grillage was not considered, three additional slabs were modelled. Those three models were identical with Lim's beam grillage models with the only difference that the torsional stiffness was defined according to Hallbjörn (2015) as in equation (4-2). The torsional rigidity factor for different width to height ratios was defined according to Table 4.1.

The investigated parameters were the bending moment, $m_y$ along the fixed edge and the vertical displacement, $u$ along the symmetry line. Figure 4.26 and Figure 4.27

shows the bending moments for the three different beam widths, modelled both with and without considering the torsional rigidity factor.
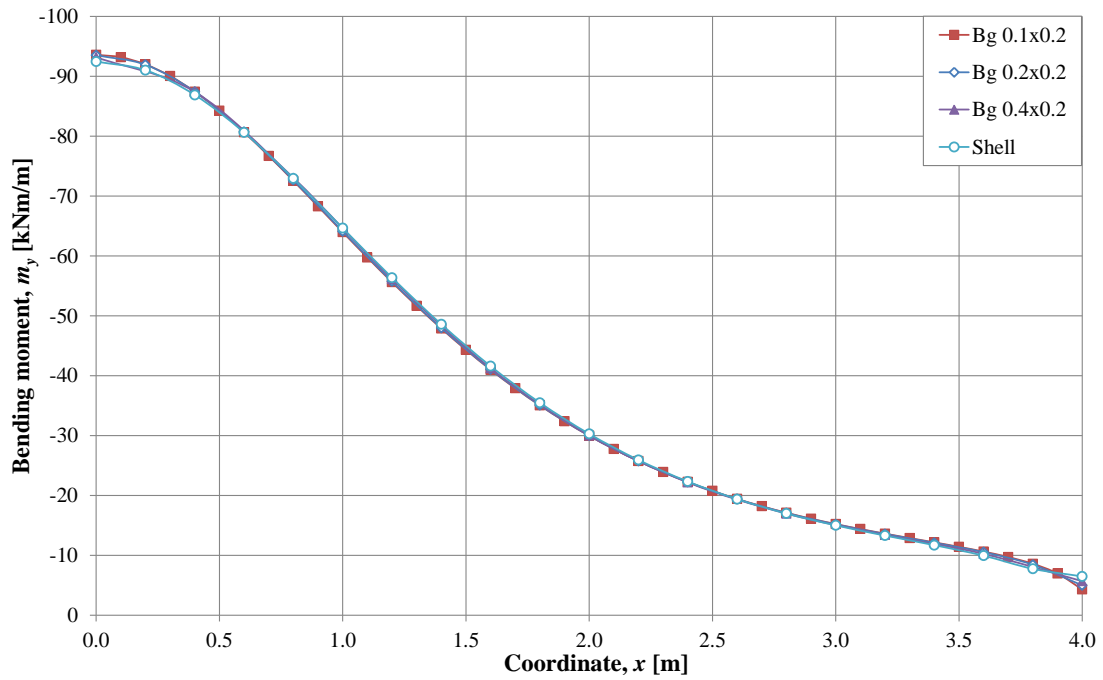


*Figure 4.26    Bending moment, $m_y$, along the fixed edge of the cantilever slab. Beam grillages modelled with modified torsional stiffness according to Table 4.1 and corresponding shell element model.*



*Figure 4.27    Bending moment, $m_y$, along the fixed edge of the cantilever slab. Beam grillages modelled with the default torsional stiffness and corresponding shell element model.*

From Figure 4.26 it can be seen that the models with modified torsional rigidity factors correlates very well to the shell element model. In addition, all three models generate almost identical results, i.e. the cross-section of the beams has negligible influence on the results. The slabs modelled as in Lim (2013) yields, as was already known, moments that deviates from the true solution, see Figure 4.27. The slab with quadratic cross-section corresponds rather well with the shell element model, but the result is nevertheless not fully similar compared to the results obtained using the shell element model.

The same tendency as was discovered for the bending moment applies to the displacement of the slab. Figure 4.28 and Figure 4.29 display the deformation curves along the symmetry line for the models with modified torsional rigidity and those modelled as in Lim (2013), respectively.



Figure 4.28    Vertical displacement, $u$, along the symmetry line for the cantilever slab. Beam grillages modelled with modified torsional stiffness and corresponding shell element model.

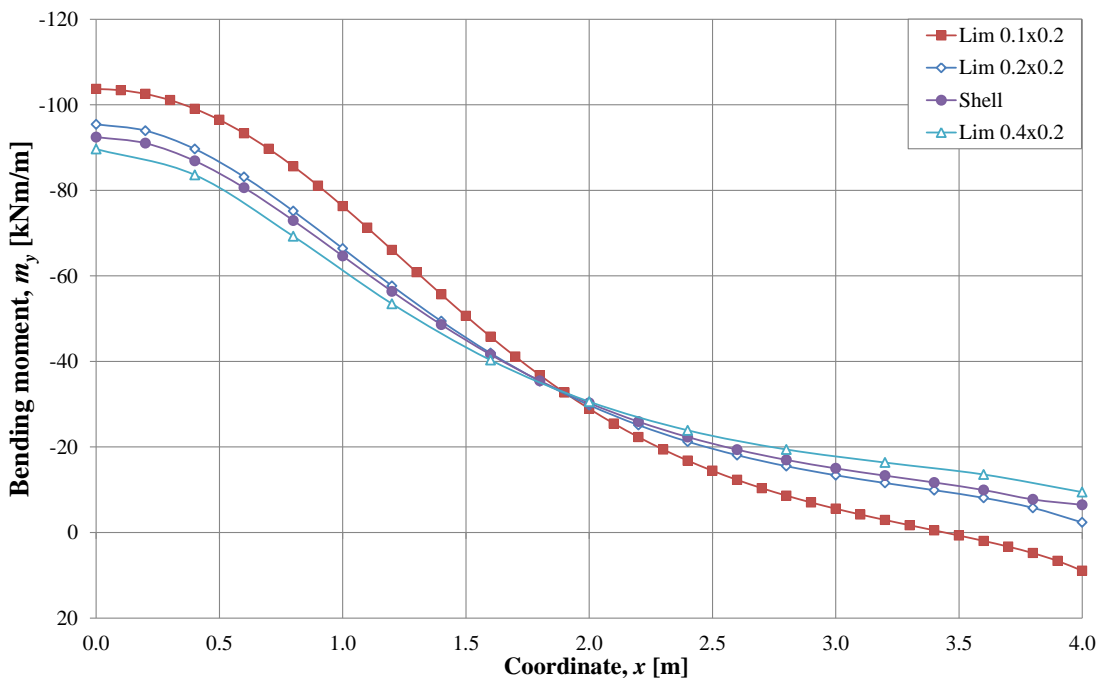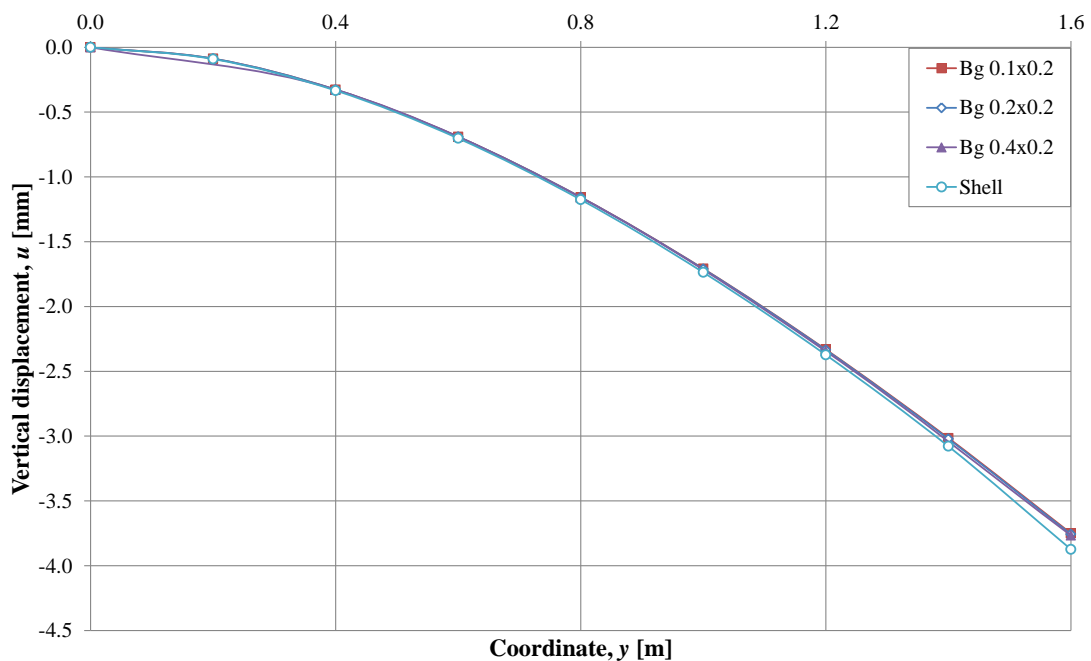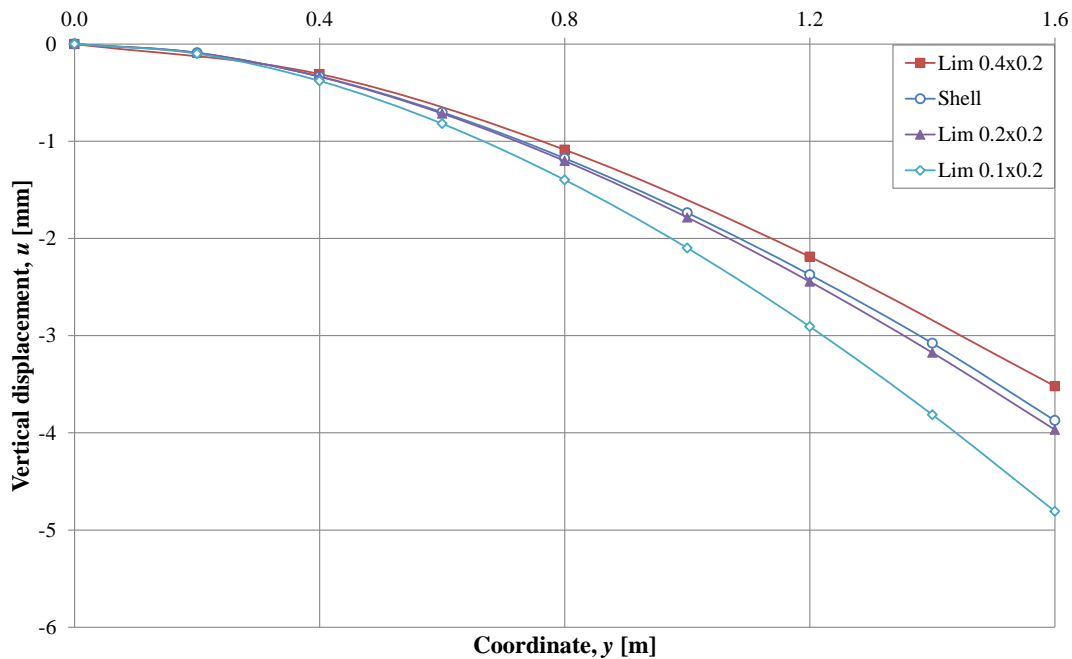*Figure 4.29   Vertical displacement, u, along the symmetry line for the cantilever slab. Beam grillages modelled with the default torsional stiffness and corresponding shell element model.*

As can be seen in Figure 4.28, the beam grillage models with modified torsional rigidity factors generate also for displacements almost identical curves. All three curves agree well with the displacement of the shell element model but deviates some in the maximum point. In contrast, for the slabs modelled as in Lim (2013), no such correlation between the displacement curves was obtained, see Figure 4.29. The slabs with rectangular beam cross-sections deviate far from the solution obtained using the shell element model. The slab with quadratic beam cross-section however, agrees rather well with the result from the shell element model. The displacement curve has a small deviation all along the symmetry line but the maximum value is closer to the true solution than for any of the slabs modelled with a modified torsional rigidity.

The displacement curve for the shell element model has a slight change of slope near the loading point, at the end of the symmetry line. This aberration was believed to be an indication of a local deviation at the point of loading. The load was applied in a single node, which as discussed in Section 3.2 may generate this type of deviation. When the moment distribution along the fixed edge is of interest, the small local deviation that occurs in the loading point can be neglected. This is due to the fact that the fixed edge is located a certain distance away from the loading point. However, in this study, where also the displacement was of concern, the load application may matter.

### 4.5.4   Response when subjected to distributed line load

To investigate if this assumption holds true, additional analyses of the cantilever slab but with a different load application was made. A 0.4 meter long line load with a magnitude of 250 kN/m was applied along the free edge, see Figure 4.30.
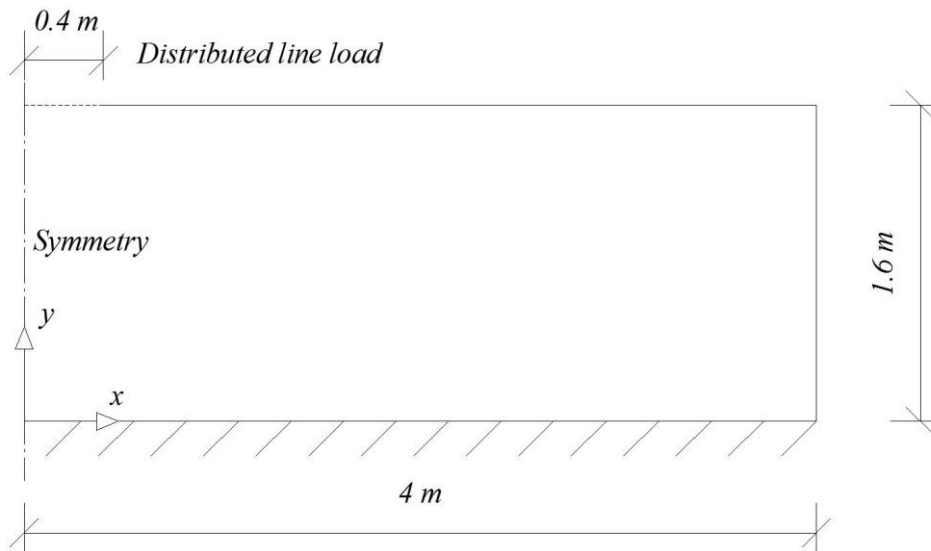
*Figure 4.30   Cantilever slab subjected to a distributed line load.*

The slabs with rectangular beam cross-sections modelled as in Lim (2013) were disregarded since the results deviate too much from the displacement of the shell element model. However, displacement curves for the other models are presented in Figure 4.31.
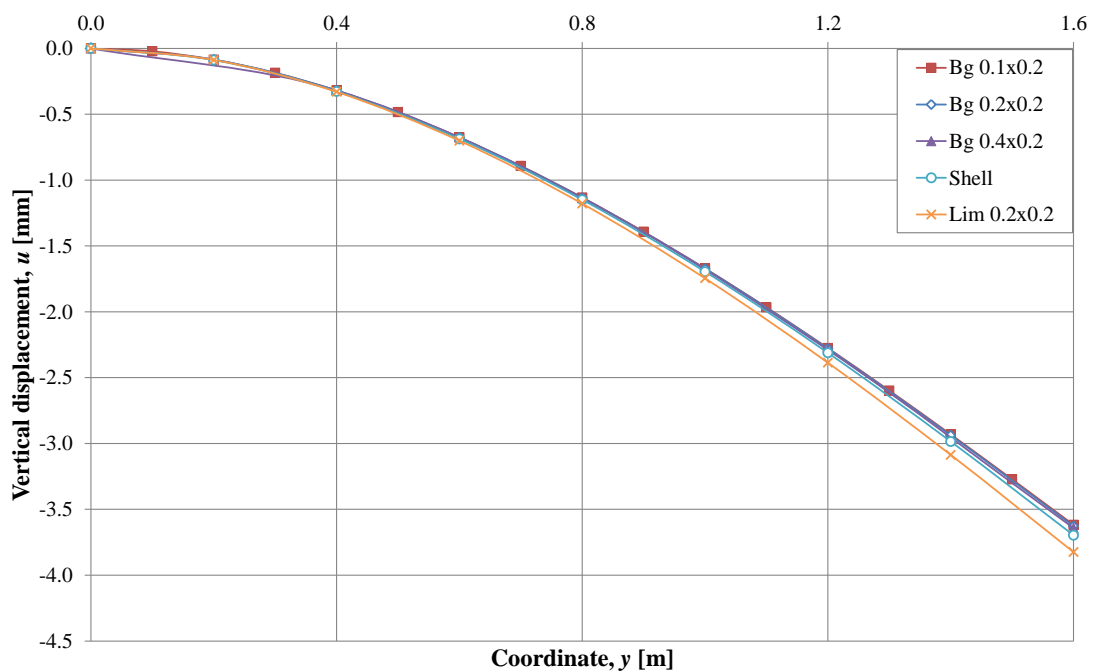


*Figure 4.31   Vertical displacement, u, along the symmetry line for the cantilever slab subjected to a distributed line load as in Figure 4.30.*

It can be seen that the displacement curve for the shell element model correlates well with the curves for the three slabs with modified torsional rigidity all along the symmetry line. The local deviation at the end of the line is eliminated. Hence, it was concluded that the application of load is of importance when studying the

displacement close to the point of loading. Furthermore, it was concluded that slabs where the torsional rigidity of the beams is defined as two times the moment of inertia generates accurate results. Additionally, and of great importance, is that the cross-section dimension has no influence on the results. Thus, the slab can be modelled with any arbitrarily chosen cross-section as long as $K_v = 2I_I$ is used.

### 4.5.5    Slab thickness versus span length

The two modelling approaches described in Section 4.4.2 and 4.5.2 generates contrary results regarding the use of rectangular beam cross-sections. Thus, it was of interest to investigate how the slab thickness versus the span length influences the results. The influence of shear deformations was believed to be a possible cause. Thus, it was decided to double the thickness of the cantilever slab to $t = 0.4$ meters. To avoid local deviations from the load application, a distributed line load was applied in the same manner as described in Section 4.5.4.

The bending moment $m_y$ was once again investigated along the fixed edge of the models. Figure 4.32 shows the moment distribution along the fixed edge.
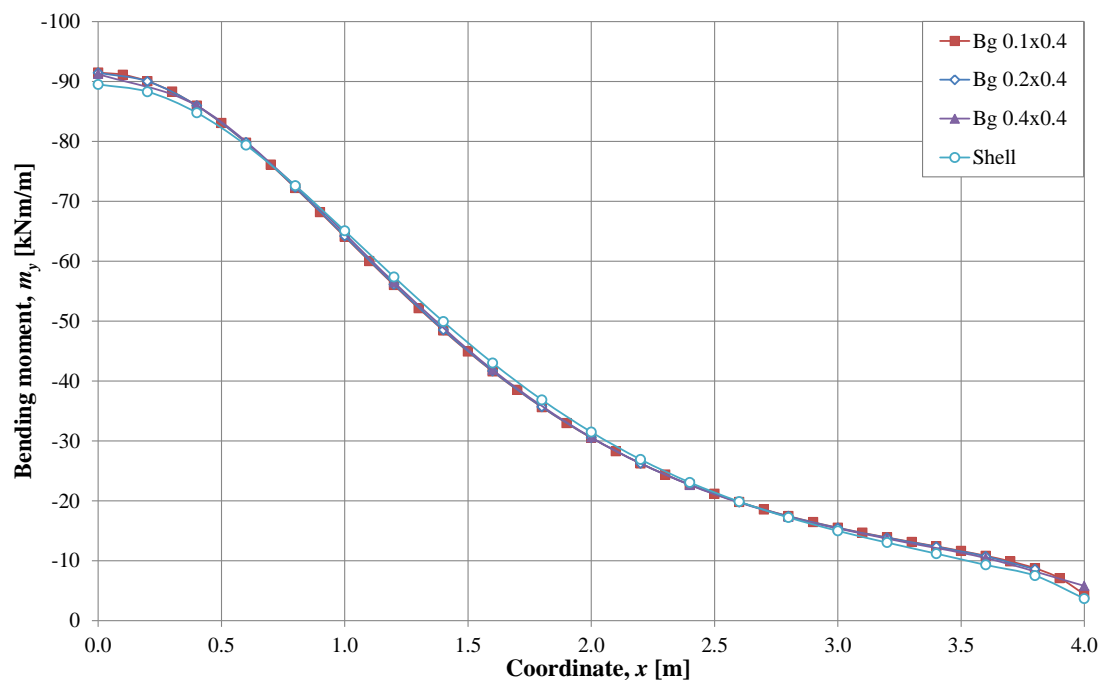


*Figure 4.32    Bending moment, $m_y$, along the fixed edge for the cantilever slab with a thickness, $t$ of 0.4 meters subjected to a distributed line load.*

As can be seen in Figure 4.32, the models with modified torsional rigidity generate a moment distribution that correlates well with the shell element model.

Increasing the thickness of the slab does not affect the moment distribution; the models with modified torsional rigidity generate accurate results. However, a study of the deformations was needed since if shear effects were present, they would probably be noticed in the displacement curves.

The displacement curves for the cantilever slab with double thickness are presented in Figure 4.33.



*Figure 4.33    Vertical displacement, u along the symmetry line for the cantilever slab with a thickness of 0.4 meters subjected to a distributed line load.*

As can be seen in Figure 4.33, similar results as presented in Figure 4.31 were acquired. The three models with a modified torsional rigidity still generate the same results irrespective of beam cross-section. However, they deviate more from the shell element model compared to the results of the thinner slab presented in Figure 4.31. Thus, it was concluded that the slab thickness versus the span length influences the displacements obtained in beam grillage models. The reason was believed to be due to shear deformations.

## 4.6    Influence of shear deformations

As was discovered in Section 4.5.5, displacements of the beam grillage models deviated from shell element models if the thickness of the cantilever slab was increased. The reason was believed to be related to shear deformations. To conclude if shear effects caused the deviations an investigation was made. For shell elements in ADINA, shear deformations are estimated as being constant over the element thickness. It is also stated that displacements disregarding shear deformations in shell elements may be estimated by multiplying the acquired deformations with a factor of 5/6 for rectangular cross-sections. To incorporate shear deformations in beam elements based on linear elastic material properties, ADINA offers the possibility to implement a shear area factor, $\beta$.

The shear area factor, $\beta$ in ADINA is multiplied with the specified cross-sectional area of the used beams to calculate the shear area, $S_A$ as in equation (4-7).

$$S_A = \beta w h \tag{4-7}$$

Where:     $S_A =$     Shear area
           $\beta =$     Shear area factor
           $w =$      Width of beam cross-section
           $h =$      Height of beam cross-section

The true value of the shear area factor varies in literature and is not straight forward to define. It depends on aspect ratio of the cross-section, the depth of the beam versus the span length and Poisson´s ratio. However, it was chosen to a value of 5/6 based on information provided in ADINA (2012).

Possible shear deformation effects were firstly investigated on the cantilever slab presented in section 4.5.5, with a thickness of the slab equal to 0.4 meters. The same beam grillage model as is presented in Figure 4.25 was tested. Displacement curves along the symmetry line with and without included shear deformations are presented in Figure 4.34.
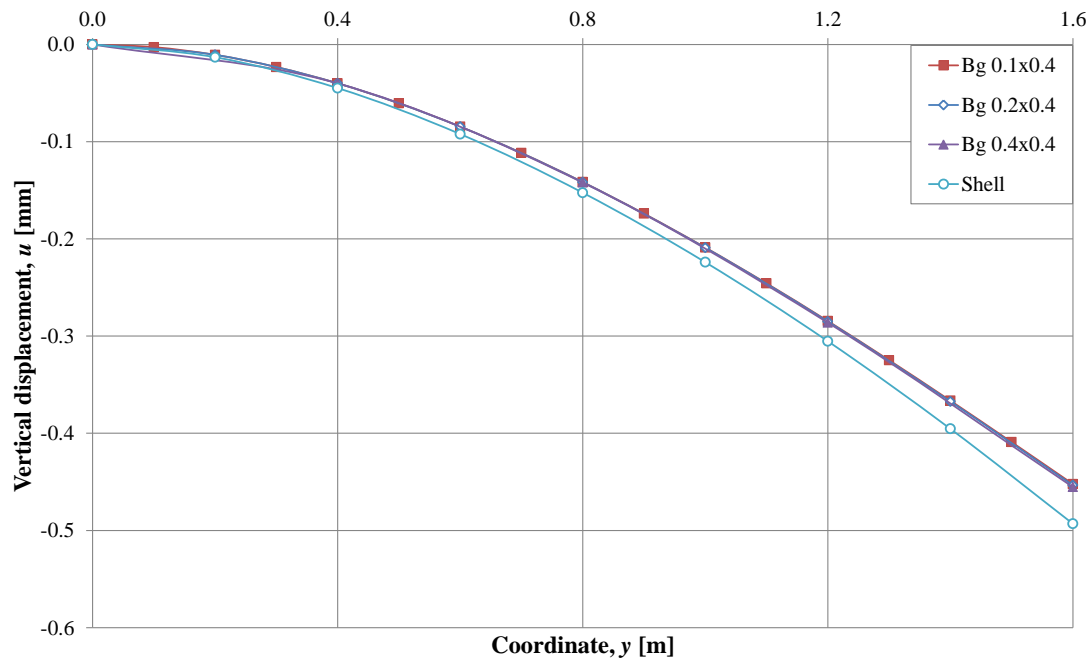


*Figure 4.34    Vertical displacement, u along the symmetry line for the cantilever slab with a thickness of 0.4 meters. Results from analyses both including and excluding shear deformations.*

As can be seen in Figure 4.34, if shear deformations are included in the analyses using beam grillage models, they generate satisfactory results in terms of displacement. The largest deviation from the shell element model is 0.8 % when shear deformations are considered. If shear deformations are disregarded the largest deviation is instead 8.3 %.

If Figure 4.31 is studied, accurate displacements were captured disregarding shear deformations. The reason for this behaviour was believed to be related to the fact that a slender slab is dominated by a flexural behaviour, i.e. no significant shear deformations take place. However, to verify this theory, shear deformations were

implemented in the beam grillage model presented in Figure 4.25, this time with a slab thickness equal to 0.2 meters. The deformation curves along the symmetry line of the cantilever slab are presented in Figure 4.35.
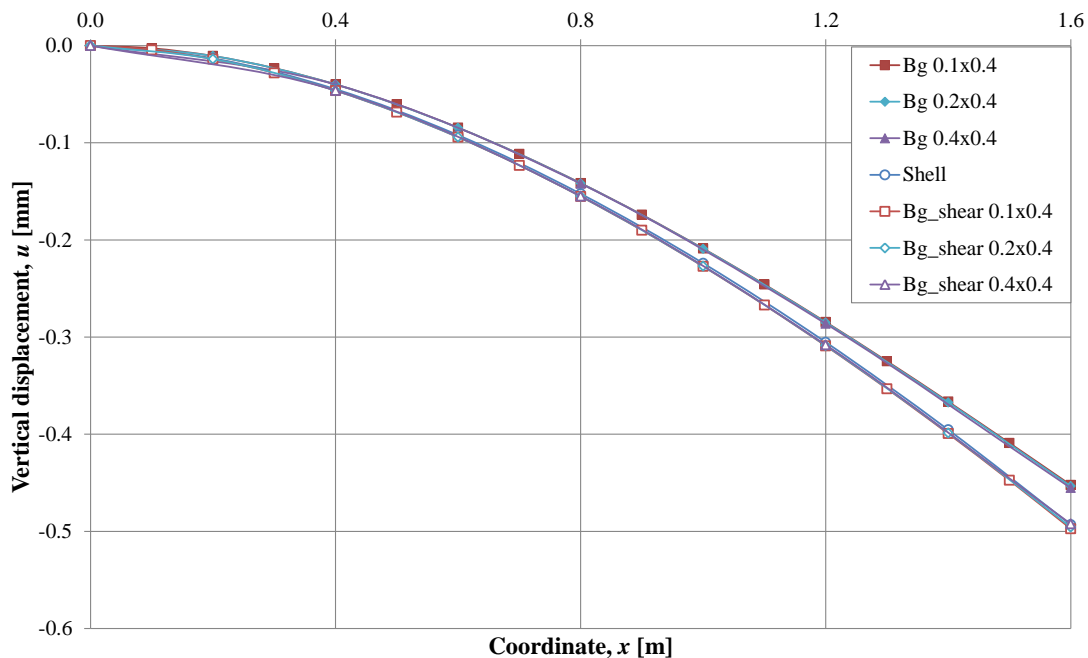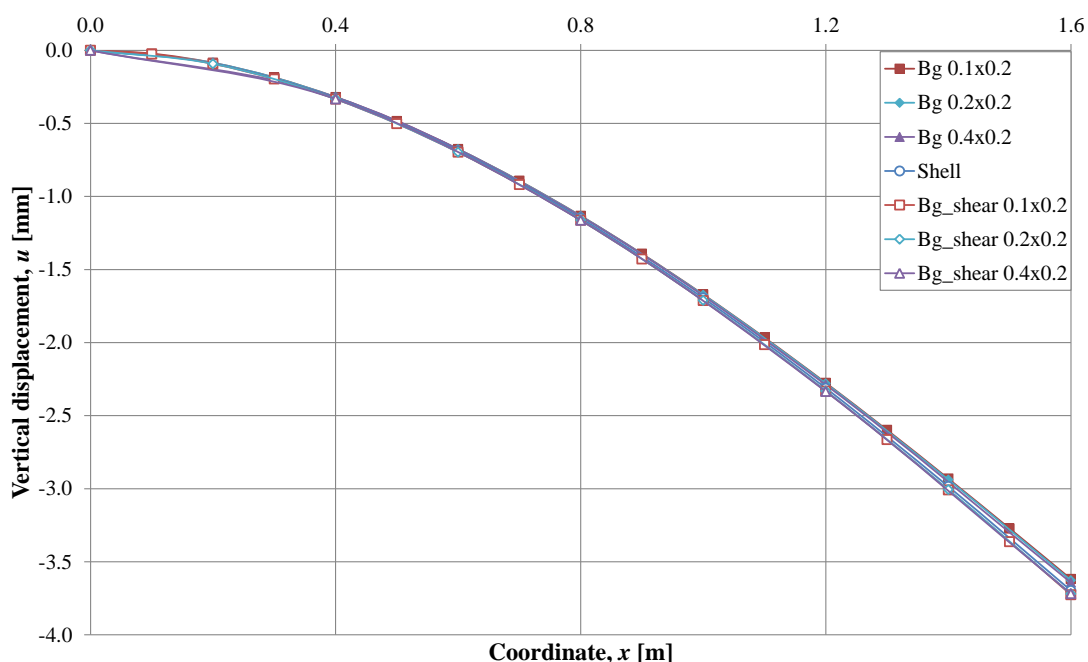


*Figure 4.35    Vertical displacement, u along the symmetry line for the cantilever slab with a thickness of 0.2 meters. Results from analyses both including and excluding shear deformations.*

Although the acquired deformations in the models disregarding shear deformations are accurate with a maximum deviation from the shell element model of 2.1 %, it can be seen in Figure 4.35 that including shear deformations yields even better accuracy where the largest deviation from the shell element model instead is 0.8 %.

From these results it seems as including shear deformations should be done for all beam grillage models intended to be compared to shell element models. Since the boundary conditions of the cantilever slab induce mainly bending action, it was of interest to study if shear deformations may also have caused the deviations investigated in Section 4.4.3, i.e. for a case predominantly subjected to torsional moments.

To investigate how shear deformations influence slabs subjected to torsion, two previously presented extreme cases were tested. The slabs presented in Figure 4.5 and Figure 4.6 are predominantly subjected to torsional moments. For width to height ratios of 0.2 and 5 both models generated displacements that deviated far from the displacement of their corresponding shell element models. This was believed to be related to the torsional stiffness of the beams.

However, since shear deformations seems to influence the acquired displacements, it was of interest to rerun the analyses including shear deformations. The displacement curves of the slabs with and without shear deformations are presented in Figure 4.36.
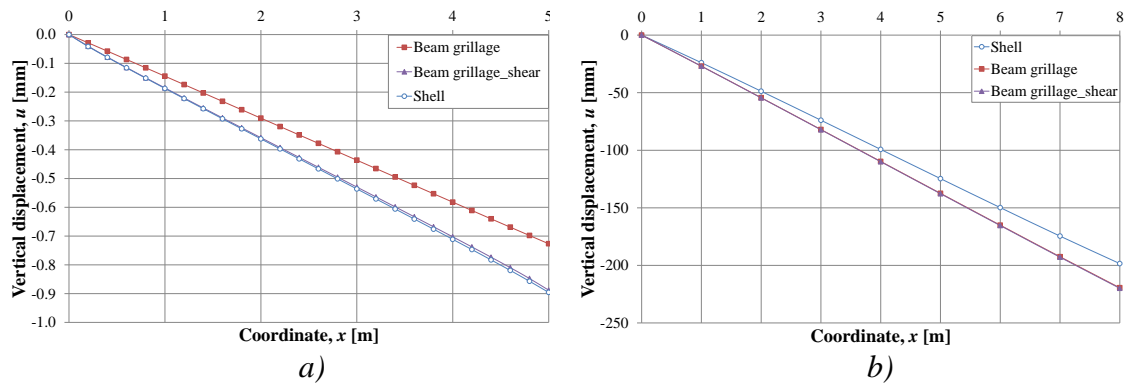
*Figure 4.36*     *Vertical displacement, u for slabs modelled as beam grillages with a width to height ratio of the beam cross-section of a) 0.2 and b) 5.0.*

From Figure 4.36a it can be stated that shear deformations have large impact on thick slabs since the 1.0-meter-thick slab deviates merely 0.9 % compared to the shell element model if shear deformations are accounted for. This should be compared to the results provided without shear deformations, which deviates by 23.3 %. Based on these results it can be concluded that shear effects should be accounted for in thick slabs.

From Figure 4.36b it can be noted that the displacement of the beam grillage model is the same irrespective if shear deformations are considered or not. This fact holds true regardless of the shear area implemented in the model. The reason why the displacement of the thinner slab is not affected by shear deformations was believed to be because the span to depth ratio is equal to 40, i.e. the slab is very slender and therefore does not transmit any significant transverse shear stresses.

Due to the limited timeframe of the project no further investigation was made regarding how the cross-section depth versus span length influences the shear deformations. It should however be noted that shear deformations in beam grillage models may generate substantial errors in terms of deformation measurements if neglected. Additionally, shear deformations were the cause of the deviations in Section 4.4.3 for width to height ratios less than 1.0. However, shear deformations do not generate the error acquired for width to height ratios larger than 1.0 which remained unsolved.

## 4.7     Torsion-twist and moment-curvature relation

As was stated in the beginning of Section 4.2 it is possible in ADINA to implement the torsional and flexural stiffness in two different ways. Instead of using the torsional rigidity factor to describe the torsional stiffness of a beam in ADINA it is also possible to define torsion versus angle of twist and flexural moment versus curvature relationships. Cross-section dimensions and material parameters are not inserted in the program, instead by defining analytically calculated torsion-twist and moment-curvature relations the equivalent torsional stiffness is computed by ADINA. Beam dimensions and material parameters are implemented when the relations are established. Angle of twist is calculated with equation (2-13) and for linear analyses the curvature is defined with equation (2-2).

If the same input parameters are used for analyses using the torsional rigidity factor or torsion-twist and moment-curvature relationships, the same results should be obtained. The slab illustrated in Figure 4.5 in Section 4.4.3, was modelled once again but this time with torsion-twist and moment-curvature relationships instead of the torsional rigidity factor to verify that both models generate same results. In both models the theory of Hallbjörn (2015), saying that $K_v = 2I$ for beam grillages, was applied. The acquired results from both models showed exactly the same vertical displacement and it was concluded that both ways of implementing the torsional stiffness of a beam in ADINA can be utilised.

## 4.8 Discussion

### 4.8.1 Modelling techniques

Two different approaches have been used to establish beam grillage models for isotropic linear elastic analyses; according to Hallbjörn (2015) in Section 4.4.2 and according to previous master's theses in Section 4.5.2. The results between the modelling techniques are not in full agreement. The most accurate results and reasonable behaviour were achieved by modelling according to Section 4.5.2 with a torsional rigidity factor based on the torsional stiffness being equal to two times the moment of inertia as in Table 4.3. The deviation in the displacement was concluded to be related to the thickness of the studied slabs.

It was also discovered that the modelling technique adapted from Hallbjörn (2015) have certain limitations. Modelling as in Section 4.4.2 prevents the placement of loads and boundary conditions at the outermost edges of the true slab geometry. Accordingly, results for the outermost strips in slabs modelled in this manner cannot be investigated. Figure 4.37 exemplifies how edge strips cannot be investigated using this modelling technique.
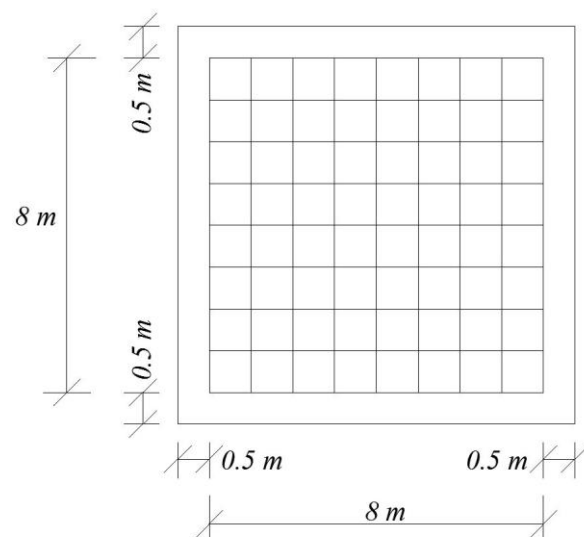


*Figure 4.37    Illustration of beam grillage geometry according to the modelling technique adapted by Hallbjörn (2015), described in Section 4.4.2.*

If beams with a width equal to 1.0 meter are used, the edge strips will be equal to 0.5 meters. The stiffness proportions of the beam grillage will match the stiffness of a 9 x 9 meters shell element model. However, no nodes will be generated at the first and last 0.5 meters along the length of the slab in both directions in the beam grillage model. The size of these edge strips can be reduced by decreasing the width of the beams, but they will always be present. Since no nodes are present at the edge strips, accordingly no results can be extracted.

With these limitations in mind all beam grillage models presented further in the Thesis are modelled with edge beams as described in Section 4.5.2. The linear elastic torsional stiffness of those models was implemented according to equation (4-2).

As is confirmed in Section 4.5.5, displacements may deviate slightly depending on the slab thickness but the moment distribution is not influenced by this effect. From a static design perspective, the moment distribution is more important than the displacements. If deformation checks are to be performed in the serviceability limit state, cracking should be taken into account.

## 4.8.2    Linear elastic torsional stiffness

From the tests of the torsional rigidity factor presented in Section 4.4 it was concluded that the usage of correction factors is case specific when the modelling technique in Section 4.4.2 is utilised. Thus, it was decided that for the modelling performed in Section 4.5.2, the torsional stiffness should be implemented as two times the moment of inertia, described in equation (4-3) without correction factors.

Satisfactory results were acquired of the cantilever slab presented in Section 4.5.3 modelled with a torsional stiffness defined as in equation (4-3). It was discovered in Section 4.5.5 that the slab thickness versus span length influences the displacements of beam grillage models when compared to shell element models. It was proven to be related to how shear deformations are handled in beam elements and shell elements in ADINA, respectively. However, the moment distribution was unaffected by the phenomenon.

Since the study also will treat the nonlinear response of reinforced concrete slabs, it is important to keep in mind that possible shear deformations might occur in load versus displacement curves used to investigate the response. Since the material parameters in the nonlinear analyses will be defined as in Section 4.7 with moment-curvature and torsion-twist relations, no shear area factor can be defined for the beams. Thus, there might be deviations based on the fact that shear deformations are not accounted for. If shear deformations are important for the studies, it is more convenient to not use moment-curvature relations to define the beams. It was also stated in Section 4.6 that the choice of shear area factor is not obvious. Since ADINA stated that a factor of 5/6 could be used to estimate deformations without shear effects in linear elastic shell element models, it was assumed to be an appropriate choice for the beam grillage models.

# 5 Non-linear analyses

## 5.1 Orientation
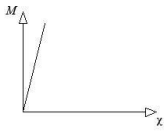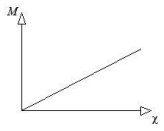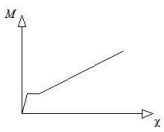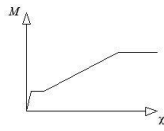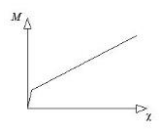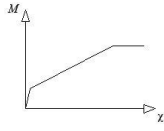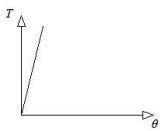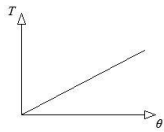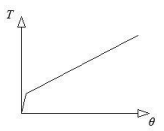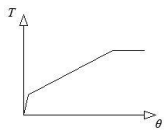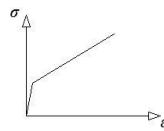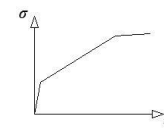
As a reasonable linear elastic behaviour of a beam grillage model was established in Chapter 4, the next step was to perform nonlinear analyses. The nonlinear response has not been successfully captured using beam grillage models in previous Theses. The problem has been believed to be related to the torsional stiffness, in specific the loss of stiffness due to cracking. This chapter intends to investigate how the transition from State I to State II should be modelled with regard to torsion. Both beam grillage models and shell element models were compared to experimental results presented in Lopes *et al.* (2014), which acts as a true nonlinear response. It was also investigated if the State II torsional stiffness could be related to the State II flexural stiffness as was the case for State I sections in linear elastic analyses. Examples of in-files used in ADINA are presented in Appendix H.

## 5.2 Notations

When performing nonlinear analyses in ADINA the material properties are defined in means of moment-curvature and torsion-twist relationships. In this chapter, several different analyses are made using varying moment-curvature and torsion-twist curves. Thus, notations describing the different curves were compiled in order to simplify the presentation of the result curves obtained. The different notations, together with a short description and a schematic figure of the relationship are presented in Table 5.1. However, explanations of the curves are presented continuous in the chapter as the different input data are acquired.

As an illustration, a curve defined as *Bg M2T3* is a beam grillage (Bg) with a linear State II moment-curvature relation (M2) and a bilinear torsion-twist relation (T3).

*Table 5.1    Notations used in Chapter 5 to describe which moment-curvature, torsion-twist and stress-strain curve that are used as input in ADINA.*

| Relation | Notation | Description | Schematic figure |
|---|---|---|---|
| Moment-curvature | M1 | Linear State I |  |
| | M2 | Linear State II |  |
| | M3 | Trilinear, cracking plateau |  |
| | M4 | Quadlinear, cracking and yielding plateau |  |
| | M5 | Bilinear, modified State II stiffness |  |
| | M6 | Trilinear, modified State II stiffness and yielding plateau |  |
| Torsion-twist | T1 | Linear State I |  |
| | T2 | Linear State II |  |
| | T3 | Bilinear |  |
| | T4 | Trilinear, yielding plateau |  |
| Stress-strain | S1 | Bilinear |  |
| | S2 | Trilinear |  |

## 5.3    Experiments performed by Lopes *et al.*

In Lopes *et al.* (2014) nine quadratic reinforced concrete slabs were subjected to torsional effects. Measurements of load versus displacement and torsion versus angle of twist were made whilst loading the slabs by displacement control until failure. The scope of the experiments was to investigate how the torsional stiffness changes due to cracking. The experimental setup is illustrated in Figure 5.1.
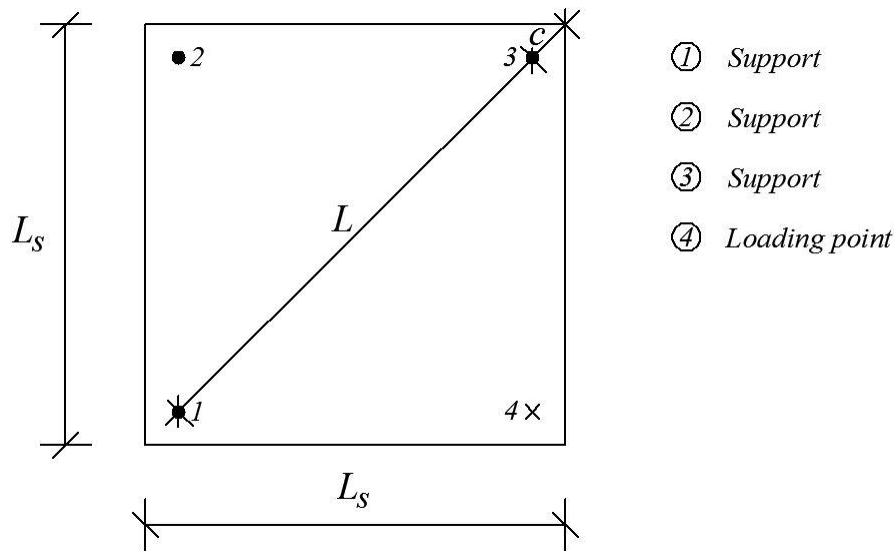


*Figure 5.1     Schematic illustration of the test setup used in Lopes et al. (2014).*

Two different sizes of slabs were used in the experiments. The diagonal measurement, $L$ between the main points of the slab was either 2.5 meters or 3.5 meters. The side length of the two slab types $L_s$ was either 2.1 meters or 2.8 meters yielding a $c$ distance of 0.25 meters in both cases. The slab thickness was supposed to be 0.15 meters for all specimens. However, some variations occurred and a mean value of the thickness was calculated for each slab.

At the day of testing the concrete used in the slabs had varying maturity. Accordingly, compression tests on cylinders in accordance with Eurocode 2, CEN (2004), were performed on the day of testing to determine the mean compressive strength $f_{cm}$ of the concrete used in each slab.

Table 5.2 states the geometrical data and material parameters of the concrete for the nine slabs used in the experiments.

*Table 5.2*     *Geometry and concrete material parameters of the nine experimental slabs presented in Lopes et al. (2014).*

| Slab no. | $L$ [m] | $L_s$ [m] | $t$ [m] | $f_{cm}$ [MPa] | $\nu$ [-] |
|---|---|---|---|---|---|
| 1 | 2.5 | 2.1 | 0.156 | 24.9 | 0.2 |
| 2 | 2.5 | 2.1 | 0.144 | 24.6 | 0.2 |
| 3 | 2.5 | 2.1 | 0.153 | 25.0 | 0.2 |
| 4 | 2.5 | 2.1 | 0.156 | 24.9 | 0.2 |
| 5 | 2.5 | 2.1 | 0.155 | 33.8 | 0.2 |
| 6 | 2.5 | 2.1 | 0.160 | 33.8 | 0.2 |
| 7 | 3.5 | 2.8 | 0.148 | 29.0 | 0.2 |
| 8 | 3.5 | 2.8 | 0.150 | 29.2 | 0.2 |
| 9 | 3.5 | 2.8 | 0.149 | 29.3 | 0.2 |

In Lopes *et al.* (2014) the mean compressive strength of the concrete was the only material parameter presented. Based on $f_{cm}$, the recommendations given in Table 3.1 in Eurocode 2, CEN (2004) were used to derive other material parameters such as Young's modulus and tensile strength.

Two different reinforcement arrangements were used in the experiments. Either $\phi 8\ s100$ or $\phi 10\ s150$ was used. The material properties of the reinforcing steel for the nine slabs are presented in Table 5.3.

*Table 5.3*     *Material properties of the reinforcing steel.*

| Slab no. | Type of steel | Bar diameter $\emptyset$ and spacing $s$ | $f_{sym}$ [MPa] | $f_{su}$ [MPa] | $\varepsilon_{su}$ [%] |
|---|---|---|---|---|---|
| 1 | Cold-worked | $\emptyset 8/s100$ | 576 | 629 | 5.40 |
| 2 | Cold-worked | $\emptyset 8/s100$ | 585 | 631 | 4.74 |
| 3 | Cold-worked | $\emptyset 10/s150$ | 620 | 669 | 5.20 |
| 4 | Cold-worked | $\emptyset 10/s150$ | 617 | 666 | 5.96 |
| 5 | Cold-worked | $\emptyset 8/s100$ | 529 | 646 | 5.60 |
| 6 | Cold-worked | $\emptyset 8/s100$ | 529 | 646 | 5.60 |
| 7 | Hot-rolled | $\emptyset 8/s100$ | 542 | 666 | 9.43 |
| 8 | Hot-rolled | $\emptyset 8/s100$ | 542 | 666 | 9.43 |
| 9 | Hot-rolled | $\emptyset 8/s100$ | 542 | 666 | 9.43 |

The reinforcement bars were placed perpendicular to each other creating a mesh with the same reinforcement amount in both directions. Two such meshes were placed in each slab. The meshes were located with certain distances $a_1$ = 20 mm and $a_2$ = 110 mm from the compressive edge of the slab. The reinforcement arrangement is depicted in Figure 5.2. Note that the measurements $a_1$ and $a_2$ are not defined to the centre of the bars, but to the bottom of each reinforcement mesh.
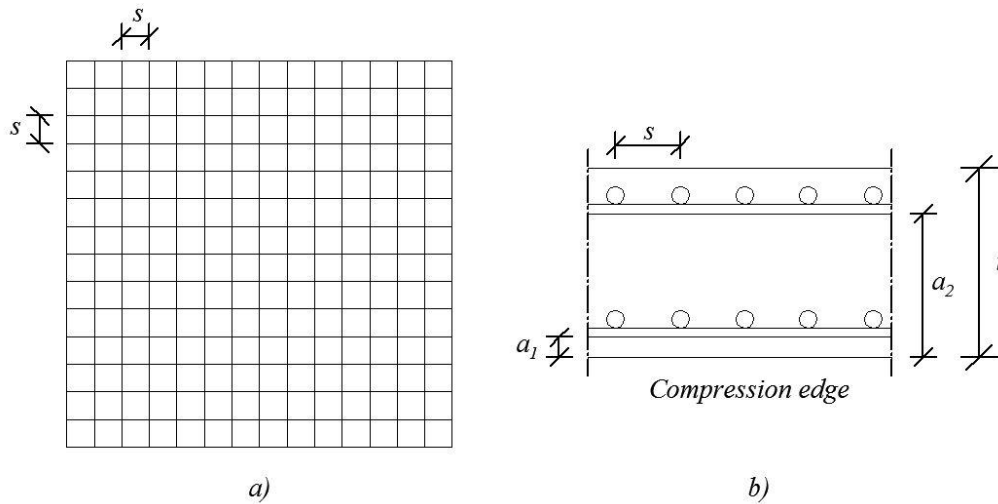


*Figure 5.2    Reinforcement arrangement as a) mesh seen from top view and b) cross-section of the slabs.*

For analytical calculations the stiffness contribution from transverse reinforcement bars was neglected. The centre distances from the compressive edge to the reinforcement bars, $d_1$ and $d_2$ were estimated by adding the diameter of one bar to the $a_1$ and $a_2$ measurements. The cross-section used for analytical calculations is presented in Figure 5.3.
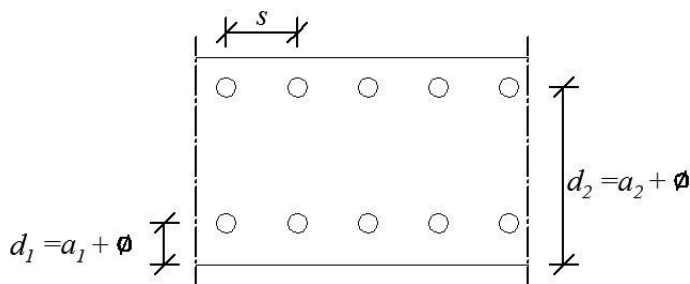


*Figure 5.3    Cross-section used for analytical calculations.*

## 5.4    Beam grillage model, simply supported slab

Slab number 1 in Lopes *et al.* (2014) was chosen for the nonlinear analysis in ADINA. For geometry and material parameters, see Table 5.2 and Table 5.3. However, when modelling a beam grillage in ADINA the beam cross-sections have to be chosen so that the outer dimensions and the diagonal length corresponds to the real measurements concurrently as nodes are generated at the point of loading and supports. It was not possible to fulfil every requirement though and a compromise was done.

The width of the beam cross-sections was defined as 0.177 meters. With thirteen beams in each direction, the outer dimension of the modelled slab was 2.124 meters and the diagonal length was 2.503 meters. That constellation also generates nodes situated close to the experimental setup. The height of the cross-sections was chosen to 0.156 meters, equal to the mean thickness of the experimentally tested slab. The geometry of the modelled slab is illustrated in Figure 5.4.
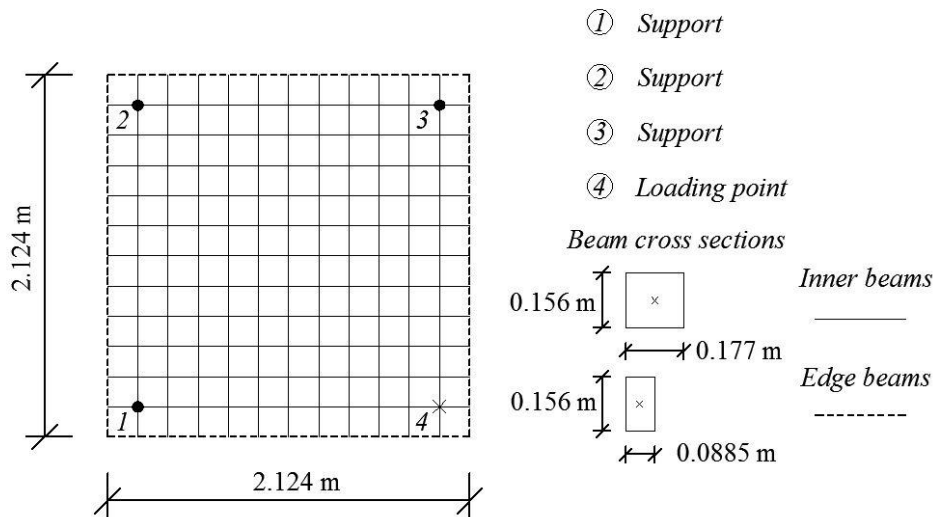


*Figure 5.4     Geometry of the beam grillage model.*

The supports were modelled in ADINA as simply supported point supports and the point load was applied to a single node to resemble the load application used in the experiments. A load of 80 kN was applied in 500 steps with equal magnitude, i.e. 0.16 kN in every step.

## 5.5     State II torsional stiffness

### 5.5.1     Orientation

In order to describe the nonlinear properties of the reinforced concrete in ADINA, torsion-twist and moment-curvature relations were used. The nonlinear response of beams subjected to bending is well known and simplified moment-curvature relationships, as described in Section 2.2, are easily established. However, the State II torsional stiffness of a beam grillage is not as thoroughly studied.

### 5.5.2     Linear elastic hypothesis

In Chapter 4, a linear elastic relationship for the torsional stiffness was defined for sections in State I. By defining the torsional stiffness of a beam grillage as two times the moment of inertia of a single beam, an appropriate stiffness was acquired, as suggested in Hallbjörn (2015). However, for State II, no such relation was pre-defined in the literature and the inclination of the torsion-twist curve was therefore hard to predict.

As a first attempt to find a relationship that describes the torsional stiffness of cross-sections in State II, the same analogy as for State I was tested. Hence, the torsional stiffness for State II was defined as two times the moment of inertia of a cracked beam, see equation (5-1).

$$K_{v,II} = 2I_{II} \tag{5-1}$$

Where: $K_{v,II}$ = Torsional stiffness of a fully cracked section.

Additionally, in order to establish a bilinear torsion-twist curve that compile the behaviour of both the uncracked and the cracked section the breakpoint, i.e. the torsional cracking moment, has to be known. Figure 5.5a illustrates a schematic bilinear torsion-twist curve. However, since it is difficult to analytically define the torsional cracking moment, a bilinear torsion-twist curve could not be established. Instead the torsion-twist was defined with two linear relationships; one for State I and one for State II, see Figure 5.5b and Figure 5.5c.
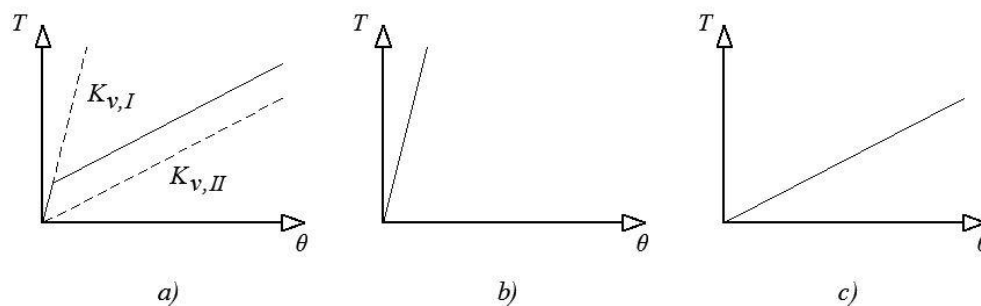


*Figure 5.5    Torsion-twist relation as a) bilinear b) linear based on State I c) linear based on State II.*

The moment-curvature relation was analytically defined as in Figure 5.6a. It is a simplified relation describing the nonlinear behaviour with a quadlinear curve. The first part of the curve corresponds to the uncracked section, then there is a plateau representing the loss of stiffness when the section starts to crack. The second inclined line describes the response of a cracked section and the last part of the curve illustrates the ultimate limit state. However, when implementing curves with plateaus in ADINA convergence problems may arise. In order to prevent such problems, the plateaus were given a small inclination. A value of 1.05 times the cracking moment and the moment resistance were computed and the curvatures were calculated accordingly. The modified moment-curvature relationship that was inserted in ADINA is shown in Figure 5.6b. This small change in inclination influences the results slightly but the deviation was assumed to be negligible.

Calculations of cracking moment, moment resistance and the corresponding curvatures can be found in Appendix D.
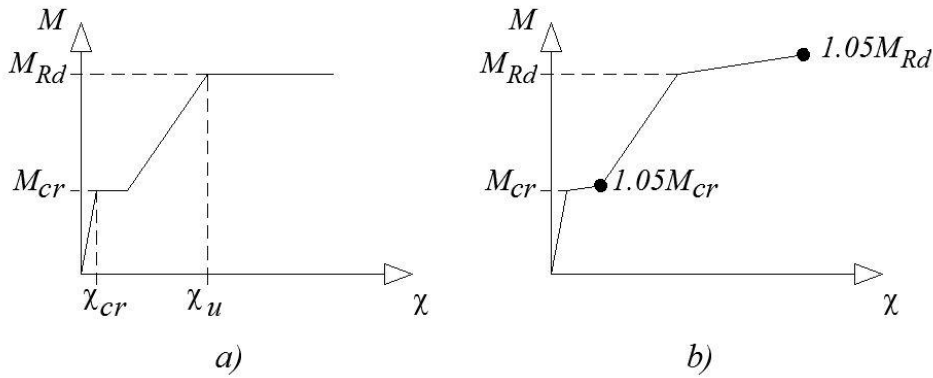
*Figure 5.6    The nonlinear moment-curvature relationship; a) analytically defined and b) the modified relationship implemented in ADINA.*

Consequently, two analyses were made. The first one had a torsion-twist relation based on the stiffness of State I and in the second analysis the relation was based on the assumed stiffness of State II. However, the nonlinear moment-curvature relationship was the same in both analyses since it describes the behaviour of all states. In Figure 5.7 the load versus displacement curve from the analysis with a torsion-twist relation based on the stiffness of State I is presented. Figure 5.8 presents the result from the analysis with a torsion-twist relation based on State II. Result from the experiment in Lopes *et al.* (2014) is also displayed in both figures.
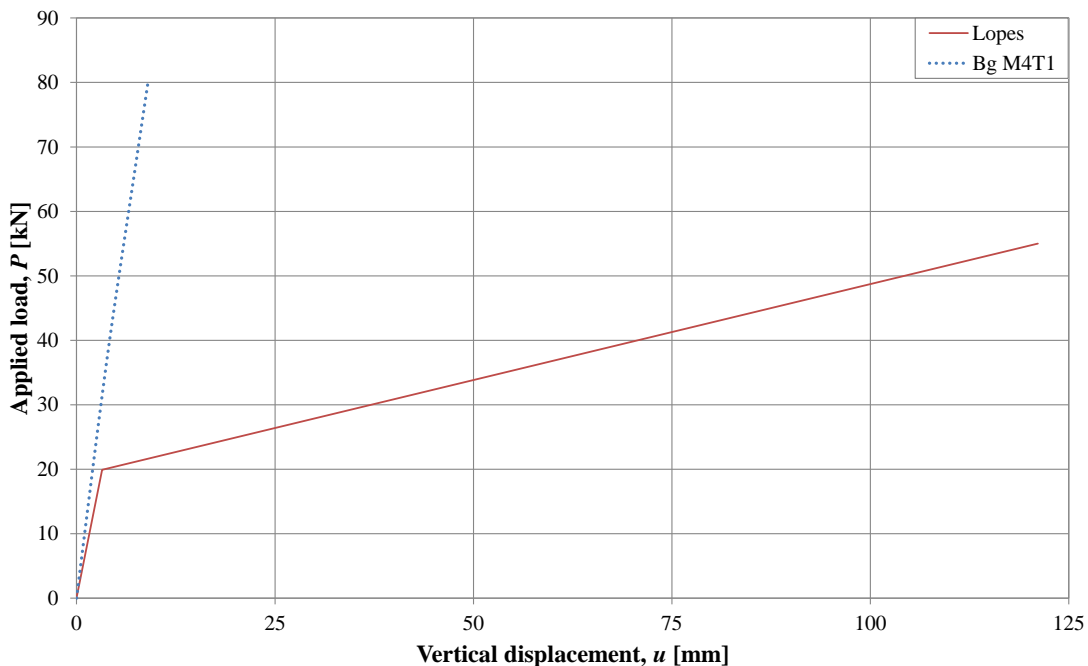


*Figure 5.7    Vertical displacement, u, at the point of loading for the studied slab with nonlinear moment-curvature relationship and linear torsion-twist relationship based on the torsional stiffness of a State I cross-section.*
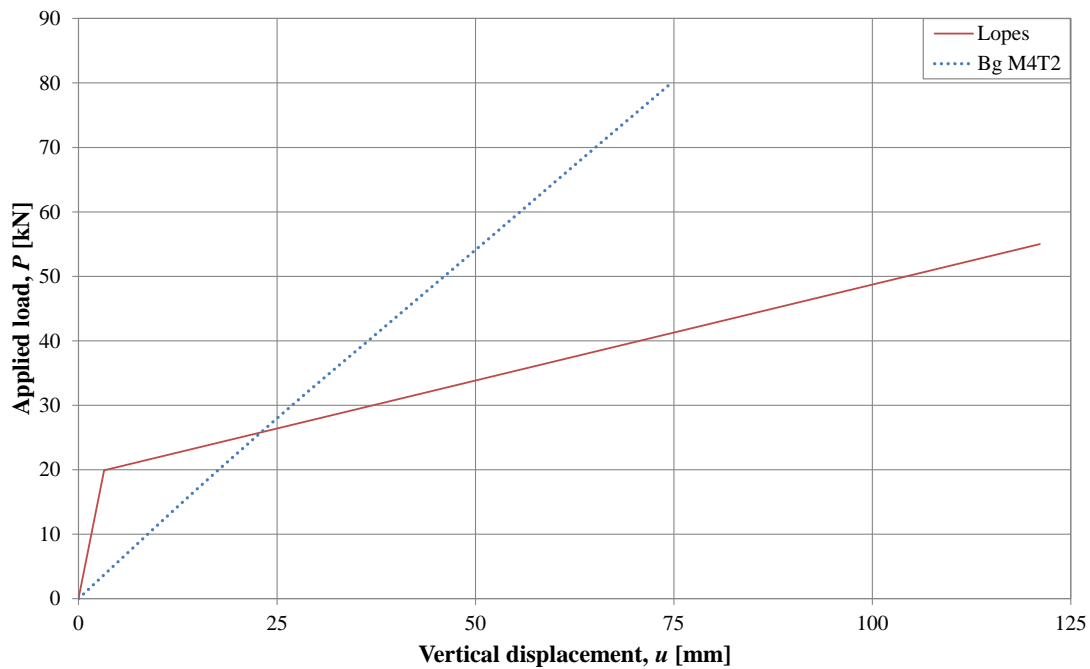
*Figure 5.8    Vertical displacement, u, at the point of loading for the studied slab with nonlinear moment-curvature relationship and linear torsion-twist relationship based on the torsional stiffness of a State II cross-section.*

The inclination of the curve from the analysis with State I stiffness corresponds rather well with the experimental result. Still, a small deviation can be seen but the reason for the divergence is not known. However, the same phenomenon was seen in the linear analyses in Section 4.4.3. The linear analyses performed on quadratic slabs with similar support and load placement, with a torsional stiffness equal to two times the moment of inertia, also differed slightly from the true solution when studying displacements.

Furthermore, by looking at Figure 5.8 it can be noted that the assumption saying that the torsional stiffness in State II should be calculated in the same manner as for State I, i.e. $K_v = 2I_{II}$, is incorrect. The inclination of the displacement curve received from ADINA is more than 3.5 times steeper than the curve from the experimental results. It seems like defining the torsional stiffness in State II as two times the moment of inertia highly overestimates the stiffness. However, to eliminate that the result received only holds true for this slab further studies were made. It was investigated if a correlation could be found between the moment of inertia and the torsional stiffness for State II for any of the nine slabs tested in Lopes *et al.* (2014). The formation and the results of the study can be read in Section 5.7.

Another interesting observation is that even though the inserted moment-curvature relationship is nonlinear, both analyses yield linear result curves. It seems like the input used to describe bending action have no or little influence of the results when the slab is subjected to mainly torsional moments. To confirm that premise, the analyses were made once again. This time also the inserted moment-curvature relations were linear; one for State I and one for State II. The same torsion-twist relations as in the previous analyses were used. The resulting load-displacement

curves, together with the results from the previous analyses and the experimental data, can be found in Figure 5.9.
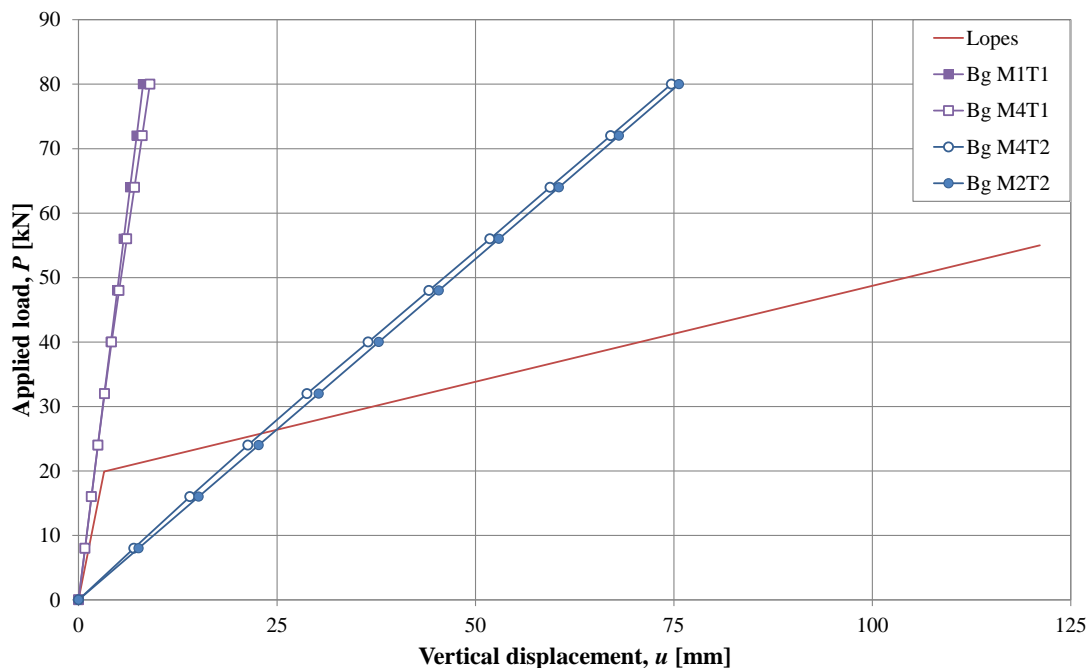


*Figure 5.9*    *Vertical displacement, u, at the point of loading for the studied slab with linear relationships for both moment-curvature and torsion-twist for State I and State II.*

By looking at the result curves in Figure 5.9 it can be concluded that the assumption above is likely to be true. For this slab, which is subjected to mainly torsional moments, the moment-curvature input has very little influence of the results. Thus, the implemented torsional stiffness seems to be a very important parameter for the studied case. The linear displacement curves are due to the linear shape of the inserted torsion-twist curves. In other words, to be able to receive the nonlinear result obtained in the experiments, nonlinear torsion-twist curves have to be defined.

In order to establish such curves, in addition to relations describing the torsional stiffness for State I and State II, the torsional cracking moment needs to be defined.

## 5.6    Torsional cracking moment

In Section 5.5 it was concluded that to achieve a nonlinear response of a beam grillage model subjected to torsion, the torsional moment versus angle of twist relationship needs to be established as a bilinear relation. To establish a bilinear response curve, the torsional cracking moment, $T_{cr}$, has to be known. However, since analytical calculations of the torsional cracking moment are complex it was of interest to study if a relation between the flexural cracking moment, $M_{cr}$, and the torsional cracking moment, $T_{cr}$, exists.

The cracking moment due to bending is calculated based on the tensile strength of the studied concrete. Since only compression tests of the concrete were made in

Lopes *et al.* (2014), only the mean compressive strength, $f_{cm}$ is presented. However, the mean compressive strength can according to Eurocode 2, CEN (2004), be used to calculate the mean axial tensile strength, $f_{ctm}$. Furthermore, $M_{cr}$, should be based on a section in bending. Thus, the flexural tensile strength $f_{ctm,fl}$ should be calculated by multiplying $f_{ctm}$ with a factor $k$ which accounts for the cross-section height or the so called size effect. The calculation of the correction factor $k$ varies in the literature. According to Eurocode 2 it should be calculated as in equation (5-2).

$$k = 1.6 - \frac{h}{1000} \tag{5-2}$$

Where:  $k = $  Correction factor due to size effect
        $h = $  Height of cross-section [mm]

In BBK04, Boverket (2004), the $k$ factor is calculated according to equation (5-3).

$$k = 0.6 + \frac{0.4}{\sqrt[4]{h}} \tag{5-3}$$

Where:  $h = $  Height of cross-section [m]

Equation (5-2) and equation (5-3) does not yield the same results, thus different flexural tensile strengths and accordingly different cracking moments will be acquired based on how calculations are made. For the experimental slabs the $k$ factor is approximately 1.45 based on Eurocode 2 as in equation (5-2), whereas it is 1.24 if the approach suggested in BBK04 is adapted, equation (5-3).

Therefore, it was decided to calculate the cracking moment due to bending for three cases of tensile strength. The calculations were made based on the mean axial tensile strength $f_{ctm}$, the flexural tensile strength $f_{ctm,fl}$ as in Eurocode 2 and the flexural tensile strength $f_{ctm,fl}$ as in BBK04. Calculations of $M_{cr}$ for the nine slabs presented in Lopes *et al.* (2014) are presented in Appendix E.

Table 5.4 presents how the flexural cracking moment based on the axial tensile strength, $f_{ctm}$ correlates with the torsional cracking moment from the experiments.

*Table 5.4    Analytical flexural bending moment based on the mean axial tensile strength, $f_{ctm}$, compared to the experimental torsional cracking moment.*

| Slab no. | $M_{cr}$ [kNm/m] | $T_{cr}$ [kNm/m] | $M_{cr}/T_{cr}$ [-] |
|----------|------------------|------------------|---------------------|
| 1        | 8.01             | 8.12             | 0.99                |
| 2        | 6.75             | 7.81             | 0.86                |
| 3        | 7.74             | 8.37             | 0.93                |
| 4        | 8.01             | 7.76             | 1.03                |
| 5        | 10.49            | 9.42             | 1.11                |
| 6        | 11.18            | 10.12            | 1.10                |
| 7        | 8.33             | 6.54             | 1.27                |
| 8        | 8.62             | 6.64             | 1.30                |
| 9        | 8.53             | 7.16             | 1.19                |
| Average: | -                | -                | 1.09                |

As can be seen in Table 5.4, the flexural cracking moments based on $f_{ctm}$ are rather close to the torsional cracking moment if the average value is studied. However, if the slabs are studied individually there is a scatter in the results. The deviation of the $M_{cr}/T_{cr}$ ratio seems to be case specific, i.e. no correlation was found to explain why certain slabs deviate more. Establishing a bilinear torsional moment versus angle of twist curve based on the assumption that $M_{cr} = T_{cr}$ will induce an error in the response of the slab. However, it could be used as a rough estimation that generates a response closer to reality than using a linear torsional moment versus angle of twist relation as was proven in Section 5.5.2.

If the flexural cracking moment instead was based on the flexural tensile strength as in Eurocode 2 the results presented in Table 5.5 were acquired.

*Table 5.5    Analytical flexural bending moment based on the flexural tensile strength, $f_{ctm,fl}$, as in Eurocode 2 compared to the experimental torsional cracking moment.*

| Slab no. | $M_{cr}$ [kNm/m] | $T_{cr}$ [kNm/m] | $M_{cr}/T_{cr}$ [-] |
|----------|------------------|------------------|---------------------|
| 1        | 11.57            | 8.12             | 1.43                |
| 2        | 9.82             | 7.81             | 1.26                |
| 3        | 11.20            | 8.37             | 1.34                |
| 4        | 11.57            | 7.76             | 1.49                |
| 5        | 15.16            | 9.42             | 1.61                |
| 6        | 16.09            | 10.12            | 1.59                |
| 7        | 12.10            | 6.54             | 1.85                |
| 8        | 12.50            | 6.64             | 1.88                |
| 9        | 12.38            | 7.16             | 1.73                |
| Average: | -                | -                | 1.58                |

In Table 5.5 it can be seen that the flexural cracking moments are greater than the torsional cracking moments when the flexural tensile strength as in Eurocode 2 was used. Using these flexural cracking moments as an approximation of the torsional

cracking moment would generate substantial errors and was therefore disregarded as a suitable solution for the studied slabs.

Finally, the flexural cracking moment calculated as in BBK 04 was evaluated and is presented in Table 5.6.

*Table 5.6*   *Analytical flexural bending moment based on the flexural tensile strength, $f_{ctm,fl}$, as in BBK 04 compared to the experimental torsional cracking moment.*

| Slab no. | $M_{cr}$ [kNm/m] | $T_{cr}$ [kNm/m] | $M_{cr}/T_{cr}$ [-] |
|----------|------------------|------------------|---------------------|
| 1        | 9.91             | 8.12             | 1.22                |
| 2        | 8.42             | 7.81             | 1.08                |
| 3        | 9.59             | 8.37             | 1.15                |
| 4        | 9.91             | 7.76             | 1.28                |
| 5        | 12.98            | 9.42             | 1.38                |
| 6        | 13.77            | 10.12            | 1.36                |
| 7        | 10.38            | 6.54             | 1.59                |
| 8        | 10.71            | 6.64             | 1.61                |
| 9        | 10.61            | 7.16             | 1.48                |
| Average: | -                | -                | 1.35                |

As can be seen in Table 5.6, the flexural cracking moment as in BBK 04 also generates a higher cracking moment due to bending than the torsional cracking moment from the experiments.

From the presented results it was concluded that the best approximation of the torsional cracking moment $T_{cr}$ for the slabs tested in Lopes *et al.* (2014) was to estimate it as the cracking moment due to bending based on the mean axial tensile strength $f_{ctm}$.

However, for moment curvature relations the cracking moment due to bending $M_{cr}$ were still based on the flexural tensile strength $f_{ctm,fl}$ as recommended in BBK 04 since it should correspond better to the true tensile strength of the material.

## 5.7    Torsional stiffness of State II, beam grillage model

When $T_{cr}$ is known, the final step to establish a bilinear torsion-twist curve is to determine the loss of torsional stiffness due to cracking, i.e. the inclination of the second branch in the relationship should describe the stiffness of a cracked section.

The flexural stiffness for a cracked section can be determined by analytical calculations. However, the change of torsional stiffness due to cracking is more complex to solve analytically. It is even more complicated when the torsional stiffness in State II is to be calculated for beams in a beam grillage model, i.e. correspond to a cracked slab.

In Section 5.5 an analysis with the torsional stiffness of State II defined as two times the moment of inertia of a State II section was studied. The analysis yielded a result

far from the true solution and it was concluded that the hypothesis was incorrect. However, to confirm that the hypothesis is incorrect not only for the tested slab, all nine slabs in Lopes *et al.* (2014) were studied. It was investigated if any correlation between the measured torsional stiffness and the torsional stiffness calculated as two times the moment of inertia could be found.

In Lopes *et al.* (2014) the ratio of the State I and State II torsional stiffness is presented for the nine slabs used in the experiments. By combining equation (4-2) and equation (5-1) the ratio of the torsional stiffness can be calculated analytically as in equation (5-4).

$$\frac{K_{v,I}}{K_{v,II}} = \frac{2I_I}{2I_{II}} = \frac{I_I}{I_{II}} \tag{5-4}$$

This relationship was compared to the stiffness ratios presented in Lopes *et al.* (2014) to see if it accurately describes the loss of stiffness due to cracking for any of the nine slabs. Table 5.7 presents the results from analytical calculations along with the values acquired from the experiments in Lopes *et al.* (2014). For calculations of the analytical values the reader is referred to Appendix F.

*Table 5.7    Ratio of State I and State II torsional stiffness based on analytical calculations and experimental data.*

| Slab no. | Analytical $I_I/I_{II}$ [-] | Experimental $K_{v,I}/K_{v,II}$ [-] |
|----------|-----------------------------|-------------------------------------|
| 1 | 9.3 | 20.7 |
| 2 | 7.4 | 18.9 |
| 3 | 8.2 | 26.4 |
| 4 | 8.7 | 12.6 |
| 5 | 9.8 | 17.3 |
| 6 | 10.8 | 22.3 |
| 7 | 8.3 | 13.4 |
| 8 | 8.6 | 15.6 |
| 9 | 8.5 | 12.9 |
| Average: | 8.5 | 17.8 |

From Table 5.7 it can be seen that the analytical values provide lower ratios than those from the experiments for all slabs. It is stated in Lopes *et al.* (2014) that uncertainties regarding the State I stiffness exists due to the sensitivity of the used measuring equipment. However, the deviations between analytical and experimental values are too large to be fully explained by these measuring uncertainties. From the presented results it was concluded that the State II torsional stiffness is highly overestimated when implementing it as two times the State II moment of inertia, just as expected. Thus, the hypothesis was determined to not be valid. Further attempts to find a suitable estimation of the transition from State I to State II with regards to torsion was made, but no accurate solution was found. Since no adequate estimation was found, it was decided to carry out the remainder of the study by using the results presented in Lopes *et al.* (2014).

## 5.8 Predefined torsional stiffness, simply supported beam grillage model

In Section 5.5 it was concluded that the torsion-twist relation implemented in ADINA has to be nonlinear to be able to describe the nonlinear response of the slab. Attempts to define such curves analytically are performed in Section 5.6 and Section 5.7 but no applicable definition could be established. Thus it was concluded to use the experimentally compiled torsion-twist curves presented in Lopes *et al.* (2014) in order to see if it is possible to receive nonlinear displacement curves from ADINA using nonlinear torsion-twist curves as input.

The torsion-twist values presented in Lopes *et al.* (2014) are the torsional cracking moment, $T_{cr}$ and the yield moment, $T_y$. The bilinear curve based on those values is presented in Figure 5.10 and the exact values are stated in Table 5.8.
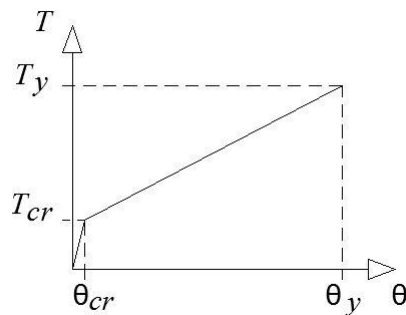


*Figure 5.10    Bilinear torsion-twist curve compiled from experimental test in Lopes et al (2014).*

*Table 5.8    Values of torsional moments and angle of twist measured in the experimental test in Lopes et al. (2014).*

| Slab no. | $T_{cr}$ [kNm] | $\theta_{cr}$ [rad/m] | $T_y$ [kNm] | $\theta_y$ [rad/m] |
|----------|----------------|-----------------------|-------------|--------------------|
| 1        | 1.437          | 0.001035              | 3.990       | 0.038800           |

The same beam grillage model as described in Section 5.3 was studied. This time the torsion-twist curve described above was implemented in ADINA along with the nonlinear moment-curvature relation described in Figure 5.6b. The obtained displacement curve is presented in Figure 5.11.
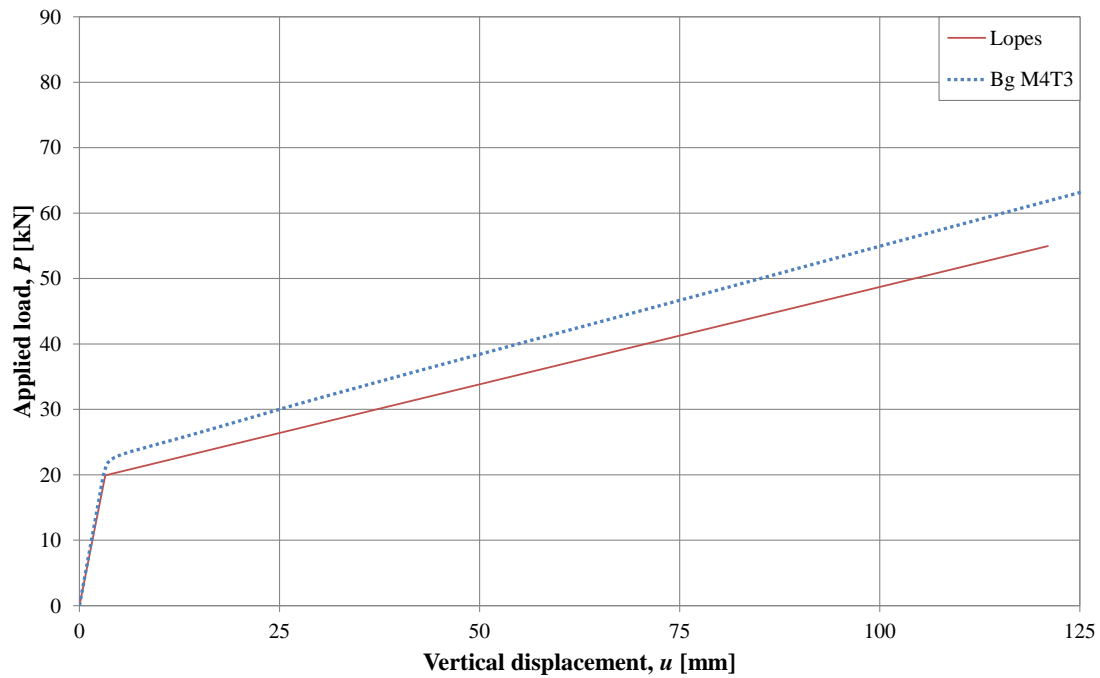
*Figure 5.11 Vertical displacement, u, at the point of loading for the studied slab with nonlinear moment-curvature relationship and a bilinear torsion-twist relationship based on the experimental measurements in Lopes et al. (2014).*

As expected, a bilinear displacement curve was obtained in the analysis. The result confirms the presumption that the implemented torsion-twist curve is of great importance when studying slabs predominantly subjected to torsional moments in ADINA.

The displacement curve received from ADINA has the same linear elastic response as the experimentally tested slab. This time also the plastic response of the cracked section corresponds well to the measurement. The result is expected since the inserted torsion-twist relation is the measured values from Lopes *et al.* (2014). The only difference is that the cracking moment is slightly higher in the ADINA model. This is believed to be due to that the values presented in Lopes *et al.* (2014) describe the global response of the slab. The input values in a beam grillage model in ADINA though, describe the local response of a beam section. With a slightly lower cracking moment, the displacement curve received from ADINA would probably correspond very well to the displacement curve in Lopes *et al.* (2014).

To further confirm the importance of the chosen torsional stiffness two more analyses were made. The experimental torsion-twist curve presented in Lopes *et al.* (2014) was still used, but the moment-curvature relation was made linear. In the first analysis the stiffness of State I was used and for the second analysis the stiffness of State II. The resulting displacement curves are presented in Figure 5.12 and Figure 5.13.
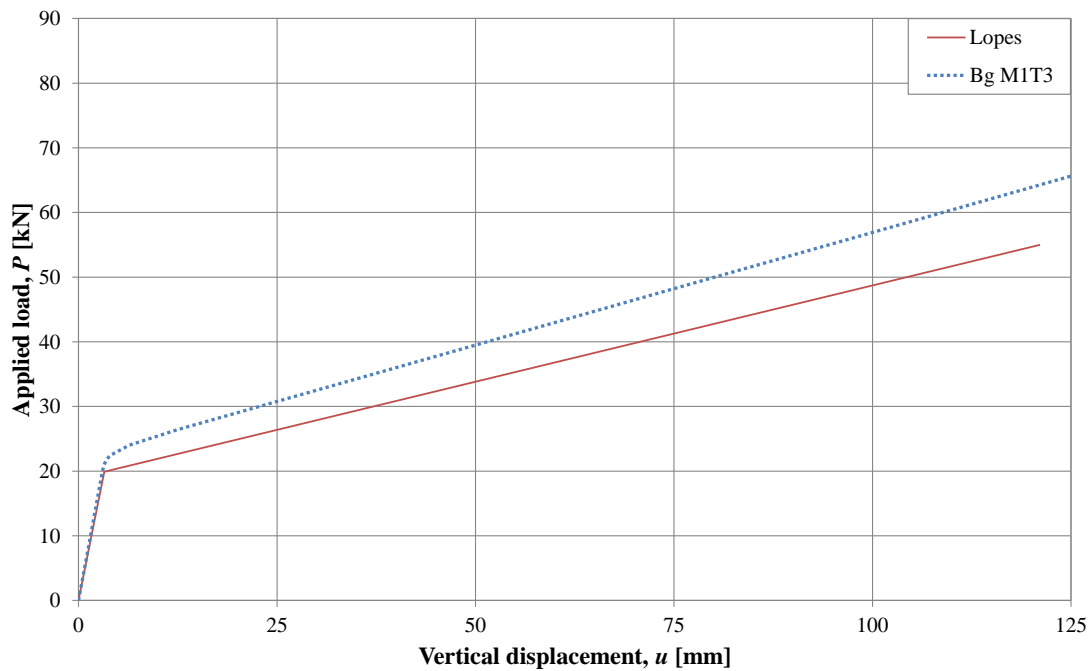
*Figure 5.12    Vertical displacement, u, at the point of loading for the studied slab with a linear moment-curvature relationship based on the stiffness of State I and a bilinear torsion-twist relationship based on the experimental measurements in Lopes et al. (2014)*



*Figure 5.13    Vertical displacement, u, at the point of loading for the studied slab with a linear moment-curvature relationship based on the stiffness of State II and a bilinear torsion-twist relationship based on the experimental measurements in Lopes et al. (2014).*
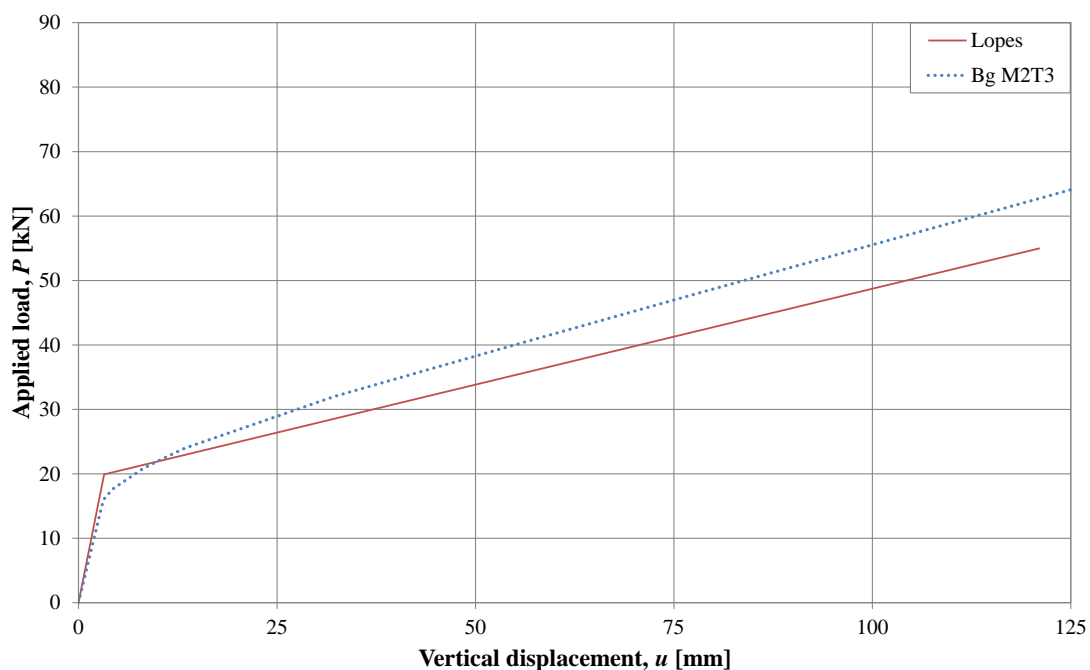
There are no distinctive differences between the displacement curves in the last two analyses, neither in comparison with the analysis using a nonlinear moment-curvature

relation. The results further affirm that the flexural stiffness has no significant influence of the result for slabs predominantly subjected to torsional moments. The implemented torsional stiffness governs the result entirely.

In order to capture the behaviour of the ultimate limit state the bilinear torsion-twist curve was made trilinear. A plateau with a small inclination was added to the bilinear relationship in Lopes *et al.* (2014), see Figure 5.14, and the analysis was run again.
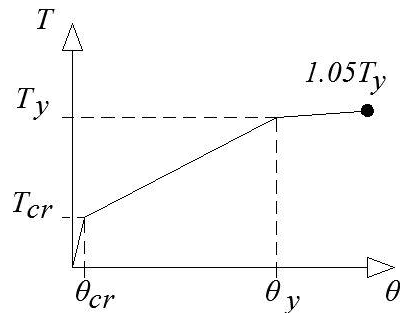


*Figure 5.14    Trilinear torsion-twist relation.*

The moment-curvature relation used in the analysis was nonlinear. However, the choice of moment-curvature relation does not influence the result much. Based on the trilinear torsion-twist curve in Figure 5.14, the behaviour presented in Figure 5.15 was acquired.
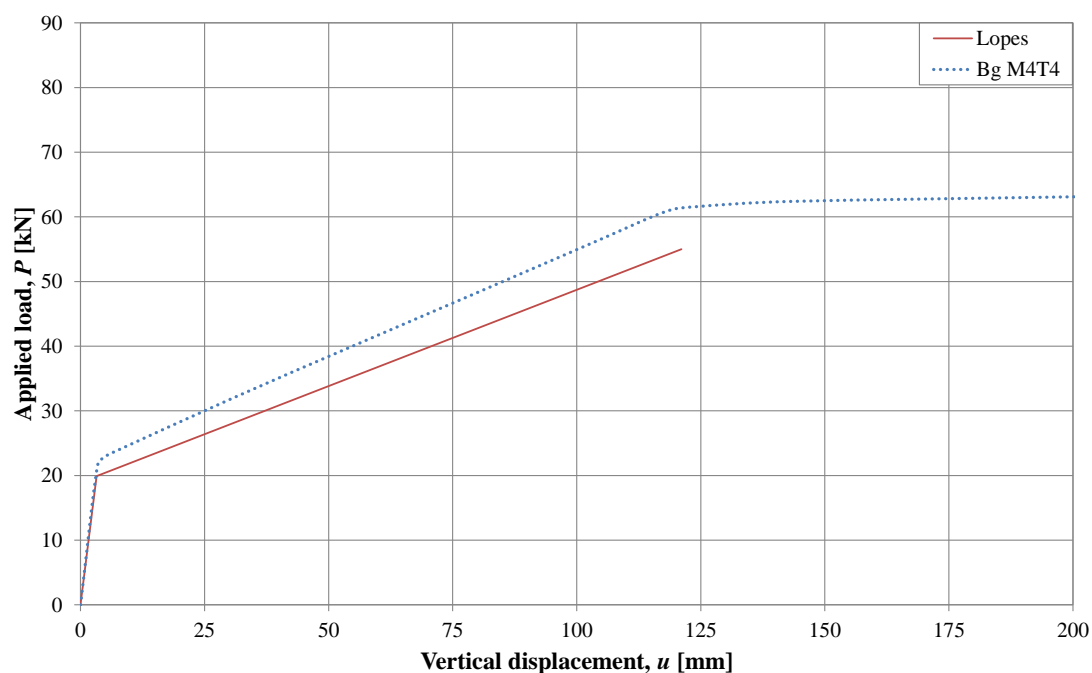


*Figure 5.15    Vertical displacement, u, at the point of loading for the studied slab with a nonlinear moment-curvature relationship and a trilinear torsion-twist relationship.*

By making the torsion-twist curve trilinear, the ultimate limit state was found. Again it was confirmed that the implemented torsional stiffness determines the response of

the slab. The modelled slab yields in torsion at a load of approximate 61 kN which is somewhat too high in comparison with the result of 55 kN obtained in the experimental test. However, with a slightly lower cracking moment as input, the whole curve would descend and the yield load would approach 55 kN.

To summarise, slabs subjected to mainly torsional moments and modelled as beam grillages in ADINA were largely influenced by the defined torsional stiffness of the beams. However, no relation for the torsional stiffness of beams in State II was found. To establish a torsion-twist relation to insert in ADINA requires, in addition to the torsional stiffness of State I and State II respectively, the torsional cracking moment. No simple way to analytically calculate the torsional cracking moment for a beam grillage exists. However, it has been observed that a fairly good approximation of the studied slabs is to define the torsional cracking moment equal to the flexural cracking moment based on the mean axial tensile strength $f_{ctm}$. Still, with no legit relationship for the torsional stiffness of State II cross-sections it is not possible to define an accurate nonlinear torsion-twist curve.

Moreover, the shape of the moment-curvature relation seems to have almost no influence of the result for tested slabs. Analyses with nonlinear moment-curvature generate similar displacement curves as analyses with linear moment-curvature relations.

## 5.9 Shell element model, simply supported slab

### 5.9.1 Orientation

In Section 5.8 it was concluded that the shape of the implemented torsion-twist relation is of great importance for analyses of slabs subjected to torsion and modelled using a beam grillage model. It was also concluded that such curves are hard to establish for several reasons. Shell element models require no torsion-twist relation as input due to the possibility of principal directions in the elements. Thus, it was of interest to see if a shell element model, which is given an appropriate nonlinear response, could be established.

### 5.9.2 Bilinear plastic model

ADINA offers a bilinear plastic material model applicable to shell elements which was used for the first analyses. The nonlinear material response aimed to describe is illustrated with the moment-curvature relation in Figure 5.16. It is a simplified bilinear relationship which defines the linear elastic stiffness and a modified stiffness, $EI'_{II}$, for State II.
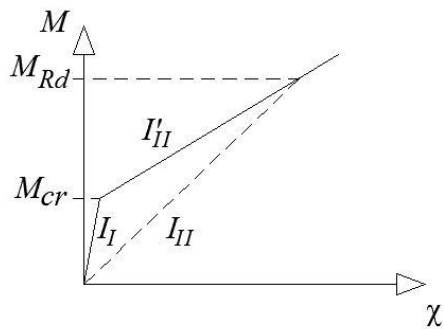
*Figure 5.16   Simplified nonlinear moment-curvature relation describing the behaviour of the shell element model.*

However, for a bilinear plastic material model in ADINA the required input data are the material yield stress and the strain hardening modulus. Thus, it is not possible to insert the moment-curvature relation directly. Instead, a stress-strain curve which corresponds to the desired moment-curvature relation has to be defined, see Figure 5.17.
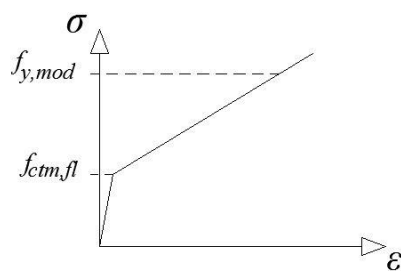


*Figure 5.17   Stress-strain relation to be inserted in ADINA. Describes the behaviour illustrated by the moment-curvature relation in Figure 5.16.*

The bilinear plastic material model in ADINA describes an elastic-plastic response. The behaviour of the material up to the inserted yield stress is linear elastic and the second branch of the bilinear curve represents the plastic behaviour.

The bilinear plastic material model is aimed to describe the behaviour of reinforcing steel. Thus, the required input data defines a bilinear stress-strain curve where the yield stress variable defines the stress at the point where the steel yields and the strain hardening modulus describes the inclination of the curve between the yield stress and the ultimate stress.

With the intention to describe the moment-curvature relation in Figure 5.16 using the bilinear material model, other input values were chosen. Since the transition from State I to State II was of interest, the first point was supposed to describe the cracking moment. Thus, the tensile strength of the concrete was used. The tensile strength can be recalculated to flexural tensile strength according to either Eurocode or BBK04, as discussed in Section 5.6. However, for this analysis the mean tensile strength $f_{ctm}$ was chosen.

The strain hardening modulus was used to describe the inclination of the modified stiffness of State II. The ratio between the stiffness of State I and the modified State II

was calculated to 14.25, which was inserted in ADINA. As the moment capacity is based on a fully plastic stress distribution, the yield stress $f_{y,mod}$ in Figure 5.17 was calculated according to Section 3.2 to account for the plastic stress distribution provided by ADINA. All calculations can be found in Appendix G.

Results from the analysis based on a bilinear stress-strain curve are presented in Figure 5.18 and compared to the experimental results from Lopes *et al.* (2014).
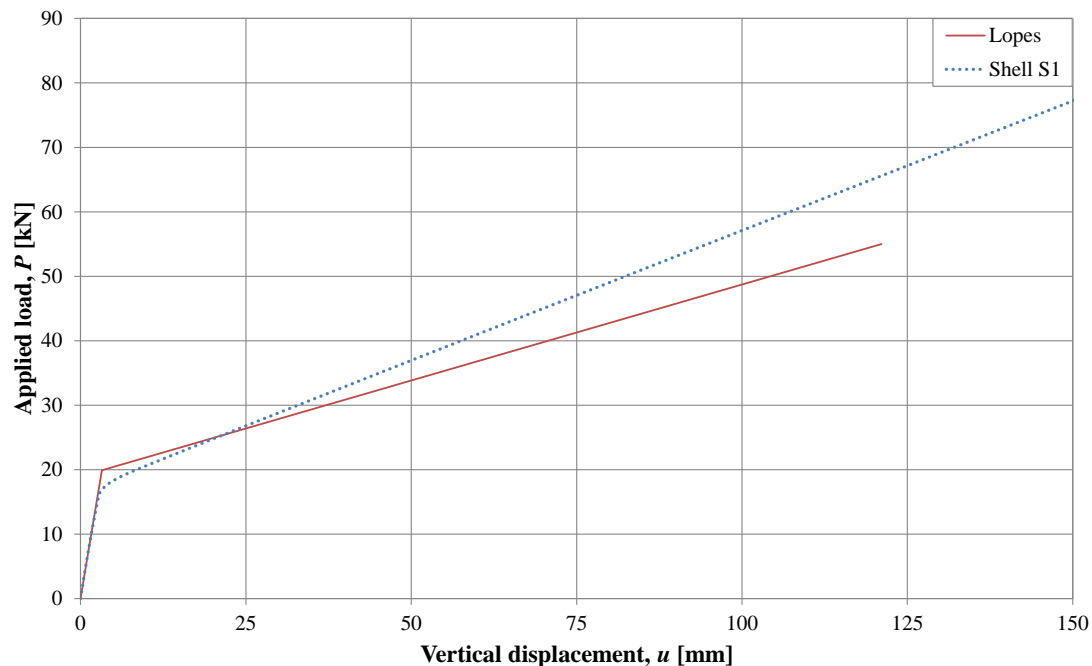


*Figure 5.18*    *Vertical displacement, u, at the point of loading for the shell element model using a bilinear plastic material model.*

As can be seen in the figure, the displacement curve obtained from ADINA does not correspond fully to the experimental results. The model in ADINA has a somewhat higher stiffness in State II than the slab tested in Lopes *et al.* (2014). However, no visible differences can be seen in State I, hence the modelled stiffness for State I seems to be true.

The cracking moment in the ADINA model is slightly lower than for the experimentally tested slab. That could be explained with the choice of the tensile strength of concrete, using the flexural tensile strength instead of the mean tensile strength may generate more correct cracking moment in the FE-model, see Section 5.6. Altogether, the shell element model does not yield satisfactory results. If it is the simplified moment-curvature relationship or the translation to the implemented stress-strain curve that causes the deviation is not known.

### 5.9.3   Multilinear plastic material model

It is also possible to use a multilinear plastic material model in ADINA. Such a material model is described with a stress-strain curve divided in an unlimited number of linear parts. The material model is elasto-plastic, i.e. the first part of the curve does always describe an elastic response. The input values are stresses and strains. In order

to capture the response of the ultimate state a trilinear curve was defined. The same stress-strain curve as in the bilinear material model was used, added with a plateau at the end to describe the ultimate state, see Figure 5.19. The plateau was inserted with a small inclination to avoid possible convergence problems.
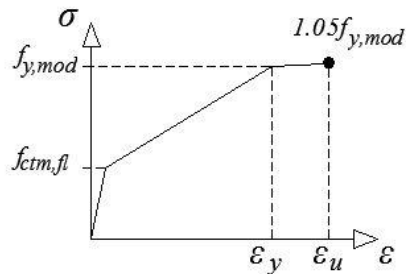


*Figure 5.19    Trilinear stress-strain relationship implemented in ADINA.*

In the Section 5.9.2, where a bilinear plastic material model was used, the obtained cracking moment and state II stiffness deviated from the experimentally tested slab. Trying to reach a better result, different input values of the tensile strength were tested. First, the mean tensile strength was used. Then the flexural tensile strength according to both Eurocode 2 and BBK 04, calculated as described in Section 5.6, was tested.

The obtained displacement curves for all analyses with different tensile strength input together with the experimental result from Lopes *et al.* (2014) are presented in Figure 5.20.
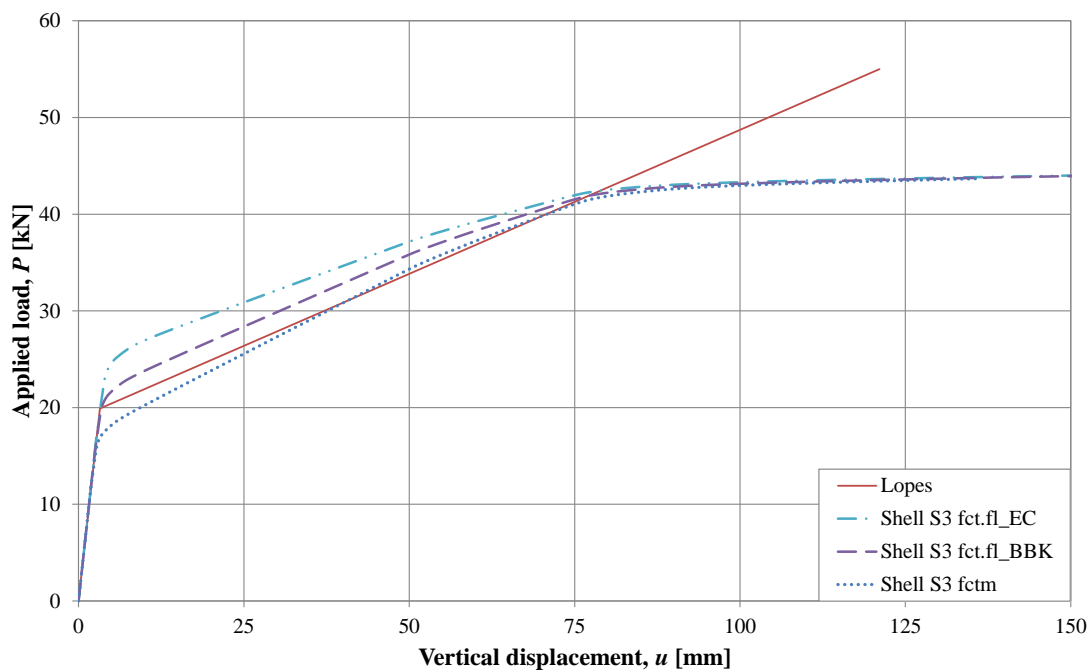


*Figure 5.20    Vertical displacement, u, at the point of loading for shell element models using a multilinear plastic material model. Different values of the concrete tensile strength were used and compared to the experimental test result.*

With the trilinear plastic material model the ULS response is captured. However, the ultimate load is far below what is observed for the experimental slab. In Lopes *et al.* (2014) a load of 55 kN was reached before the slab failed, for the ADINA model the corresponding load is merely 44 kN.

It can also be concluded that the different input values in terms of tensile strength generates different cracking moments. The flexural strength according to Eurocode yields the highest cracking moment since the method used there gives the highest flexural tensile strength of the concrete. The model based on the mean tensile strength renders the lowest cracking moment. However, all three FE-models generate the same linear elastic and ultimate limit state response. Hence, with altering cracking moment, the stiffness of State II varies between the models. Although the results from the FE-models differ slightly from the experimentally tested slab, they were considered to be adequate.

The choice of concrete tensile strength to be used is not obvious. Eurocode and BBK 04 give different recommendations of how to calculate the flexural strength. According to Eurocode a value 1.45 times the mean tensile strength should be used, $f_{ct,fl\_EC}$. On the contrary, BBK 04 recommend the value 1.24 times the mean tensile strength, $f_{ct,fl\_BBK}$. It should be noted that those values correspond to a slab with a height of 0.15 meters. Hence, it differs 45% between the lowest and highest recommended values. The divergences in the obtained cracking moment in the analyses in ADINA are therefore not hard to perceive. Which value of the tensile strength that gives the most correct result in general cannot be determined; it varies from case to case. However, for this specific slab, the flexural strength according to BBK 04 was believed to give the most accurate result. It yields a cracking moment slightly higher than the experimentally tested slab but the stiffness of State II corresponds well. Thus, the flexural strength according to BBK 04 was chosen and used in the further analyses.

## 5.10 Beam grillage model, fixed edges

As the tested slab in Section 5.8 and Section 5.9 were mainly subjected to torsional moments, it was of interest to study a case more prone to bending action. Thus, a slab with the same dimensions and reinforcement arrangement as described in Section 5.4, but with two fixed edges instead of simply supported point supports was studied. Such a load case will generate larger bending moments compared to the experimental setup in addition to the torsional moments. Thus, the dependency of the inserted moment-curvature relationship was believed to increase.

Since no way to describe the torsional stiffness of a beam grillage in State II has been found, it is difficult to define the torsion-twist curve to implement in ADINA. Thus, the torsion-twist curve compiled in Lopes *et al.* (2014) was used as an approximation. However, it should be noted that it is an estimate and that results received may deviate from the true solution.

No experimental test performed on such a slab has been found. Thus, no results that can act as references in comparison with the beam grillage model exist and no comparison with experimental data was made. To be able to examine the results

received from the beam grillage model, a corresponding shell element model was created. The comparison between the beam grillage model and the shell element model is presented in Section 5.11. First, in this section though, the behaviour of the beam grillage model using different input data is investigated.

The geometry of the beam grillage model together with boundary conditions and load placement are illustrated in Figure 5.21.
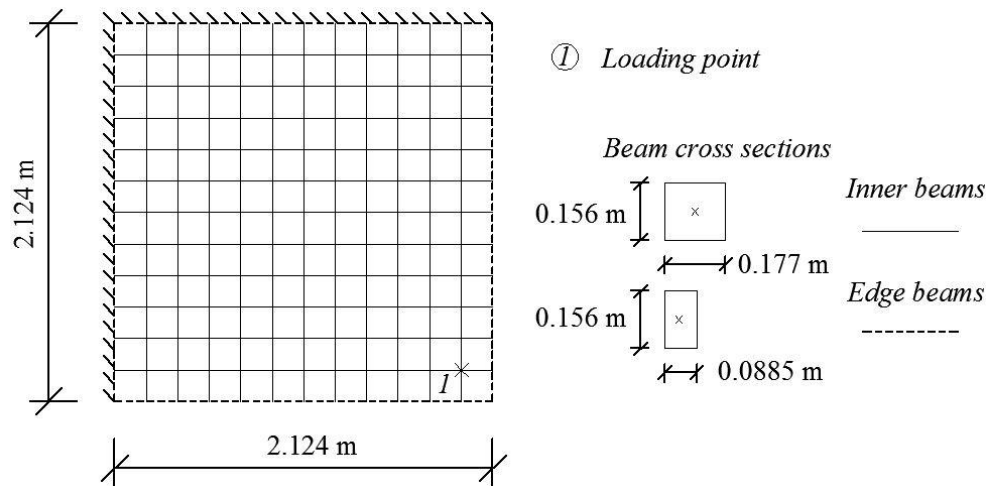


*Figure 5.21    Geometry of beam grillage model with two fixed edges.*

First it was investigated if the moment-curvature relationship inserted influences the result for this slab. Thus, three analyses were made. The torsion-twist relation from Lopes *et al.* (2014) was used for all three analyses but the moment-curvature relationship inserted in ADINA varied.

The moment-curvature relationship was defined with a modified State II stiffness as in Figure 5.16 in order to be able to directly compare the results from the beam grillage model with the results from a shell element model. The shell element model is modelled with a stress-strain relation that aims to describe the moment-curvature in Figure 5.16 with a modified State II stiffness. Hence, the flexural stiffness for the beam grillage model is defined in the same manner.

The first analysis had the bilinear moment-curvature relation illustrated in Figure 5.16, the second and third analysis uses the linear moment-curvature relation based on the stiffness of State I and State II, respectively. The resulting load-displacement curves for all three analyses are presented in Figure 5.22.
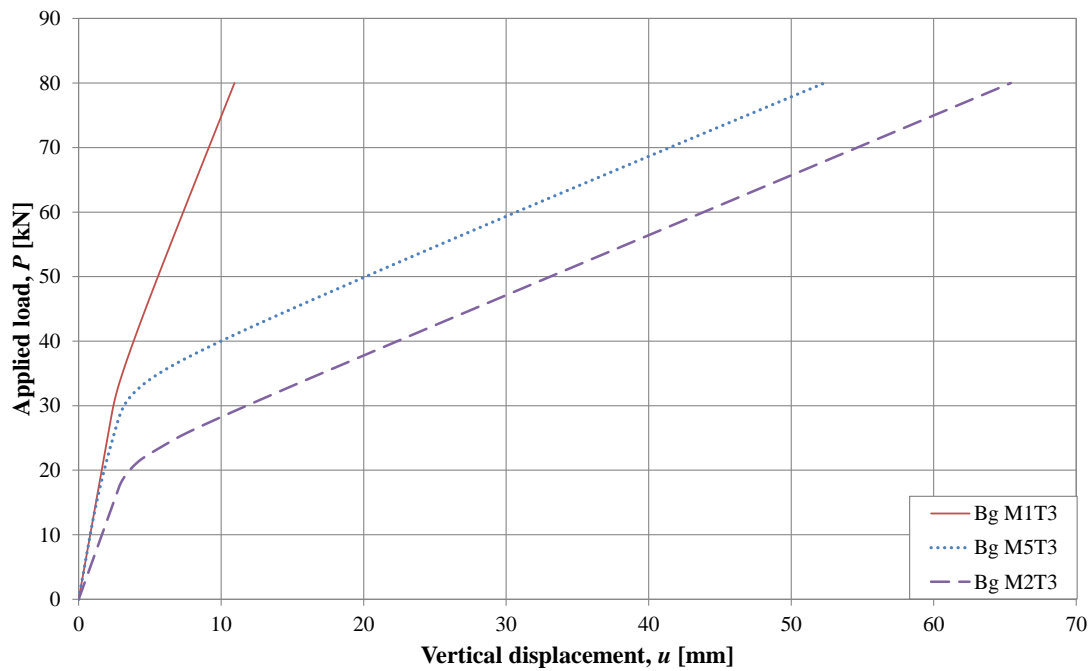
*Figure 5.22    Vertical displacement, u, at the point of loading for the beam grillage model with two fixed edges. Bilinear torsion-twist curve as input for all slabs together with a) linear State I moment-curvature relation (Bg M1T3), b) bilinear moment-curvature relation (Bg M5T3) and c) linear State II moment-curvature relation (Bg M2T3).*

From Figure 5.22, it can be noted that all analyses yield nonlinear displacement curves. Both models with linear moment-curvature input generate bilinear result curves which mean that the nonlinearity is due to the implemented bilinear torsion-twist curve. The same conclusion can also be drawn by looking at curve b) and c) in Figure 5.22. Those curves have the same shape even though curve c) has a linear moment-curvature input. At the point in the displacement curves where the inclination changes, the torsional cracking load has been reached and the torsional stiffness of the beam grillage decreases. However, the analyses give three different displacement curves which indicate that the moment-curvature input also influences the results for this slab. Hence, to capture the most accurate behaviour of the slab both the inserted moment-curvature and torsion-twist relation should be nonlinear.

Next step was to create a model that can capture also the response of the ultimate limit state. First, the moment-curvature relationship was added with a yield plateau while the torsion-twist curve was kept bilinear and the analysis was run again. The plateau has a small inclination to avoid possible convergence problems. The trilinear curve has the same shape as illustrated in Figure 5.23.
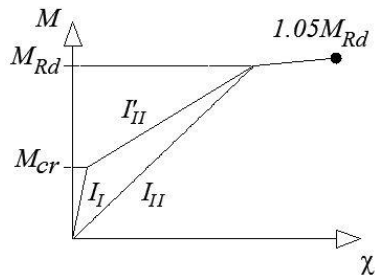
*Figure 5.23    Trilinear moment-curvature relation based on a simplified State II stiffness.*

No failure of the slab could be noted; thus the load was increased from 80 kN to 160 kN in case the failure load not yet was reached. The analysis was then run again and the resulting displacement curve can be seen in Figure 5.24.
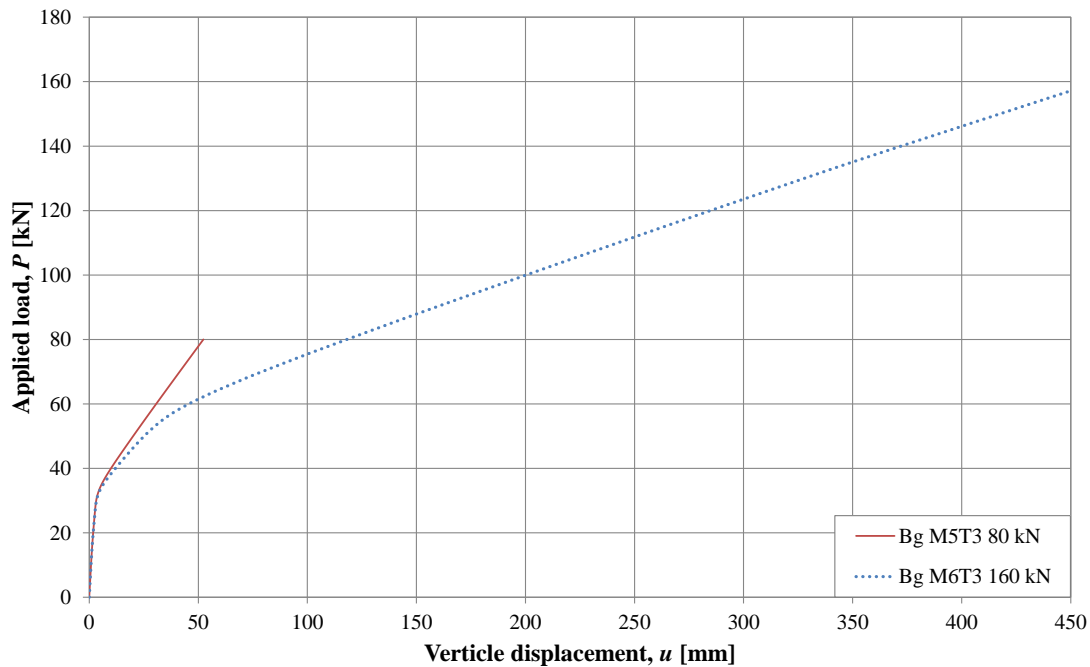


*Figure 5.24    Vertical displacement, u, at the point of loading for the beam grillage model with two fixed edges. Bilinear torsion-twist curve was used as input for both slabs together with a) bilinear moment-curvature relation (Bg M5T3) and b) trilinear moment-curvature relation (Bg M6T3).*

The increased load did not result in any rupture or failure of the slab; thus the trilinear moment-curvature input could not capture the ultimate limit response. However, the displacement curve has changed from bilinear to trilinear. The first change in inclination is still representing the torsional cracking moment and the second change is where the bending moment resistance is reached. The load can still be increased after that point though, without any visible signs of a failure.

Next, the moment-curvature relation was made bilinear again and the torsion-twist curve was made trilinear instead. A yield plateau with a small inclination was added to the bilinear relationship to see if it was possible to capture the ultimate limit

response with a limited torsional stiffness. The implemented trilinear curve is the same as illustrated in Figure 5.14. The load of 160 kN was also kept in the further analyses. The resulting displacement curve is presented in Figure 5.25.
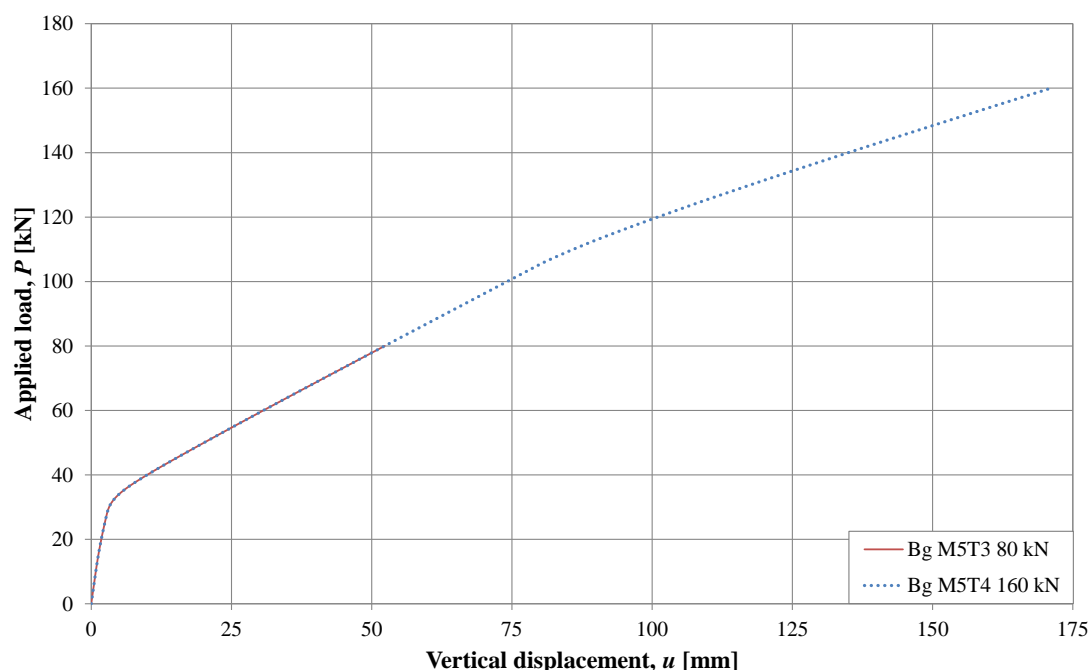


*Figure 5.25*    *Vertical displacement, u, at the point of loading for the beam grillage model with two fixed edges. Bilinear moment-curvature relation was used as input for both slabs together with a) bilinear torsion-twist relation (Bg M5T3) and b) trilinear torsion-twist relation (Bg M5T4).*

The ultimate response was not captured with a trilinear torsion-twist relation either. The displacement curve for the model with a trilinear torsion-twist relation is identical to the model with a bilinear torsion-twist input up to a load of approximate 108 kN. When studying the obtained moments in the model at that load it can be determined that the moment corresponding to the maximum torsional resistance of the beam grillage has been reached. After that the stiffness of the slab decreases, but still no failure can be seen.

It seems like for a slab with a defined maximum torsional resistance, that after that point is reached, the moment is redistributed and the unlimited bending resistance of the beams continue to carry the load. The same phenomenon was seen in the analysis where the maximum bending resistance was defined. In that case, the torsional stiffness of the beams carries the load after the maximum bending moment resistance is reached. In conclusion, it appears like both input curves need to have a yield plateau where the maximum moment resistances are defined in order to find the ultimate limit response. Thus, an analysis with trilinear moment-curvature and torsion-twist relationships, see Figure 5.23 and Figure 5.14, as material input was performed. The result is illustrated in Figure 5.26.
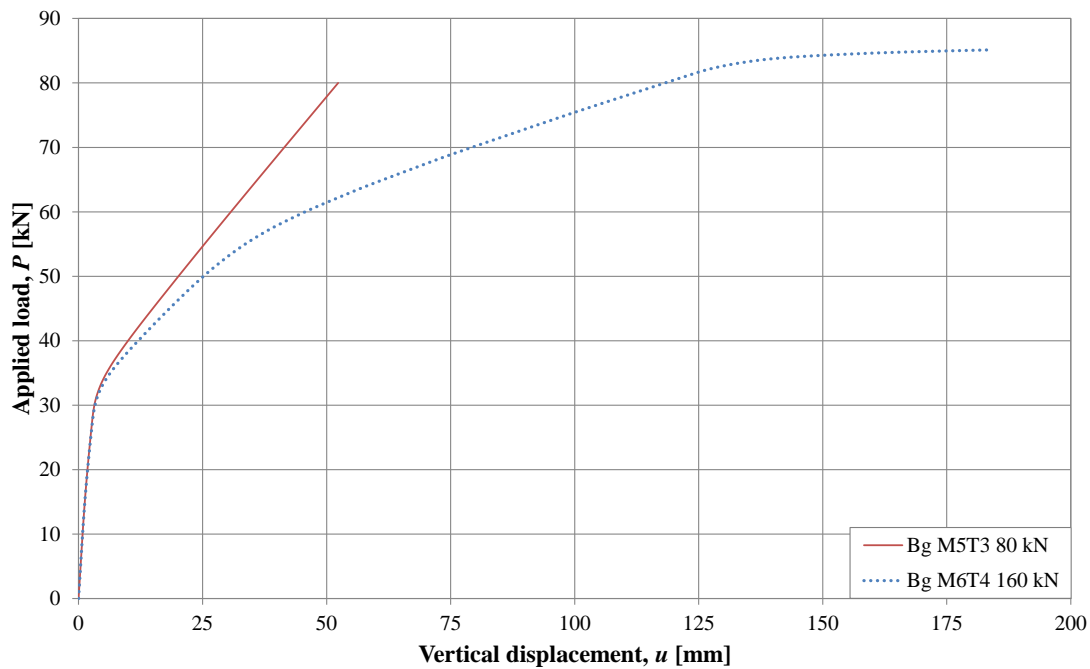
*Figure 5.26    Vertical displacement, u, at the point of loading for the beam grillage model with two fixed edges. Trilinear torsion-twist and moment-curvature relations were used as input.*

As expected, with trilinear input curves that defines the maximum moment resistance in bending and torsion respectively, the ultimate limit response was found. The slab fails at a load of approximate 82 kN. The displacement curve is now quadlinear which indicates that the failure happens after both the maximum bending and torsional stiffness are utilised. Torsional moments and bending moments at every breakpoint were controlled in ADINA and compared with the input values. In that way it could be concluded that the first change in inclination corresponds to the torsional cracking moment and at a load of approximate 47 kN the bending moment resistance is reached in the first beam elements. At approximately 55 kN all bending resistance is utilised. Thereafter, the moment is redistributed and the load is carried by the remaining torsional stiffness until all resistance is depleted, at a load of about 82 kN.

To summarise, the shape of the torsion-twist curve still has a major influence of the results for the studied slab. However, when also bending moments are present in the slab, the inserted moment-curvature relation will influence the results too. Moreover, to capture the ultimate limit response both a maximum bending moment resistance and a torsional moment resistance needs to be defined.

## 5.11    Shell element model, fixed edges

In Section 5.10 a beam grillage model with two fixed edges was tested to investigate if the moment curvature relation used has more influence with such boundary conditions. Since no experimental data was available for such a load case, it was of interest to establish a shell element model supported along two fixed edges. It was done to compare the behaviour between models based on beam or shell elements. The shell element model was given the geometry and loading seen in Figure 5.27.
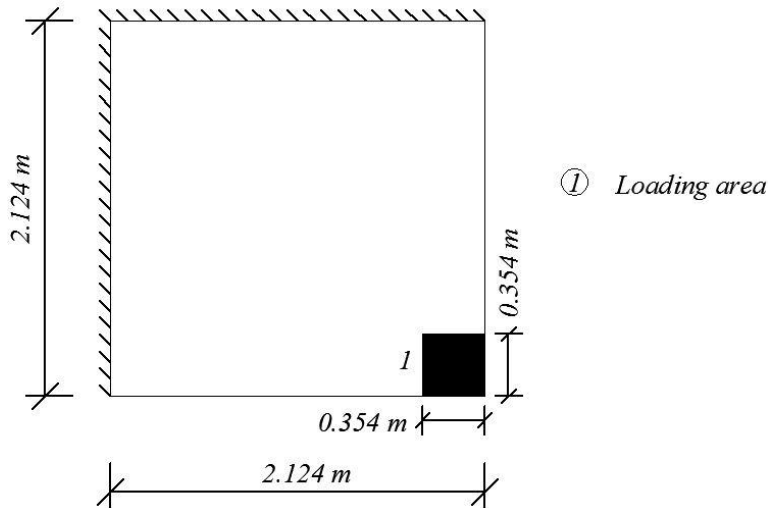
*Figure 5.27    Geometry of the shell element model with two fixed edges.*

As a first step it was determined to use a bilinear stress-strain relation in the shell element model. The stress-strain curve used was the same as is presented Figure 5.17 in Section 5.9.2. An appropriate beam grillage model for comparison is the model presented in Section 5.10 with bilinear torsion-twist and moment-curvature relations. For the first analysis, the beam grillage model was not given a yield plateau in the moment-curvature relation to better enable comparison and avoid any irregularities that might occur by introducing a specific bending capacity. Schematic illustrations of the input data in the models are presented in Figure 5.28.
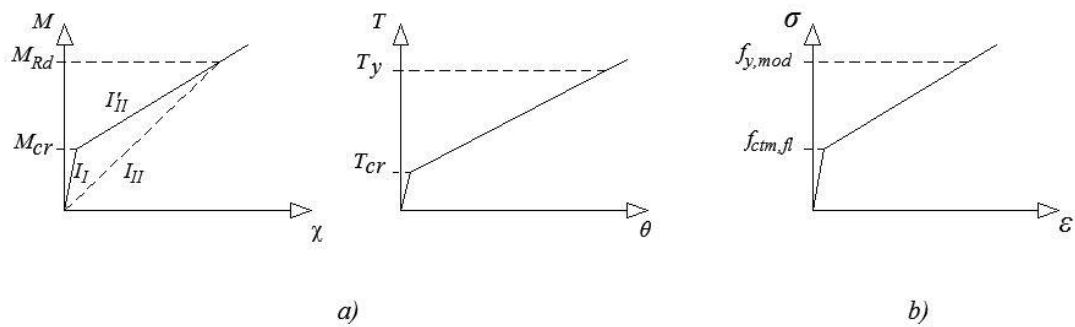


*Figure 5.28    Bilinear material input data for a) beam grillage model and b) shell element model.*

By using the input data presented in Figure 5.28, the load versus displacement curves in Figure 5.29 were acquired.
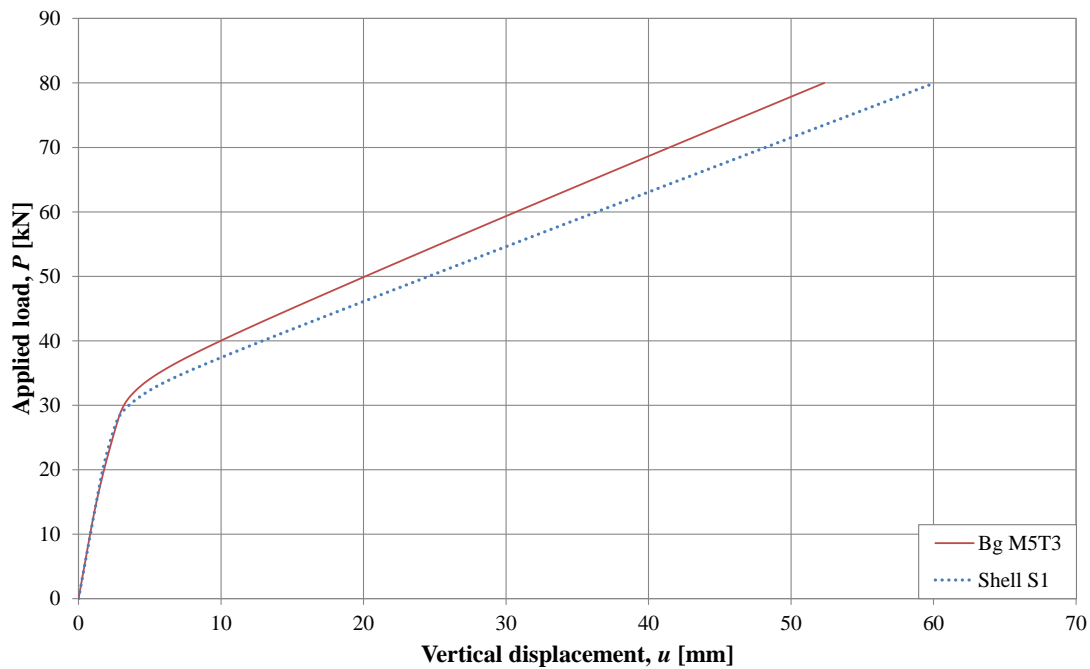
*Figure 5.29    Comparison of the vertical displacement, u at the point of loading for a slab with two fixed edges modelled with either shell elements or beam elements. Bilinear material input data were used.*

From Figure 5.29 it can be stated that both models have a similar behaviour during their uncracked phase. A slight deviation in the cracking load of the models can be seen. This was believed to be related to the fact that the experimental torsion-twist curve from Lopes *et al.* (2014) was used for the beam grillage model although new boundary conditions were implemented. Since the new boundary conditions make a larger portion of the load to be carried in bending, the torsional cracking moment is reached at a higher load level. Post-cracking, both models exhibits a linear State II behaviour as expected. The beam grillage model has a somewhat stiffer State II behaviour which also was believed to be related to the approximation of using the experimental torsion-twist relation.

Since the models based on bilinear relations showed agreement to a certain extent, it was of interest to introduce a yield limit for both models. With yield limits defined in the models the failure load of the models could be compared. For the shell element model this means that a trilinear stress-strain curve was used as input. The beam grillage model was given trilinear torsion-twist and moment-curvature relations. An illustration of the curves used as input data in the models is depicted in Figure 5.30.
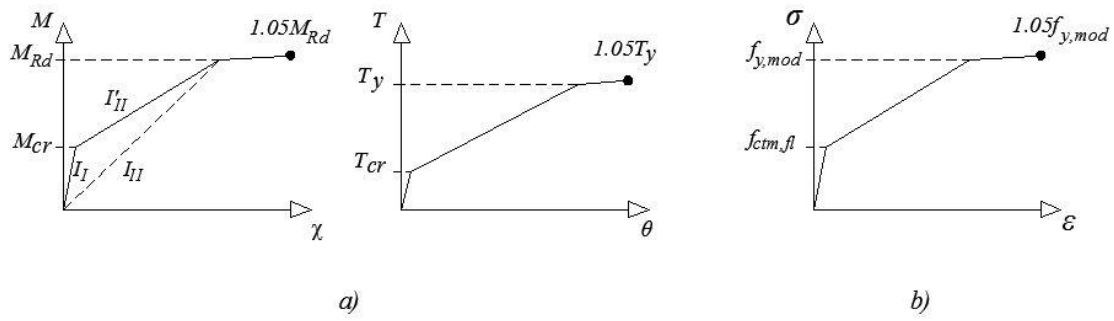
*Figure 5.30   Trilinear material input data for a) beam grillage model and b) shell element model.*

From the input data presented in Figure 5.30, the results displayed in Figure 5.31 were obtained.
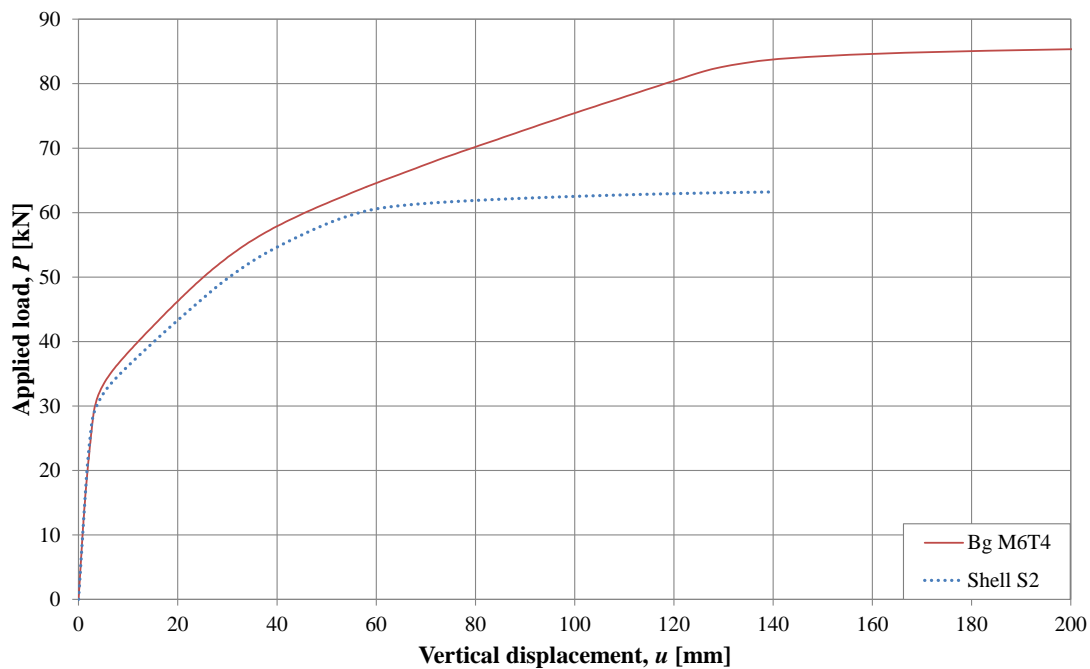


*Figure 5.31   Comparison of the vertical displacement, u at the point of loading for a slab with two fixed edges modelled with either shell elements or beam elements. Trilinear material input data were used.*

As the only difference between the results presented in Figure 5.30 and Figure 5.31 is related to the addition of yield limits in the input data, the point of interest in this comparison was the ultimate load capacity. As can be seen, the beam grillage model shows a far greater load capacity than the shell element model. This means that the models do not redistribute the load in a similar manner. The shell element model uses the principal moment as reference for calculations whereas the beam grillage model uses pure bending and torsional moments. The shell element model yields when the principal stress reaches the yield stress. On the contrary the beam grillage model has two yielding conditions; either it yields due to torsion or it yields due to bending.

Once again the torsion-twist relation calculated from experimental data was used although the boundary conditions of the model are not in agreement with the experiment. Thus, the torsional yielding moment is reached at a higher load level due to more loads being carried in bending. It can be seen in the curve that the beam grillage model starts to change stiffness at a load level of 47 kN. This load magnitude was investigated and it was found that the first beams in the grillage reaches the yielding limit in the provided moment-curvature relation. The yielding due to bending spreads out with increasing load until a load magnitude of 62 kN is reached. Further the model redistributes the load and starts to use the remaining capacity in torsion. The failure of the beam grillage model occurs at 82 kN, where enough beams yields in bending and torsion to form a collapse mechanism as shown in Section 5.10. It is of importance to note that no yielding plateau is reached in the beam grillage model if a bilinear torsion-twist relation is used. This means that the plateau starting at 82 kN in Figure 5.31 corresponds to yielding due to torsion.

Since the torsion-twist relation used in the beam grillage model is an approximation, the ultimate load of the model is uncertain, i.e. it does not represent a real case. If comparisons are made with Figure 5.15 where the torsion-twist relation is correct, the beam grillage model probably have a more correct ultimate load capacity. However, independent of the used boundary conditions, the beam grillage models overestimate the ultimate load capacity.

From this study it can be stated that the torsion-twist relation used in the beam grillage models has significant influence of the response, irrespective of applied boundary conditions. Since no clear relation between moment-curvature and torsion-twist is known, no practical way to establish a correct torsion-twist relation was found. Thus, it was concluded that it is not possible to capture a realistic nonlinear response when torsional effects are present using a beam grillage model.

## 5.12  Discussion

### 5.12.1  Simply supported slab

In Section 5.5 it was discovered that a nonlinear torsion-twist relation is required to capture a nonlinear response in beam grillage models mainly subjected to torsional moments. Thus, it was investigated if any simplified way of establishing such curves existed. The torsional stiffness of State II was found hard to define in a simplified manner since the implemented torsional stiffness of the beam element should correspond to the torsional stiffness of the slab portion that it represents. As a clear relation between bending and torsion in beam grillage models existed for linear elastic analyses, it was believed that a similar relation might exist also after cracking. However, the hypothesis saying that two times the moment of inertia of a single beam corresponds to the torsional stiffness of a beam in a beam grillage model did not hold true for cracked sections.

In previous Theses different choices and estimations of the torsional stiffness has been made. Although the results presented in Section 5.5 does not present a good estimation of the State II torsional stiffness in beam grillage models, it verifies that the choice of stiffness has a major influence when torsion is present in the structure. Hence, it was argued that the advantages of using a beam grillage model,

i.e. orthotropic stiffness properties, cannot be accurately implemented for nonlinear analyses.

Since the attempts to establish nonlinear torsion-twist relations failed, it was decided to use the torsion-twist relation presented in Lopes *et al.* (2014) to focus the study more towards the general behaviour of beam grillage models. With the experimental torsion-twist curve used as input the results presented in Figure 5.15 were acquired. The results were considered to be adequate, i.e. the model behaves well compared to the experimentally tested slabs except for the cracking load which deviates. This was believed to be related to the fact that provided material parameters such as the tensile strength of the concrete is based on a normal distribution, i.e. the material data provided in Lopes *et al.* (2014) will not be exactly the same in each section of the real slab. Since the FE-model has one defined tensile strength that is consistent in every section whilst a real slab always has local defects, deviations were expected. Although a satisfactory behaviour was acquired, it was based on using a pre-known torsion-twist relation. Hence, the intention of defining a general solution to model the slab with beam elements was not found.

Thus, it was of interest to analyse if a developed plastic shell element model could capture the response. The idea was that shell elements do not require a defined torsional stiffness due to the existence of principal directions in the elements. As is presented in Figure 5.20 in Section 5.9.3, the tensile strength of the model governs the cracking and also the State II stiffness since the ultimate capacity is a fixed value. The ultimate capacity of the shell element models deviated quite far from the experimentally measured capacity.

The reason for this deviation may be related to the fact that cold worked steel was used in the slab. Since no clear yielding plateau exists for cold worked steel, the experimental slab might have reached its ultimate strain $\varepsilon_{su}$ at a load magnitude of 55 kN. The ultimate capacity of the model was based on analytical calculations as in Appendix G, were the capacity was defined at the yielding limit of the steel, $\varepsilon_{sy}$.

However, as the theory in Section 3.2 states, the shell elements are based on the von Mises yield condition using a Poisson's ratio $v = 0.5$ in elements that reach their plastic limit. Thus an overestimation of the moment capacity should be acquired due to the incorrect appearance of biaxial stress states in the slab. However, an underestimation was calculated in ADINA and no explanation to this phenomenon was found.

### 5.12.2 Fixed edges

In Section 5.10, a slab more prone to bending was evaluated although torsion was still present. It was discovered that in such a case the implemented bending properties govern more of the structural response. Furthermore, it was found that to capture the ultimate limit state of any of the studied slabs modelled as a beam grillage, both the torsion-twist relation and moment-curvature relation needed to have defined yielding plateaus. As the theory in Section 2.3.4 suggests, analytical calculations based on the strip method assumes that all torsional stiffness is depleted in the ultimate limit state and all load carrying is done in pure bending by means of reinforcement. However, the beam grillage model was given a torsional stiffness, and as was illustrated in

Figure 5.26 the modelled slab carries load in pure torsion after the bending moment capacity is utilised. Thus, it is not possible to verify the results with analytical calculations.

Accordingly, it was believed that some kind of failure criterion should have been implemented in ADINA, i.e. the slab should be able to acquire a pure bending failure when all flexural capacity is used. For the fixed case this was noticed in Figure 5.31 were a beam grillage model was compared to a plastic shell element model. The shell element model based on principal directions fails at the same load magnitude as all moment capacity is used in the beam grillage model. However, the beam grillage carries further load in torsion. As was stated for this comparison, the torsion-twist curve used is the one defined in Lopes *et al.* (2014) which is not correct for a fixed case. However, the magnitude of this error is unknown. It is difficult to estimate how much the incorrect torsion-twist curve influences the results of the beam grillage model. Since there are uncertainties regarding the torsional stiffness modelled for the fixed slab, the results linked to the beam grillage model should be seen as a parametric study of what input data influences the results rather than focusing on the numerical values achieved in the analyses.

# 6    Final remarks

## 6.1    Conclusions

This Thesis intends to investigate if a reinforced concrete slab can be evaluated accurately by means of a beam grillage model in the FE-software ADINA. Both the linear elastic response and the non-linear response are studied and compared to shell element models and experimental results. The scope of the study was to find a general modelling method together with appropriate stiffness properties of the beam elements used in the beam grillage model.

From linear elastic analyses it was concluded that the choice of torsional stiffness is of great importance and also governs the structural response if the model is predominantly subjected to torsion. By choosing a torsional stiffness as two times the moment of inertia for each beam element, an accurate response in terms of moment distribution was found.

As shell element models were used as reference for a true linear elastic response, the influence of shear deformations caused certain deviations in terms of displacement. This was related to the fact that shear deformations always are accounted for in shell elements in ADINA, whereas for beam elements, they have to be included by a user defined shear area. By defining the shear area as 5/6 of the cross-sectional area of the beam elements, accurate displacements were measured in all beam grillage models based on beam cross-sections with a width to height ratio less than or equal to 1.0. For beam grillage models based on beam cross-sections with a width to height ratio larger than 1.0, displacements deviated irrespective if shear deformations were accounted for or not. No appropriate way to capture completely accurate displacements for beam width to height ratios larger than 1.0 was found.

For non-linear analyses, experimental results presented in Lopes *et al* (2014) acted as reference for a true solution. Replicas of one of the slabs used in the experiments were generated both by shell and beam elements, respectively. It was concluded that a nonlinear torsion-twist curve had to be established for the beam grillage model to acquire a non-linear response. However, as the torsional cracking moment and the State II torsional stiffness were impossible to estimate in a simple manner, the idea with a general beam grillage model was disregarded. It was still of interest if the modelling technique could generate an accurate response if the correct input parameters were known. Thus, the experimental results were used as input data in the beam grillage model and a reasonable response was acquired.

As using a beam grillage was concluded to be a non-viable modelling method due to the complexity of estimating an appropriate torsional behaviour, the next step was to use plastic shell element models. Since shell elements are based on principal moments which do not exist in beam elements, no specific torsion-twist relation needs to be established for such models.

The shell element models were able to capture an accurate response in terms of stiffness properties for State I and State II. However, the ultimate limit state, i.e. failure load in the studied load-displacement curves, got significantly underestimated when using a plastic shell element model in comparison to the

experimental results. As the stiffness properties were good in the shell element models it was considered as a more applicable modelling technique than a beam grillage model for non-linear analyses.

## 6.2 Further studies

The use of a beam grillage model in linear elastic analyses was thoroughly improved by the findings regarding the torsional stiffness and the influence of shear deformations. However, there still exist deviations in terms of displacements as the width to height ratio is increased beyond 1.0. As the error increases with increasing width to height ratio it would be of interest to further study the linear elastic response focusing on using beams with a width to height ratio larger than 1.0 to find the cause of these deviations. If such a study is successfully performed, it would lead to a modelling technique that could be considered as general. This would also give an alternative modelling technique to shell element models, with the advantage that concentrated forces and supports can be applied to single nodes without any risk of local deviations.

For the non-linear response, research regarding elasto-plastic shell element models would be interesting to better capture the ultimate load capacity of such models. Since the stiffness properties acquired in this Thesis were reasonable, a solution to the deviation in the ultimate limit state would lead to a model that can capture a simplified non-linear response of reinforced concrete slabs.

Furthermore, it would have been interesting to adapt a modelling technique that models concrete and reinforcement separately. This could possibly be done by combining shell elements representing the concrete and beam elements connected to appropriate nodes, acting as reinforcement bars. Such a model would avoid the problem with defining a torsion-twist relation since principal directions will exist in the shell elements. It could also be compared and verified with other FE-software that has embedded reinforcement as a modelling option.

# 7 References

ADINA R and D, Inc. (2014). *ADINA System 9.0 Release Notes.* Watertown: s.n.

ADINA (2012) *Theory and Modelling Guide,* Vol 1: ADINA Solids & Structures Report ARD 12-8, ADINA R & D inc., Watertown, MA. USA.

Al-Emrani, M. Engström, B. Johansson, M. and Johansson, P. (2011) *Bärande konstruktioner, del 1.* Göteborg: Chalmers University of Technology.

Andersson, J. and Antonsson, J. (2015) *Design with regard to collision impact.* Göteborg: Chalmers University of Technology.

Augustsson, R. and Härenstam, M. (2010) *Design of reinforced concrete slab with regard to explosions.* Göteborg: Chalmers University of Technology.

Blake, A. (1985) *Handbook of Mechanics, Materials, and Structures.* New York: John Wiley & Sons Inc.

Boverket (2004) *Boverkets handbok om betongkonstruktioner, BBK 04,* Boverket, Sweden.

CEN (2004) *Eurocode 2: Design of concrete structures – Part 1-1: General rules and rules for buildings,* European Committee for Standardization , Brussels, Belgium.

Dahlberg, T. (2002) *Teknisk hållfasthetslära.* Lund: Studentlitteratur AB.

Dahlblom, A. Olsson, K-G. (2010) *Strukturmekanik, Modellering och analys av ramar och fackverk.* Lund: Studentlitteratur AB.

Engström, B. (2014) *Design and analysis of slabs and flat slabs.* Göteborg: Chalmers University of Technology.

Engström, B. (2015) *Design and analysis of continious beams and columns.* Göteborg: Chalmers University of Technology.

Hallbjörn, L. (2015) *Betongplattor, beräkning och dimensionering.* Stockholm: Sveriges Bygguniversitet.

Lim, S. (2013) *Redistribution of force concentrations in reinforced concrete cantilever slab using 3D non-linear FE-analyses.* Göteborg: Chalmers University of Technology.

Lindelöf, A. and Walhelm, B. (2014) *Moment distribution and cumulative plastic rotation in reinforced concrete slabs subjected to concentrated forces.* Göteborg: Chalmers University of Technology.

Lopes, A.V. Lopes, S.M.R. Carmo, R.N.F. (2014) *Stiffness of reinforced concrete slabs subjected to torsion.* Department of civil engineering, University of Coimbra.

Pacoste, C. Plos, M. and Johansson, M. (2012) *Recommendations for finite element analysis for design of reinforced concrete slabs.* Stockholm: Royal Institute of Technology.